

2011

Development of a Monte Carlo based correction strategy for a TG-43 based brachytherapy treatment planning system to account for applicator inhomogeneities

Bobby Chon Mathews

Louisiana State University and Agricultural and Mechanical College, bcmathews84@gmail.com

Follow this and additional works at: https://digitalcommons.lsu.edu/gradschool_theses



Part of the [Physical Sciences and Mathematics Commons](#)

Recommended Citation

Mathews, Bobby Chon, "Development of a Monte Carlo based correction strategy for a TG-43 based brachytherapy treatment planning system to account for applicator inhomogeneities" (2011). *LSU Master's Theses*. 1339.
https://digitalcommons.lsu.edu/gradschool_theses/1339

This Thesis is brought to you for free and open access by the Graduate School at LSU Digital Commons. It has been accepted for inclusion in LSU Master's Theses by an authorized graduate school editor of LSU Digital Commons. For more information, please contact gradetd@lsu.edu.

DEVELOPMENT OF A MONTE CARLO BASED CORRECTION STRATEGY FOR A TG-43
BASED BRACHYTHERAPY TREATMENT PLANNING SYSTEM TO ACCOUNT FOR
APPLICATOR INHOMOGENEITIES

A THESIS

Submitted to the Graduate Faculty of the
Louisiana State University and
Agricultural and Mechanical College
in partial fulfillment of the
requirements for the degree of
Master of Science

In

The Department of Physics and Astronomy

by
Bobby Mathews
B.S. University of Arkansas in Little Rock, 2007
May, 2011

Acknowledgements

I thank my committee chair, Dr. Michael Price for providing me the needed direction, understanding and professional enrichment. He has been an invaluable mentor that not only developed this project, but also had the remarkable patience with me during the writing process. I cannot thank him enough. Also, I acknowledge my supervisory committee members, Dr. Kenneth Matthews, Dr. Jonas Fontenot, Dr. John Gibbons, Dr. Jonathan Dowling, and Dr. Charles Wood for their guidance and support throughout the course of this research. Special thanks to Dr. Matthews who I personally asked to serve on my committee. His extra dedication to detail in the classroom and on this committee has been very constructive to my education.

I thank the Mary Bird Perkins Cancer Center and staff for allowing me to use their facility for my thesis research. Also, I thank the clinical physicists at Mary Bird Perkins Cancer Center for their help in the clinic. Special thanks to Connell Chu for his interest in this project and support with computer programming obstacles.

I am also grateful and many thanks are due to Dr. Kenneth Hogstrom, program director, because of his constant commitment to student success which does not go unnoticed. I also thank Yvonne Thomas for her help with everything over the years. If I ever had a question, she always had an answer.

Thank you to my close friends who have made my time at Louisiana State University an incredible experience. Special thanks to my mom and dad for their constant support and encouragement they have given me not only as a student but throughout my entire life.

“..for I have learned to be content whatever the circumstances. I know what it is to be in need, and I know what it is to have plenty. I have learned the secret of being content in any and every situation, whether well fed or hungry, whether living in plenty or in want.”

–Philippians 4:11-12

Table of Contents

Acknowledgements	ii
List of Tables	v
List of Figures.....	vi
Abstract.....	ix
Chapter 1 Introduction.....	1
1.1 Brachytherapy for the Treatment of Cervical Carcinoma	1
1.2 Prescription Methodologies for Gynecological ICBT	2
1.2.1 Manchester System.....	2
1.2.2 International Commission on Radiation Units (ICRU) Report 38 Guidelines for ICBT of Cervical Disease	3
1.2.3 American Brachytherapy Society Guidelines for ICBT of Gynecological Disease.....	4
1.3 Dose Calculation Methods for Brachytherapy	4
1.3.1 Analytical Method: American Association of Physicist in Medicine Task Group-43 (AAPM TG-43) Methodology.....	5
1.3.2 Deterministic Method: Monte Carlo Technique.....	7
1.4 ICBT Applicators and Their Dosimetric Effect	9
1.5 Hypothesis and Specific Aims	11
1.5.1 Aim 1. Confirm a Monte Carlo Model of A Paired Nucletron Fletcher CT-MR Ovoid Applicator.	11
1.5.2 Aim 2. Create a Library of 3D Correction-Attenuation Matrices.	11
1.5.3 Aim 3. Apply Attenuation-Correction Matrices To Treatment Planning System-Calculated Dose Distributions And Compare To Monte Carlo Calculations.....	12
Chapter 2 Methods and Materials.....	13
2.1 Aim 1: Monte Carlo Confirmation Method	13
2.1.1 Nucletron CT-MR Compatible, ICBT Ovoid MC Modeling.....	13
2.1.2 Radiochromic Film Model Confirmations	18
2.2 Aim 2: Development of 3D Attenuation Correction Factor Database	24
2.2.1 Method 1: Ovoid-Based Correction Factor, c_O	26
2.2.2 Method 2: Source-Based Correction Factor, c_S	27
2.2.3 Analysis Software Development	28
2.3 Aim 3: Application of 3D Correction Strategy to Patient Cases.....	28
2.3.1 DICOM.....	28
2.3.2 Application of Correction Factors to TPS-Calculated Plans	29
2.3.3 Case Selection	30
2.3.4 Analysis	31
Chapter 3 Results and Discussion	32
3.1 Aim 1: MC Modeling of a Nucletron ICBT CT-MR Fletcher Ovoid Applicator.....	32
3.1.1 Model Confirmation via Radiochromic Film	32
3.2 Aim 2: Development of Ovoid and Source-Based Correction Factors	34
3.2.1 Nucletron MicroSelectron High-Dose Rate Ir-192 Source	34

3.2.2 Nucletron CT-MR Compatible Applicator.....	35
3.2.3 MC Applicator Modified to Include High-Z Inhomogeneities	40
3.3 Aim 3: Application of Source- and Ovoid-Based 3D Correction Strategies	44
3.3.1 Nucletron CT-MR compatible Fletcher Ovoid Applicator	44
3.3.2 MC Applicator Modified to Include High-Z Inhomogeneities	56
3.3.3 Summary of Results	74
3.4 Discussions.....	76
Chapter 4 Conclusions.....	78
4.1 Summary of Results	78
4.2 Evaluation of Hypothesis	78
4.3 Future Work	79
References.....	80
Appendix 1 Process Digitized Film (.tiff images) and Calculate Standard Deviation	82
Appendix 2 Compile Dose Grid from a RD DICOM File	85
Appendix 3 Dose Tolerance and Distance to Agreement Algorithm	86
Appendix 4 Define Plan Parameters from RP, RD DICOM Files	89
Appendix 5 Dose Grid 3D Rotation.....	93
Vita.....	94

List of Tables

Table 2.1: Materials of structures used in the CT-MR Fletcher ovoid set Monte Carlo simulations, their compositions listed by weight and density. Dry air is defined at sea level (1 atm) and 20° C.	15
Table 2.2: Estimated relative uncertainties of the radiochromic film dose interpretations per measured unit reference air kerma rate.	24
Table 3.1: Agreement of MC simulation with TG-43 data set, Ovoid-correction plan, and Source-correction plan. Agreement metric: 2% or 2mm.	74
Table 3.2: Agreement of modified MC model simulation with TG-43 data set, Ovoid-correction plan, and Source-correction plan. Agreement metric: 2% or 2mm.	75

List of Figures

Figure 1.1: CT-MR Fletcher applicator set.....	2
Figure 1.2: Anatomy illustration to show relationship of points A and B to the vaginal fornices and uterus as described using the Manchester system.....	3
Figure 1.3: Definition of the coordinate system utilized within the AAPM TG-43 formalism.....	6
Figure 2.1: Two-dimensional plots of the CT-MR Fletcher ovoid applicator set using the MCNPX graphical plotter	16
Figure 2.2: RCF measured calibration points used to convert RCF readings to dose.	20
Figure 2.3: Monte Carlo model film confirmation phantom	22
Figure 2.4: Illustration of comparison algorithm.	24
Figure 2.5: Two-dimensional plots of the modified CT-MR Fletcher ovoid applicator set using the MCNPX graphical plotter	25
Figure 2.6: Illustration of 3D dose tolerance and distance-to-agreement algorithm	29
Figure 3.1: Anterior rectal wall MC/RCF isodose contour comparison. Comparison of MC (dashed) simulated and RCF (solid) measured dose, in cGy, for a plane located 1.7 cm distal to the distal surface of a single ovoid. This plane serves as a surrogate to the anterior rectal wall of a patient.....	33
Figure 3.2: Lateral disease wall MC/RCF isodose contour comparison. Comparison of MC (dashed) simulated and RCF (solid) measured dose, in cGy, for a plane located 3.3 cm lateral to the long-axis of a single ovoid. This plane serves as a surrogate to the disease wall, lateral to the cervix, of a patient.....	34
Figure 3.3: Comparison of MC (red dashed) and TG-43 (solid blue) dose distribution, in Gy, resulting from a single source in water with equivalent source activities and dwell-time	36
Figure 3.4(a-b): Comparison MC and TG-43 dose distribution for dwell index (a) 1500 mm and (b) 1495 mm, in Gy, within a plane bisecting the right ovoid, resulting from a single source with equivalent source activities and dwell-times	37
Figure 3.5(a-b): Comparison MC and TG-43 dose distribution for dwell index (a) 1490 mm and (b) 1485 mm, in Gy, within a plane bisecting the right ovoid, resulting from a single source with equivalent source activities and dwell-times	38
Figure 3.6: Comparison MC and TG-43 dose distribution for superimposed dwell indexes: 1500 mm, 1495 mm, 1490 mm, and 1485 mm, in Gy, within a plane bisecting the right ovoid, resulting from four source dwell-positions with equivalent source activities and dwell-times. .	39

Figure 3.7(a-b): Comparison MC and TG-43 dose distribution for dwell index (a) 1500 mm and (b) 1495 mm, in Gy, within a plane bisecting the right ovoid, resulting from a single source with equivalent source activities and dwell-times	41
Figure 3.8(a-b): Comparison MC and TG-43 dose distribution for dwell index (a) 1490 mm and (b) 1485 mm, in Gy, within a plane bisecting the right ovoid, resulting from a single source with equivalent source activities and dwell-times	42
Figure 3.9: Comparison MC and TG-43 dose distribution for superimposed dwell indexes: 1500 mm, 1495 mm, 1490 mm, and 1485 mm, in Gy, within a plane bisecting the right ovoid, resulting from four source dwell-positions with equivalent source activities and dwell-times. .	43
Figure 3.10: Comparison of MC simulation of a mHDR v2 Ir-192 source contained in a CT-MR compatible Fletcher ovoid applicator (red) vs. TG-43 calculations for a source in water (blue). Maximum adjacent dwell-time gradient is zero.....	45
Figure 3.11(a-b): Comparison of MC simulation of a mHDR v2 Ir-192 source contained in a CT-MR compatible Fletcher ovoid applicator vs. TG-43 corrected plans that account for applicator heterogeneities. Maximum adjacent dwell-time gradient is zero	46
Figure 3.12: Comparison of MC simulation of a mHDR v2 Ir-192 source contained in a CT-MR compatible Fletcher ovoid applicator (red) vs. TG-43 calculations for a source in water (blue). Maximum adjacent dwell-time gradient is 30%	48
Figure 3.13: Comparison of MC simulation of a mHDR v2 Ir-192 source contained in a CT-MR compatible Fletcher ovoid applicator vs. TG-43 corrected plans of a source in water. Maximum adjacent dwell-time gradient is 30%	49
Figure 3.14: Comparison of MC simulation of a mHDR v2 Ir-192 source contained in a CT-MR compatible Fletcher ovoid applicator (red) vs. TG-43 calculations for a source in water (blue). Maximum adjacent dwell-time gradient is 60%	51
Figure 3.15(a-b): Comparison of MC simulation of a mHDR v2 Ir-192 source contained in a CT-MR compatible Fletcher ovoid applicator vs. TG-43 corrected plans of a source in water. Maximum adjacent dwell-time gradient is 60%	52
Figure 3.16: Comparison of MC simulation of a mHDR v2 Ir-192 source contained in a CT-MR compatible Fletcher ovoid applicator (red) vs. TG-43 calculations for a source in water (blue). Maximum adjacent dwell-time gradient is 70%	54
Figure 3.17: Comparison of MC simulation of a mHDR v2 Ir-192 source contained in a CT-MR compatible Fletcher ovoid applicator vs. TG-43 corrected plans of a source in water. Maximum adjacent dwell-time gradient is 70%.....	55
Figure 3.18: Comparison of MC simulation of a mHDR v2 Ir-192 source contained in a modified CT-MR compatible Fletcher ovoid applicator to include a high-Z shield (red) vs. TG-43 calculations for a source in water (blue). Maximum adjacent dwell-time gradient is zero	57

Figure 3.19(a-b): Comparison of MC simulation of a mHDR v2 Ir-192 source contained in a modified CT-MR compatible Fletcher ovoid applicator to include high-Z shield vs. TG-43 corrected plans of a source in water. Maximum adjacent dwell-time gradient is zero..... 58

Figure 3.20: Comparison of MC simulation of a mHDR v2 Ir-192 source contained in a modified CT-MR compatible Fletcher ovoid applicator to include a high-Z shield (red) vs. TG-43 calculations for a source in water (blue). Maximum adjacent dwell-time gradient is 5%..... 60

Figure 3.21: Comparison of MC simulation of a mHDR v2 Ir-192 source contained in a modified CT-MR compatible Fletcher ovoid applicator to include high-Z shield vs. TG-43 corrected plans of a source in water. Maximum adjacent dwell-time gradient is 5% 61

Figure 3.22: Comparison of MC simulation of a mHDR v2 Ir-192 source contained in a modified CT-MR compatible Fletcher ovoid applicator to include a high-Z shield (red) vs. TG-43 calculations for a source in water (blue). Maximum adjacent dwell-time gradient is 10%. . 63

Figure 3.23(a-b): Comparison of MC simulation of a mHDR v2 Ir-192 source contained in a modified CT-MR compatible Fletcher ovoid applicator to include high-Z shield vs. TG-43 corrected plans of a source in water. Maximum adjacent dwell-time gradient is 10% 64

Figure 3.24: Comparison of MC simulation of a mHDR v2 Ir-192 source contained in a modified CT-MR compatible Fletcher ovoid applicator to include a high-Z shield (red) vs. TG-43 calculations for a source in water (blue). Maximum adjacent dwell-time gradient is 15%.... 66

Figure 3.25: Comparison of MC simulation of a mHDR v2 Ir-192 source contained in a CT modified CT-MR compatible Fletcher ovoid applicator to include high-Z shield vs. TG-43 corrected plans of a source in water. Maximum adjacent dwell-time gradient is 15% 67

Figure 3.26: Comparison of MC simulation of a mHDR v2 Ir-192 source contained in a modified CT-MR compatible Fletcher ovoid applicator to include a high-Z shield (red) vs. TG-43 calculations for a source in water (blue). Maximum adjacent dwell-time gradient is 30%.... 69

Figure 3.27: Comparison of MC simulation of a mHDR v2 Ir-192 source contained in a modified CT-MR compatible Fletcher ovoid applicator to include high-Z shield vs. TG-43 corrected plans of a source in water. Maximum adjacent dwell-time gradient is 30%. 70

Figure 3.28: Comparison of MC simulation of a mHDR v2 Ir-192 source contained in a modified CT-MR compatible Fletcher ovoid applicator to include a high-Z shield (red) vs. TG-43 calculations for a source in water (blue). Maximum adjacent dwell-time gradient is 60%.... 72

Figure 3.29(a-b): Comparison of MC simulation of a mHDR v2 Ir-192 source contained in a modified CT-MR compatible Fletcher ovoid applicator to include high-Z shield vs. TG-43 corrected plans of a source in water. Maximum adjacent dwell-time gradient is 60% 73

Abstract

Purpose: The purpose of this work was to investigate the use of pre-calculated Monte Carlo (MC) ovoid and source-based attenuation-correction factors that would correct a commercially-available brachytherapy treatment planning system (TPS) generated plan in order to account for any dosimetric effects due to the presence of intracavitary brachytherapy (ICBT) applicators during treatment delivery.

Methods: A MC model of an ICBT CT-MR compatible ovoid applicator set was confirmed utilizing radiochromic film (RCF). MC was used to simulate dose distributions resulting from eight source-dwell-positions within the ICBT applicator. Also, the American Association of Physicist in Medicine Task Group 43 Report (AAPM TG-43) was utilized to calculate absolute dose rate around a microSelectron version 2 ^{192}Ir source contained in water. With these dose distributions, a library of ovoid and source-based 3D attenuation-correction factor datasets characterizing the dosimetric effects of the ICBT applicator was developed. Appropriate attenuation-correction factors were then applied to correct a brachytherapy TPS-calculated plan. Several plans with different maximum dwell-time gradients (∇_{dt}) were compared to evaluate the effectiveness of both correction methods with respect to criteria of acceptability being within +/- 2% absolute dose or +/- 2 mm distance-to-agreement (DTA).

Results: RCF confirmation measurements from 3 active dwell-positions in a single ovoid agreed with MC simulated planes with over 96% of points agreeing within 2% or 2 mm DTA. Plans generated by Oncentra TPS can be corrected utilizing either the ovoid-based or source-based correction methods to agree with full simulated Monte Carlo datasets to within +/- 2% or +/- 2mm DTA. Although, dwell-time combinations utilized in this study with a maximum dwell-time gradient above 10% is a threshold for the ovoid- based correction scheme to correct the TG-

43 calculation. The source- based correction method consistently results in 100% agreement between a corrected plan and the equivalent MC generated plan.

Conclusions: The MC model is sufficient to predict measured RCF dose distributions accurately. Source- based correction factors can be applied to correct a TG-43 based treatment plan to match a full MC simulation.

Chapter 1 Introduction

1.1 Brachytherapy for the Treatment of Cervical Carcinoma

Intracavitary brachytherapy (ICBT) has an advantage over external beam radiotherapy (EBRT) for local control because it allows for dose escalation while sparing normal tissue surrounding the treatment volume. Cervical cancer treatment is typically a combination of EBRT and ICBT. EBRT is generally delivered first in order to reduce the volume of the primary disease before ICBT as well as to control the spread of disease at the periphery of the tumor bed. Unlike in EBRT, where radiation is directed at the disease from outside the body, ICBT involves placing a radioactive source within close proximity or inside the target tissue. Due to the inverse square law, *i.e.* the exposure due to a source is inversely proportional to the square of the distance from the source; the high-dose region delivered from a radioactive source is localized and has a very steep dose gradient.

The current ICBT cervical technique is to remotely afterload radioactive sources into a tandem and ovoids once they have been placed in the uterine canal. A photo of Nucletron's computed tomography, magnetic resonance (CT-MR) compatible tandem and ovoids is shown in Figure 1.1. During an ICBT treatment, the radioactive source is remotely after loaded into the applicator and the source steps to varying positions (*i.e.*, 5 mm back) within the applicator shaft. The process of moving a single source to multiple positions in the applicator simulates a single-long source in the applicator. The design of an applicator allows delivery of the radioactive source and a specific dose distribution around the disease.

A tandem is a hollow tube and is inserted directly through the cervical opening into the endometrial cavity (inner uterine lining). Although only 5 cm of the tandem is placed in the uterus, tandems are approximately 25 cm in length and are available in varying curvatures (*i.e.* 15°, 30°, 45°) to accommodate variations in disease location and patient anatomies. The ovoids

are positioned lateral to the cervical opening on opposite sides within the vaginal fornices. In addition to the ICBT technique, a “packing” procedure holds the ovoids relatively stationary post-insertion and displaces the rectum and bladder away from the high dose volume. “Packing” refers to inserting gauze around the ovoids in the patient’s anterior and posterior directions. This additional procedure takes advantage of the distortable characteristic of the vagina and the inverse-square dose falloff applicable with ICBT.

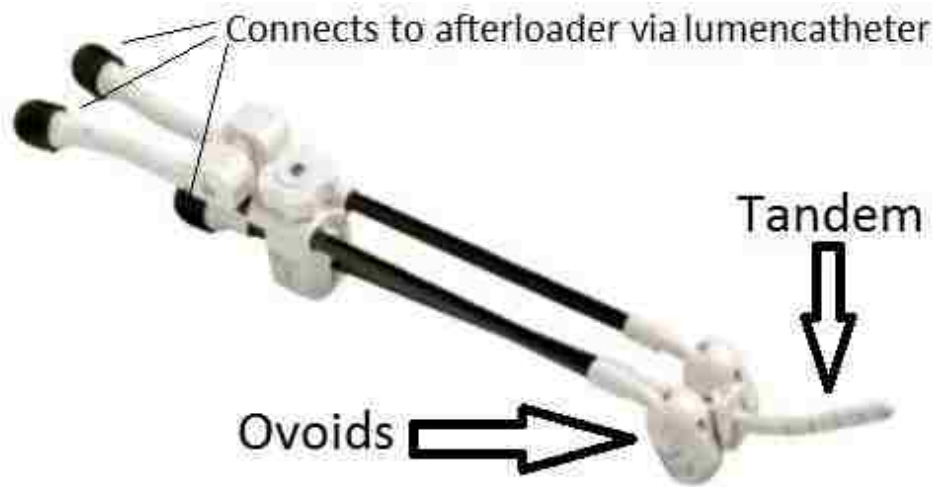


Figure 1.1: CT-MR Fletcher applicator set.

1.2 Prescription Methodologies for Gynecological ICBT

Dosimetry systems for brachytherapy consist of a set of rules which, when followed, would deliver dose in a clinically desirable distribution to a designated anatomical region. These guidelines specify treatment delivery parameters in terms of dose, time, and source position in an attempt to deliver a prescribed dose in a reproducible manner. Dosimetry systems also provide standardization for treatments which allow inter-institutional comparison of results.

1.2.1 Manchester System

The Manchester system, developed by Ralston Paterson, M.D. and Herbert Parker, Ph.D. at Manchester Hospital, defines four points at which delivered dose rates are to be considered: point A, point B, a bladder point, and a rectum point. The duration of the implant is based on the

dose rate calculated at point A, although the dose at the other points are recorded and evaluated during the treatment planning process. As illustrated in Figure 1.2, the left and right point A's were defined as 2 cm superior and lateral to the vaginal fornices. Point B was defined 3 cm lateral to the left and right point A's. Ideally, Point A represents an anatomical location where the uterine vessels cross the ureter, and point B represents the location of lymph nodes. Within the Manchester system, the locations of prescription points are a function of source orientations and not specified directly in terms of a patient's anatomical structures. For an ICBT cervical treatment, the delivered dose distribution ideally resembles a "pear shape" when viewed in the anterior-posterior (AP) plane. In some patient instances, this method of defining prescribed doses to a specific point risks under dosage of a large cervical tumor or over dosage of small tumors [1].

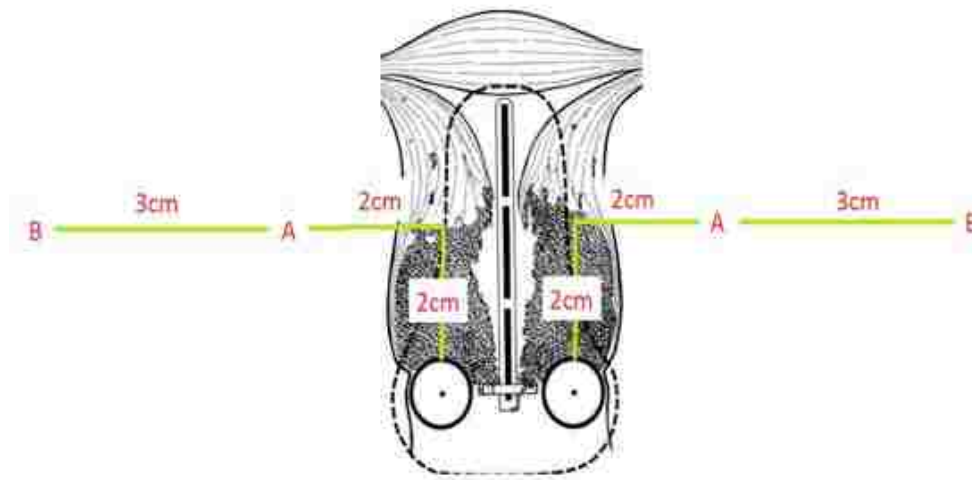


Figure 1.2: Anatomy illustration to show relationship of points A and B to the vaginal fornices and uterus as described using the Manchester system.

1.2.2 International Commission on Radiation Units (ICRU) Report 38 Guidelines for ICBT of Cervical Disease

The International Commission on Radiation Units (ICRU) Report 38 introduced a dosimetry system, incorporating recommendations of the European Group of Brachytherapy, which recommends specifying prescription dose to a target volume, rather than to a discrete

point [2]. The method addresses the inherent ambiguity of dose delivered to a target volume when merely prescribing dose to a set of points. For an ICBT cervical treatment, the report recommends dose to be prescribed as an isodose surface that surrounds the target volume (uterus, cervix). Recommendations are given to use certain points for reporting dose to organs at risk (OAR) such as the bladder point, rectal point, lymphatic trapezoid of Fletcher points, and pelvic wall points. However, it has been shown that the ICRU reference points for the bladder and the rectum do not necessarily indicate the maximum dose delivered to these OARs [3]. 3D treatment planning analysis has shown maximum bladder doses and maximum rectal doses can be as much as 2.3 and 1.3 times higher, respectively, when determined using computed tomography (CT) relative to the ICRU reference points [4].

1.2.3 American Brachytherapy Society Guidelines for ICBT of Gynecological Disease

The American Brachytherapy Society recommends prescribing dose for cervical ICBT to a new point, other than point A, where it is farther from the high-dose gradient fall off from the ovoids [5]. This point, designated point H, relocates the prescription point away from the high-dose high-gradient fall off region that the ICRU/Manchester point A lies within, to an area of high-dose, low dose-gradient fall off. It was suggested as a minor change in the location of point A because it results in a significant difference in dose which may lead to inconsistencies in patient treatments. This new point (Point H) is located 2 cm superiorly to the cervical os plus the radius of the ovoids, and then 2-cm in the lateral direction.

1.3 Dose Calculation Methods for Brachytherapy

Accurate dose calculation of an ICBT cervical treatment is an important and challenging task. In general, radiation dose calculations involve the determination of the amount of energy deposited within a volume or point of interest. Manual dose calculations utilize published tables which characterize a dose distribution for a specified isotope and encapsulation in a

homogeneous material where the reference dose rate is estimated and the treatment time is calculated. Although manual tables are convenient for two dimensional (2D) dose calculations, treatment planning system (TPS) computers are able to quickly calculate dose to a three dimensional (3D) volume. Also, because the human body is not homogeneous, it would be advantageous for a calculation method to take into account tissue heterogeneities.

1.3.1 Analytical Method: American Association of Physicist in Medicine Task Group-43 (AAPM TG-43) Methodology

Most commercially available brachytherapy TPS utilize the dose calculation methods presented within the American Association of Medical Physics Task Group-43 (AAPM TG-43) report published in 1995 which characterizes the dose distribution in water as a function of isotope and source construction. This report presented a formalism that clearly defines the necessary physical quantities for point dosimetry [6]. The formalism has one dimensional and 2D formats: the point-source approximation and the line-source approximation. For dose distributions resulting from multiple sources or single source plans with multiple dwell-positions, this methodology relies on superposition of single-source dose distributions. This method assumes a 3D cylindrically symmetrical dose distribution as the calculation utilizes a 2D dataset for commissioning.

The AAPM TG-43 2D dose rate calculation equation is:

$$\dot{D}(r, \theta) = S_k \cdot \Lambda \cdot \frac{G(r, \theta)}{G(r_0, \theta_0)} \cdot g(r) \cdot F(r, \theta) \quad (1.1)$$

where r denotes the distance from the center of the radioactive source to the point of interest, and θ denotes the polar angle specifying the point-of-interest relative to the source longitudinal axis. As illustrated in Figure 1.3, the reference angle, θ_0 , and reference distance, r_0 , define a point on the source transverse plane, and are specified to be 90° and 1 cm, respectively.

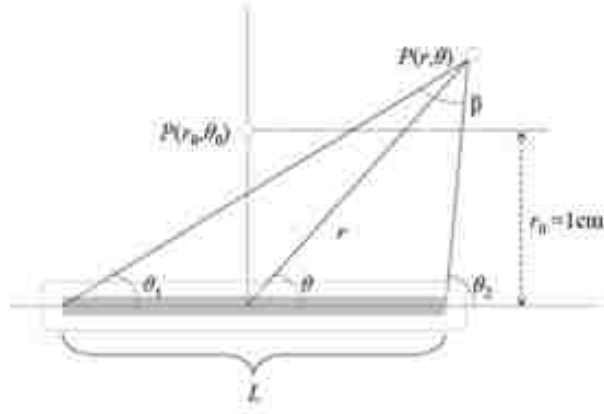


Figure 1.3: Definition of the coordinate system utilized within the AAPM TG-43 formalism.

Air-kerma strength, S_K , is the air-kerma rate, $K_\delta(d)$, *in vacuo*, due to photons with energies greater than δ , at distance d from the source, multiplied by the square of this distance. Air kerma rate measurements should be made in air and corrected for photon attenuation and scattering in air between the source and detector. In lieu of measurements, Price *et al.* has shown that a Monte Carlo (MC) simulation can be used to calculate air kerma rate [7]. The distance d can be any distance that is large relative to the maximum linear dimension of the radioactivity distribution so that S_K is independent of distance [1]. The units of air-kerma strength, denoted as U , are $\mu\text{Gy h}^{-1} \text{m}^2$.

The dose-rate constant, Λ , depends on both the radionuclide and source model, and is influenced by the source encapsulation's internal design. The definition of the dose-rate constant in water is the ratio of dose rate at the reference position to S_K :

$$\Lambda = \frac{\dot{D}(r_0, \theta_0)}{S_k} \quad (1.2)$$

The radial dose function, $g(r)$, accounts for dose fall-off on the transverse-plane due to photon scattering and attenuation, and is defined as:

$$g(r) = \frac{\dot{D}(r, \theta_0) \cdot G(r_0, \theta_0)}{\dot{D}(r_0, \theta_0) \cdot G(r, \theta_0)} \quad (1.3)$$

At the reference point, the radial dose function is equal to unity.

The 2D anisotropy function, $F(r, \theta)$, describes the variation in dose due to self-absorption of radiation as a function of polar angle relative to the transverse plane.

$$F(r, \theta) = \frac{\dot{D}(r, \theta) \cdot G(r, \theta_0)}{\dot{D}(r, \theta_0) \cdot G(r, \theta)} \quad (1.4)$$

At the reference point, the anisotropy function is equal to unity.

Physically, the geometry function, $G(r, \theta)$, neglects scattering, attenuation, radionuclide energy spectrum, and accounts for the inverse square dose fall off and distribution of radioactive material inside the radioactive source on the dose distribution at a given point.

$$G(r, \theta) = \begin{cases} \frac{\beta}{L \cdot r \cdot \sin \theta}, & \theta \neq 0 \\ (r^2 - L^2/4)^{-1}, & \theta = 0 \end{cases} \quad (1.5)$$

where L is the length of the radioactive source, and β is the angle subtended by the radioactive source with respect to the point of interest.

1.3.2 Deterministic Method: Monte Carlo Technique

The transport of radiation through matter is a stochastic process and can be simulated modeling physical law combined with the probabilities of interactions. For this type of application, a MC simulation is based on a repeated random sampling of particle histories to simulate random trajectories of individual particles. A single history finishes when the primary particle and all its liberated secondary particles lose enough energy that the remainder is considered negligible. Each history serves as an independent sample contributing towards the simulation result or tally, which is a statistical estimate of an actual dose distribution. When

enough histories are simulated, the central limit theorem applies and accurate dosimetric information on the transport process may be obtained by averaging over the entire simulation tally. Also, Strong's theory of large numbers says that results obtained from a large set of trials should be close to the expected value, and will tend to become closer as more trials are performed. Applications of MC techniques in medical physics, especially radiation therapy physics, have been discussed in numerous publications [8-10]. MC is considered the "gold standard" for dose computation accuracy once its application has been validated experimentally.

To accurately simulate a dose distribution using MC, the user must correctly model the geometry of the problem. The MC input file contains information about the geometry and material specification; the location and characteristics of the source; and any type of answers or tallies applicable. MC is able to simulate photon interactions such as the photoelectric effect, characteristic x-rays, coherent scattering, Compton scattering, and pair production [11].

Serial computation of millions of histories involves a significantly large amount of computing time. The MC calculation time is affected by the solid-angle effect and inverse-square law fall off of the radiation from the radioactive source since they result in fewer simulated photons at a distance away from the source. According to the central limit theorem, the relative error is proportional to $1/\sqrt{N}$, where N is the number of histories; and is used as a surrogate for computational time. The serial MC method requires long calculation times to generate dose distributions with satisfactory statistical uncertainties. To circumvent long computation times, MC parallel processing is able to simulate and track particle histories independently and simultaneously; the histories can be separated into several batches and executed in parallel. As of 2010, the Monaco TPS version 2.03 is the only commercially available MC-based treatment planning system for EBRT.

1.4 ICBT Applicators and Their Dosimetric Effect

Unfortunately, current clinical TPS are typically unable to accurately account for the dosimetric effects of additional source encapsulation, such as polysulfone and high-Z shielding, provided by the applicator in certain HDR ICBT techniques. These TPS systems utilize the TG-43 algorithm which does not provide a method to quantify the attenuative effects when calculating dose. The TG-43 formalism assumes calculations are in water. As such, errors of 5% - 30% or more may occur in planned dose to OARs [12-13]. Also, brachytherapy applicators which produce a non-cylindrically symmetric dose distribution cannot be incorporated into the TG-43 2D formalism.

One way to account for these dose perturbations is through the use of the MC technique. But, due to the intense computational time requirements for MC dose calculations, clinical use of MC for ICBT treatment planning is impractical. Investigations have been made into the use of pre-calculated MC data sets which characterize common brachytherapy dose distributions which are then applied to patient-specific geometries [14-15]. The technique presented by Rivard et al. (*i.e.* the Tufts technique) treats the brachytherapy applicator as an additional source encapsulation and employs MC to generate new TG-43 2D relative parameters (*i.e.* radial dose function, anisotropy function) specific to the radioactive source and brachytherapy applicator combination [15] which is then implemented into the TG-43 2D dose calculation. The TPS is then able to generate a 3D dose distribution that incorporates the applicator's attenuative effect into superposition calculations using MC-generated dose distribution parameters. However, this technique is only applicable to brachytherapy applicators that deliver a cylindrically symmetric dose distribution as TG-43 methods are limited to 2D.

Price *et al.* developed a rudimentary TPS that utilized pre-calculated MC data sets to simulate patient ICBT treatments delivered using a shielded tandem and ovoid applicator [16].

Because the system determined total dose to the patient through the superposition of dose distributions resulting from individual source dwells, a large number of MC simulations were required for commissioning. The systems required, as input, a simulated distribution for each possible source dwell-position, for each ovoid (left and right), for all possible ovoid lateral separations. As such, robust commissioning of the system was time prohibitive when one considers that for acceptable accuracy, a simulation of a few hundred million histories is required for each possible source position. In spite of these shortcomings, when commissioned with limited data applicable to a specific patient geometry, Price *et al.* reported a 94% agreement in dose to a clinically-applicable volume for a simulated patient treatment when compared to an equivalent volume whose ICBT delivered dose was simulated explicitly using MC techniques. The benefit of Price *et al.*'s system was in that their results were obtained nearly 5000 times faster than explicit MC system modeling and simulation. To reduce the commissioning requirements and extend the practicality of Price's system, the minimum amount of commissioning data required to produce a clinically viable pre-calculated MC-based TPS for ICBT must be determined.

In this work we present a modification to the method of Price *et al.* that, rather than employing pre-calculated MC data sets directly for dose determination, implements MC-based correction factors that correct for shortcomings intrinsic to TG-43 methods (more detailed discussion on correction factors in Chapter 2). When applied to TG-43 calculated dose, these correction factors will account for any dosimetric effects due to the presence of ICBT applicators during treatment delivery. The motivation driving this modification is that it facilitates the method's integration into existing, commercially-available TPS. Additionally, it is thought that by taking into account the dominant dosimetric effects of inverse-square falloff of dose with distance from the source (via TG-43 methods) as well as the attenuative effects of the ICBT

applicator (via MC-correction factors), an accurate patient dose calculation can be made while by-in-large ignoring the secondary influence of scatter due to tissue inhomogeneities. However, verifying this expectation is beyond the scope of the presented work.

1.5 Hypothesis and Specific Aims

A 3D Monte Carlo-simulated dose distribution of the ovoid contribution to a cervical intracavitary brachytherapy (ICBT) treatment administered via Nucletron's Fletcher CT-MR ovoid applicator (Nucletron Corporation, Veenendaal, The Netherlands), modeled with and without a rectal shield surrogate, will agree, within criteria, with the dose distribution resulting from an equivalent treatment calculated using AAPM Task Group-43 (TG-43) methodology when corrected for heterogeneities using pre-calculated MC correction factors applied (a) to individual source dwell-positions and (b) individual ovoids acting as multi-source surrogates for varying adjacent dwell-time gradients (∇_{dt}). Criteria are defined as agreement within +/- 2% dose or +/- 2 mm distance-to-agreement (DTA).

Three aims have been completed to test this hypothesis:

1.5.1 Aim 1. Confirm a Monte Carlo Model of A Paired Nucletron Fletcher CT-MR Ovoid Applicator.

A Monte Carlo (MC) model of the Nucletron high-dose rate (HDR) ICBT CT-MR compatible Fletcher ovoid set will be created and experimentally confirmed via film dosimetry. Absolute dose measurements will be made in two perpendicular planes, (a) 1 cm beyond the distal end and (b) 3.3 cm from, and parallel to, the long axis of a single ovoid. Measurements will be carried out in water.

1.5.2 Aim 2. Create a Library of 3D Correction-Attenuation Matrices.

Two MC models will be used to simulate 3D dose distributions in water for clinically relevant microSelectron HDR (mHDR) Ir-192 dwell-positions. The two MC models will model (1) the commercially-available CT-MR compatible Fletcher ovoid confirmed in Aim 1 and (2) a

modified version of that includes a high-Z heterogeneity acting as a rectal shield surrogate.

These distributions will take into account source loading geometry as well as dose perturbations due to the ovoids. From this data, a library of 3D attenuation-correction matrices will be developed that characterize the dosimetric effect of the commercial ovoid as well as the modified ovoid model to create both source- and ovoid-based correction factors.

1.5.3 Aim 3. Apply Attenuation-Correction Matrices To Treatment Planning System-Calculated Dose Distributions And Compare To Monte Carlo Calculations.

The two sets of ovoid and source-based correction attenuation matrices will be applied to 3D dose distributions calculated by the Oncentra Brachytherapy treatment planning system, which utilizes TG-43 dose-calculation methodology, in an attempt to reproduce MC-simulated dose distributions of equivalent treatment geometries. The two sets of correction factors will be applied to different plans varying the ∇_{dt} of each ovoid. Agreement criteria will be applied and the hypothesis will be tested.

Chapter 2 Methods and Materials

2.1 Aim 1: Monte Carlo Confirmation Method

For Monte Carlo (MC) modeling of the Ir-192 high dose-rate source and ICBT applicator ovoids, Monte Carlo N-Particle eXtended (MCNPX) transport code was employed. This MC package is capable of simulating transport of a variety of particles in complex, three dimensional geometries [11]. The validated MC model of the microSelectron v2 HDR (mHDR v2) Ir-192 source (Nucletron Corporation, Veenendaal, The Netherlands) presented by Price *et al.* is utilized for all source simulations within this study and its design and material description can be found in their work [7]. Price *et al.* showed that MC simulated dose for a medial plane with effects from a high-Z shield was in agreement with radiochromic film measurements for 91% of the comparison points within +/-2% or +/- 2mm and approximately 98% were within +/-10% or +/-2mm distance-to-agreement (DTA) [17].

2.1.1 Nucletron CT-MR Compatible, ICBT Ovoid MC Modeling

Detailed physical measurements of Nucletron's CT-MR compatible tandem and ovoid applicator were performed in-house to facilitate construction of a MC model of the device. The model consists of an ovoid set and does not include the intrauterine tandem. The tandem was excluded due to its cylindrical symmetry and thin wall (≈ 1 mm) construction of nearly tissue equivalent material. As such, dose calculated using TG-43 based or MC methods in a heterogeneous volume differ within the uncertainty of the MC calculation method.

To ensure dosimetrically accurate simulations, it is important to model the entire physical system with sufficient precision when utilizing MC methods. Therefore, the model used for this study included a paired of left and right ovoids that can house the mHDR v2 Ir-192 source in a variety of clinically applicable dwell-positions. For this work, dwell-positions were limited to four (4) per ovoid with a separation of 5 mm between possible source positions. Although only

one ovoid can be “active” (*i.e.* contain the stepped radioactive source) at any one time, all simulations included its “inactive” pair as it has been shown that dose discrepancies up to 14% may result when the inactive ovoid is not explicitly modeled [16]. This effect is especially true for shielded applicators. The material, density, and composition of each component of the MC model used within this study are shown in Table 2.1. A two-dimensional graphical representation of the study’s MC model is shown in Figure 2.1 (a) through (c).

A few geometric features of the components were simplified to reduce the complexity of the MC input file while maintaining dosimetric accuracy at relevant clinical distances from the ovoid surface. These include: (1) omitting the long handle of each ovoid, (2) approximating the retaining screw as a cylinder, (3) simplifying the shape of the intrauterine tandem flange spacer, (4) approximating the curvature of the colpostat shaft as two intersecting cylinders, and (5) modeling a length of 2 cm to approximate the braided steel cable attached to the proximal end of the mHDR v2 Ir-192 source. It is also assumed for simulations that the mHDR v2 Ir-192 source, when deployed from the after loader, lays exactly along the central shaft of the ovoid. As the nominal inner diameter of the source lumen within the ovoid shaft is 3.5 mm, the modeled source, which has a 0.9 mm outer diameter, could be off center by, at most, 1.3 mm [16]. Assuming inverse square is the predominate effect; the uncertainty of absolute dose, directly adjacent to the ovoid, may be affected by the source being off center.

The superposition of simulated dose matrices of individual Ir-192 source dwell-positions is required due to the density of the iridium source causing large anisotropy effects when sources are simulated simultaneously. Multiple dwell-positions simulated simultaneously are not an accurate representation of an actual loaded HDR ICBT treatment where a single source is positioned at varying dwell points within the ovoid shaft at different times.

Table 2.1: Materials of structures used in the CT-MR Fletcher ovoid set Monte Carlo simulations, their compositions listed by weight and density. Dry air is defined at sea level (1 atm) and 20° C.

Structures	Material	Composition (% by weight)	Density (g cm ⁻³)
Source encapsulation, braided steel cable	AISI 316L stainless steel, conductor ^a	Mn 2.0 Si 1.0 Cr 17.0 Ni 12.0 Fe 68.0	8.02 4.81 ^a
Film phantom	Liquid water	H 11.2 O 88.8	1.0
Ovoids	Polysulfone	C 66.0 O 22.0 S 7.4 H 4.6	1.29
Outside of water phantom, interior of ovoid, interior of ovoid shaft, canal where retaining screw is fitted	Dry air gas = 1 ^b	C 0.0124 N 75.5267 O 23.1781 Ar 1.2827	1.205 x 10 ⁻³
Radioactive source	Iridium-192	Ir 100	22.42

^a Braided steel cable density is 4.81 g • cm⁻³

^b Gas state defined on material card in MCNPX

2.1.1.2 The ¹⁹²Ir Energy Spectrum

The mHDR Ir-192 source has a half-life of 73.83 days and an average energy of 0.38 MeV. It decays by emitting beta particles and gamma radiation. It is produced by neutron activation of iridium metal in a nuclear reactor. The energy spectrum utilized for ¹⁹²Ir source simulations is that reported by Glasgow and Dillman[18]. They reported that gamma and x-rays of energies less than 11.3 keV cannot penetrate through the high-Z source encapsulation and should not be included in the determination of the total specific gamma-ray constant, total specific x-ray constant, and total exposure rate constant. The total number of photons emitted per disintegration was determined to be 2.32 by Price *et al.* [7]. This factor was used to convert the MC dose rate estimate per photon to the dose rate estimate per source contained activity in Equation 2.1.

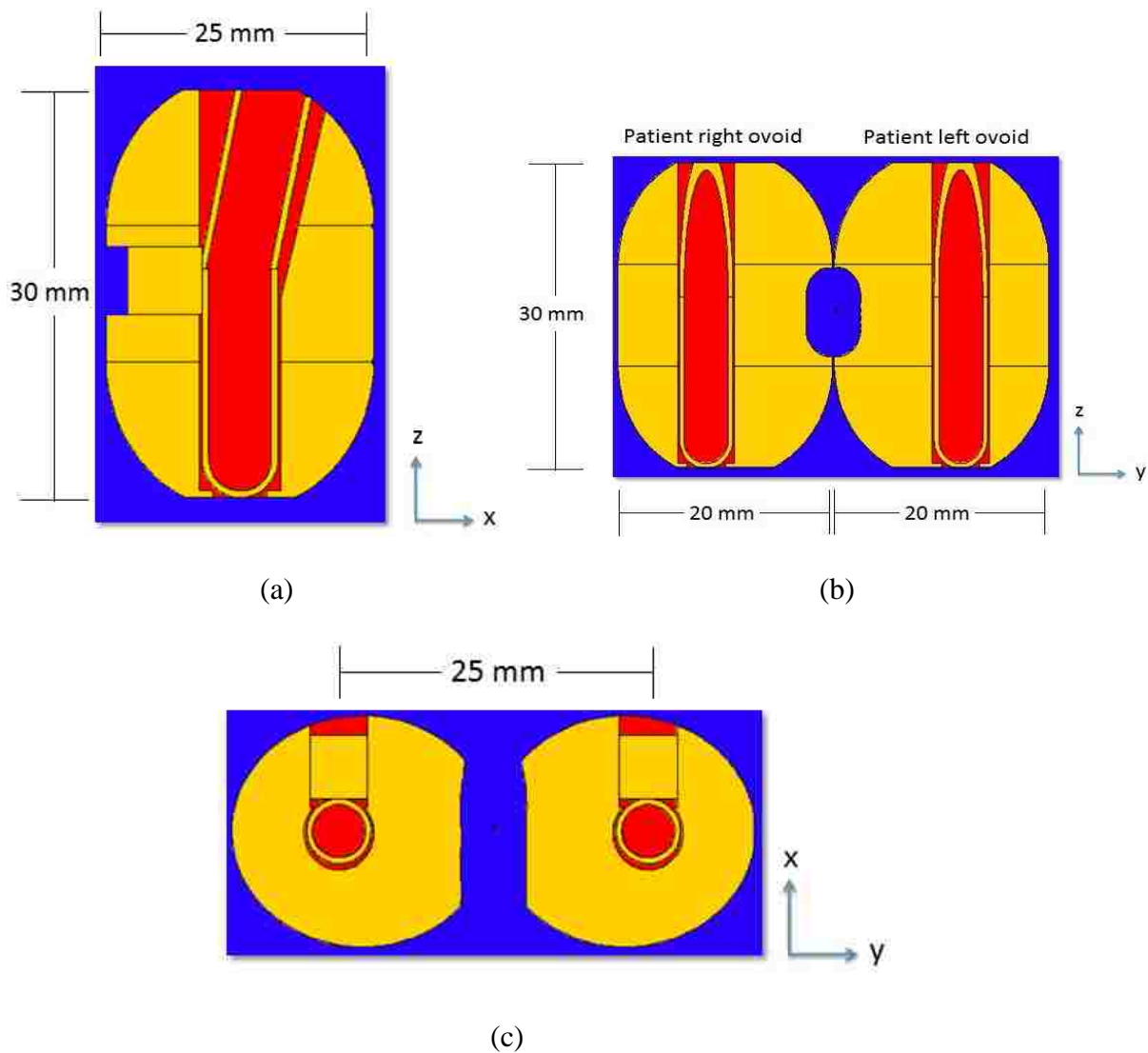


Figure 2.1: Two-dimensional plots of the CT-MR Fletcher ovoid applicator set using the MCNPX graphical plotter through a.) the ZX-plane bisecting the ovoid shaft, b.) the ZY-plane bisecting the ovoid shafts in the left/ right ovoids and c.) the XY-plane bisecting the ovoid shaft. Colors show different materials where blue, yellow, and red are water, Polysulfone, and air, respectively.

2.1.1.3 The Tally Type, Mesh Size, and Relative Error of MC Dose Estimates

The MCNPX “mesh” tally (F6:photons) type was utilized for study simulations. The tally size for this study was a $10 \times 10 \text{ cm}^3$ plane with 1 mm^3 voxels. The type of tally utilized in this study scores the average energy deposition per unit volume ($\text{MeV cm}^{-3} \text{ particle}^{-1}$). Tracked

particle interactions were limited to photons as the energy deposition for non-tracked secondary particles (*i.e.*, electrons) was assumed to be constrained to within close proximity of the collision site [11]. Since secondary particles from low energy photons have a relatively short path length, compared to the voxel size, this tally yields a good approximation of collision kerma [16, 19-21]. The normalization is per unit cell volume, not per unit mass, since the mesh cell may cover regions of different masses.

Due to the inverse-square law fall off of emitted radiation, voxels far from a simulated source will record fewer histories compared to those more proximal. For each tally voxel, MC reports an estimation of relative error, R , corresponding to one estimated standard deviation. The relative error is proportional to $1/\sqrt{N}$, where N is the number of particle histories. Therefore, relatively large number of particle histories must be simulated in order to obtain energy depositions of acceptable error. Since MC estimates of collision KERMA depend largely on simulated interaction cross-section data, the accuracy of these libraries plays an important role in the validity of simulated interactions. As such, all cross-section libraries utilized in this work have been vetted by Los Alamos National Laboratory [11]. Finally, an additional source of error may lie within the inaccuracies of modeled geometries. If errors exist in any of these study components (modeled geometry, energy spectrum, and interaction cross-section) disagreements will exist between simulated and measured dose distributions. Therefore, film measurements have been performed to confirm the accuracy of the MC modeling of the ovoids.

2.1.1.4 Conversion of MC Calculated Quantities to Absolute Dose

MCNPX mesh tally simulations are recorded as units of energy deposition per unit volume per simulated particle [$\text{MeV cm}^{-3} \text{ particle}^{-1}$]. To convert to absolute dose rate per contained activity, a method presented by Price *et al.* (2005) is utilized:

$$\begin{aligned}
\dot{D} \left[\frac{\text{Gy}}{\text{mCi} \cdot \text{hr}} \right] &= x \left[\frac{\text{MeV}}{\text{cm}^3 \cdot \text{particle}} \right] \times 1.602 \cdot 10^{-6} \left[\frac{\text{erg}}{\text{MeV}} \right] \times 3.7 \cdot 10^7 \left[\frac{\text{Bq}}{\text{mCi}} \right] \times \left[\frac{\text{dis.}}{\text{Bq} \cdot \text{sec}} \right] \times \dots \\
&2.324 \left[\frac{\text{particle}}{\text{dis.}} \right] \times 3600 \left[\frac{\text{sec}}{\text{hr}} \right] \times 1.13 \left\{ \frac{\text{contained}}{\text{apparent}} \right\} \times 10^{-7} \left[\frac{\text{Joule}}{\text{erg}} \right] \times \dots \\
&\rho^{-1} \left[\frac{\text{cm}^3}{\text{g}} \right] \times 1000 \left[\frac{\text{g}}{\text{kg}} \right] \times \left[\frac{\text{Gy} \cdot \text{kg}}{\text{Joule}} \right]
\end{aligned} \tag{2.1}$$

Defining terms that are not simple conversions, 2.324 particles disintegration⁻¹ is determined from the source spectrum utilized for MC simulations [18]. The conversion factor of 1.13 contained to apparent activity was determined by Price *et al.* 2005. A 1-Ci apparent activity of an encapsulated radioisotope source is defined to be the amount of encapsulated source that gives rise to the same exposure in air as an unencapsulated source of the same isotope of 1-Ci (contained) activity. The definition of 0.243 mCi \equiv 1 $\mu\text{Gy m}^2 \text{h}^{-1}$ defines the relationship of S_k to apparent activity for Ir-192 [1, 19].

To calculate the absolute dose per dwell-position for an ICBT HDR administration, Equation 2.2 was used:

$$D[\text{Gy}] = \dot{D} \left[\frac{\text{Gy}}{\text{mCi} \cdot \text{hr}} \right] \times S_k [\text{U}] \times 0.243 \left[\frac{\text{mCi}}{\text{U}} \right] \times t[\text{min}] \times 60^{-1} \left[\frac{\text{hr}}{\text{min}} \right] \tag{2.2}$$

where $t[\text{min}]$ is the active dwell-time. The conversion factor for air kerma strength to apparent activity for an Iridium-192 source is 0.243 mCi U⁻¹ [1].

2.1.2 Radiochromic Film Model Confirmations

For model confirmation, the mHDR v2 ¹⁹²Ir source was positioned at three dwell-positions within the colpostat and films were exposed in two perpendicular orientations. Radiochromic film (RCF) was utilized for this work due to its high spatial resolution, minimal energy dependence, insensitivity to ambient light, its ability to be immersed in water and near

tissue equivalence [22]. RCF consists of a thin (7 - 23 μm), radiosensitive layer of monomer crystals, dispersed in gelatin, bonded to a Mylar base [1]. When high-energy radiation interacts with the active layer, the monomer is polymerized, increasing the saturation of the dye's color in proportion to the amount of radiation absorbed. Gafchromic dosimetry media type MD-55-2 (International Specialty Products Technologies, Wayne, NJ) radiochromic film (Lot # R0419MDV2) was used for MC model confirmation of the CT-MR ovoid applicator set in a liquid water phantom. Since dose distributions in water were required for this MC model confirmation, the ability to submerge the film in water and to handle film in room light greatly simplifies the setup process. According to the vendor, RCF is suitable for dose measurements within the range of 3 to 100 Gy. The American Association of Physicists in Medicine (AAPM) has published detailed characteristics of this type of film and their suggested film handling recommendations were followed [22].

2.1.2.1 Film Calibration

A single calibration curve was used to calibrate films from the same manufacturing lot. Calibration curves were determined using 13 measurements acquired using 2 x 2 cm^2 pieces of film cut from a single sheet. The same corner of each individual pieces of film were marked in order to allow consistent, identical film orientation for film digitization [22]. Films were calibrated by placing the film perpendicular to an *en face* 4 MV beam set to 100 cm source to axis distance (SAD), placing 10 cm of Plastic Water on top of the film with 5 cm below for sufficient backscatter. The pieces of film were then separately irradiated in the center of an open 10 x 10 cm field to: 3, 5, 10, 23, 25, 28, 30, 33, 35, and 38 Gy. One piece of film was not irradiated and used to provide the background / fog color saturation (optical density) level of the film.

As recommended by AAPM Task Group-55, irradiated RCFs were stored for at least 48 hours prior to scanning to allow for film development under ambient conditions (temperature $\approx 23^\circ\text{C}$, relative humidity $\approx 30\%$) with nominal exposure to fluorescent room lights. Irradiated films were digitized using an Epson Perfection V700 Photo flatbed scanner (Seiko Epson Corporation, Nagano, Japan). The 16-bit red channel image was exported for film analysis as the absorption peak of RCF film lies at $\approx 773\text{ nm}$, which corresponds to the scanner's red channel. A scanning resolution of 96 dpi ($\approx 0.3\text{ mm pixel}^{-1}$) was used for film digitization.

After digitization of the calibration films, Image J (Image J, Bethesda, Maryland) software was utilized to measure the average scanner value for a 1 cm^2 region in the center of each film piece to correlate the scanner value to known dose values. Image J freeware is a public domain image processing program that can be used for image analysis [23]. After plotting the scanner values vs. absorbed dose, a second order polynomial was fit to the resulting curve to convert film scanner values to absorbed dose as shown in Figure 2.2.

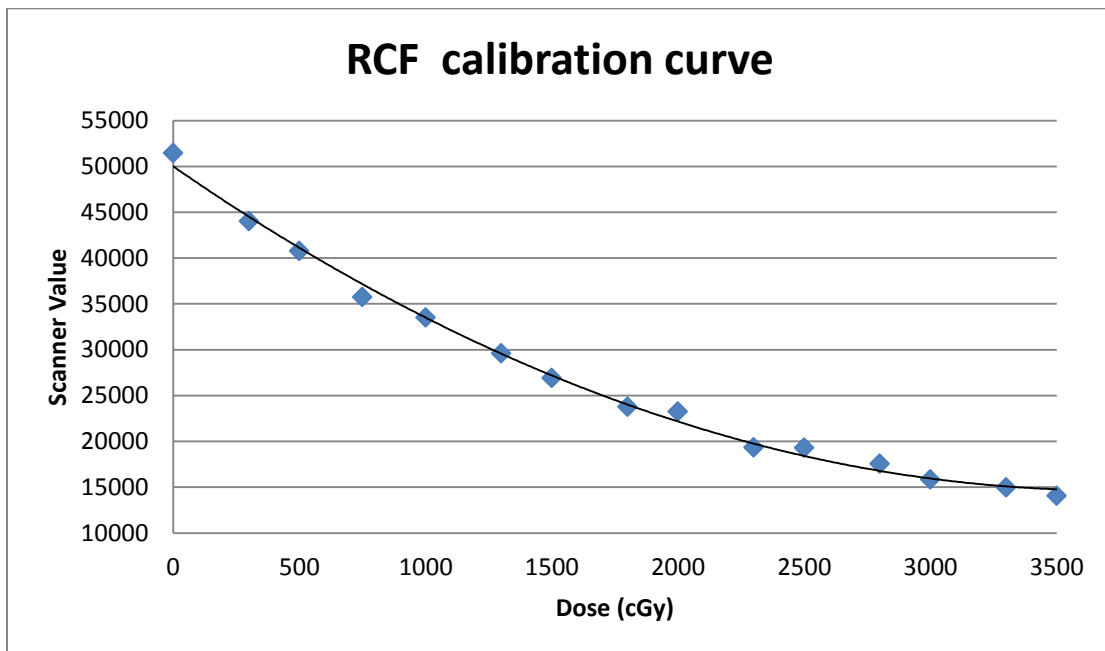


Figure 2.2: RCF measured calibration points used to convert RCF readings to dose.

2.1.2.2 Treatment Planning for Model Confirmation Film Irradiations

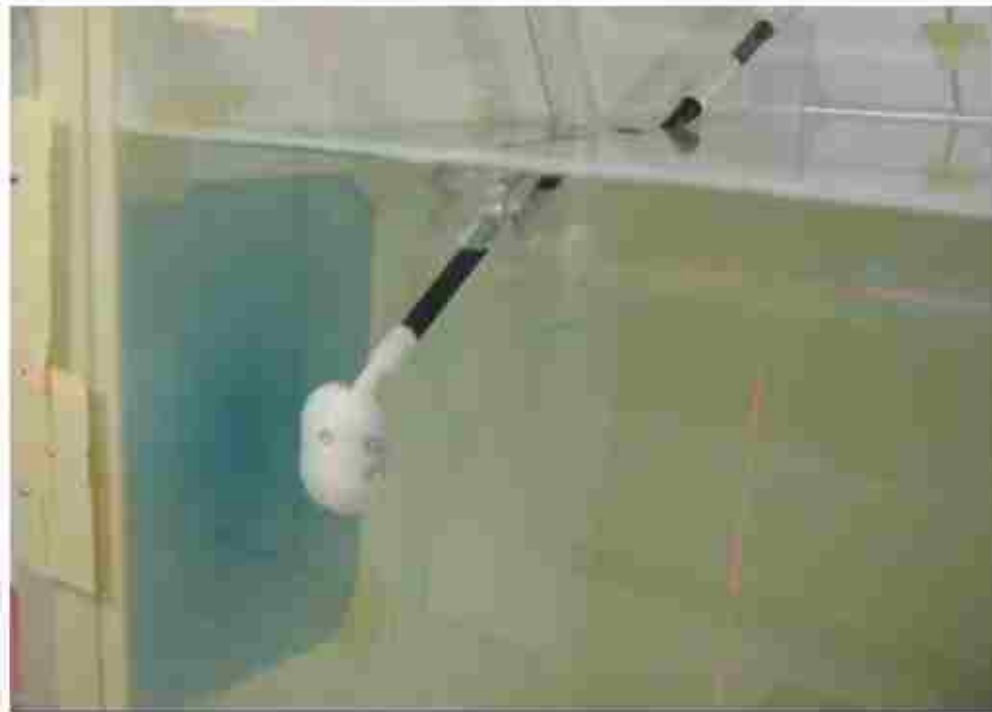
The Nucletron Corporation Oncentra brachytherapy treatment planning system (Veenendaal, The Netherlands) was used to determine the dwell-time required to deliver a 10 Gy to a point 1.7 cm away and perpendicular to the long-axis of a source positioned 5mm proximal and distal to, two adjacent dwell-positions (three dwell-positions total) (*c.f.* Figure 2.3). An additional plan was constructed that determined dwell-times for three sources in an equivalent orientation that delivered 10 Gy to a point that lay 3.3 cm away and parallel to the long-axis of the middle dwell-position (*c.f.* Figures 2.3). These points were selected to act as surrogates for the rectal and disease plane, respectively. With air kerma strength of $32701 \mu\text{Gy m}^2 \text{h}^{-1}$, the resulting treatment plan for both planes called for indexer lengths of 1500 mm, 1495 mm, and 1490 mm with a total dwell-time evenly distributed for all dwell-positions of 10.9 min and 18.3 min for the rectal plane and disease plane, respectively. A radiograph was inspected to confirm source position / indexer length correspondence of the ovoid applicator set to the MC modeling of the source position within the ovoid.

2.1.2.3 Phantom Film Measurement Setup

In-room patient setup lasers were used to align the colpostat shaft perpendicularly to the rectum surrogate film plane (*c.f.* Figure 2.3a) or parallel to the disease surrogate film plane (*c.f.* Figure 2.3b). Films were placed atop slabs of Solid Water submerged within the water phantom. Room lasers were also used to carefully orient each film in a reproducible fashion. Once properly aligned, the ovoid was attached to the mHDR afterloader (Nucletron, Veenendaal, The Netherlands) and plans were delivered. Each plan was delivered three times to for a total of 6 measurements.



(a)



(b)

Figure 2.3: Monte Carlo model film confirmation phantom. (a) The GafChromic film is shown in the “rectum plane” orientation. (b) The GafChromic film is shown in the “medial plane” orientation. The ovoid, water tank, and film were aligned using vault lasers.

2.1.2.4 Film Data Processing and Analysis

The average of three measurements was acquired for each plane measured for the MC model confirmation. The standard deviation, σ , between three measurements was calculated to compare pixel to pixel for each film.

MC confirmation RCF measurements were processed following the same methods utilized for RCF calibration. All films were scanned in equivalent orientations and locations on the flatbed scanning window. In-house software was developed using Matlab v7.8 (2007a, The MathWorks, Natick, MA) for all data processing. The software was written to facilitate importation and processing of the digitized TIFF images as well as the conversion of raw image data (scanner values) to absorbed dose [Gy]. To reduce inherent image noise, an adaptive 2-D Wiener filter was applied to all scanned film data. To perform an analysis, the algorithm first down-sampled the red channel of the TIFF image so as to spatially match the MC dose array and then registered the RCF film data to the MC simulated dose. Software written in Matlab allowed incremental 1 mm shifts to the film data in the up, down, left, and right directions in order to spatially match the MC simulated dose. Table 2.2 lists the uncertainty components associated with MC model confirmation film measurements. An expanded uncertainty of 11% is the total uncertainty in measurements.

Film measured dose distributions were compared to MC simulations to evaluate the dosimetric accuracy of the MC model. The comparison consisted of determining the number of points within an arbitrary percent agreement as well as distance-to-agreement (DTA). The algorithm selected a corresponding point from both data sets and determined whether or not the percent difference passed the dose criteria (*e.g.* 2%) using:

$$\% \text{Difference} = \frac{|Film(i, j) - MC(i, j)|}{MC(i, j)} \cdot 100\%, \quad (2.3)$$

where i and j are indexes used to define pixel location (row and column). If this point is within the dose criterion, the algorithm continues to the next point in the data set. If the point is not within criteria, the algorithm searches for a point within the distance criteria (e.g. 2 mm) for a value that meets the dose criteria. This is repeated for all corresponding points in the MC and image data set. An overview of this process is shown in Figure 2.4.

Table 2.2: Estimated relative uncertainties of the radiochromic film dose interpretations per measured unit reference air kerma rate.

Uncertainty component	Relative one standard uncertainty (%)
Calibration of the 4MV LINAC	3.0
Response of the film exposed to the LINAC	3.0
Response of the films exposed to the source under test	3.0
S_k calibration for source under test	1.67 ^a
Combined standard uncertainty	5.5
Expanded uncertainty (k=2)	11

^aNucletron Certificate for Sealed Sources.

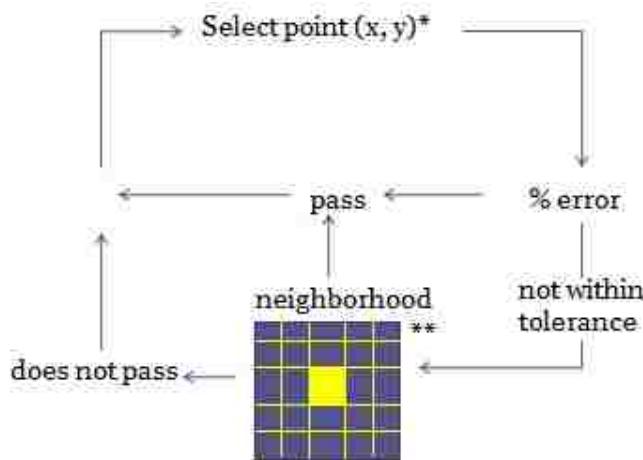


Figure 2.4: Illustration of comparison algorithm. *Values below 3 Gy (as recommended by TG-55) are not included in the comparison. **If one point passes the tolerance and distance condition, then point (x, y) passes.

2.2 Aim 2: Development of 3D Attenuation Correction Factor Database

Two MC models will be used to simulate 3D dose distributions in water for clinically relevant mHDR Ir-192 dwell-positions. The two MC models will model (1) the commercially-available CT-MR compatible Fletcher ovoid confirmed in Aim 1 and (2) a modified version of

that includes a high-Z heterogeneity acting as a rectal shield surrogate. A two-dimensional graphical representation of the study’s modified MC model is shown in Figure 2.5. Because the CT/MR compatible Fletcher ovoids are not available in a shielded model, this modification was included in this study as a proof of principle for this correction scheme. Clinical shielded ovoid applicators contain 1.7 mm tungsten “half discs” compared to the rounded distal end being comprised of metal. Dose perturbations are expected to be significant with the modified shield as opposed with an actual clinically available shield.

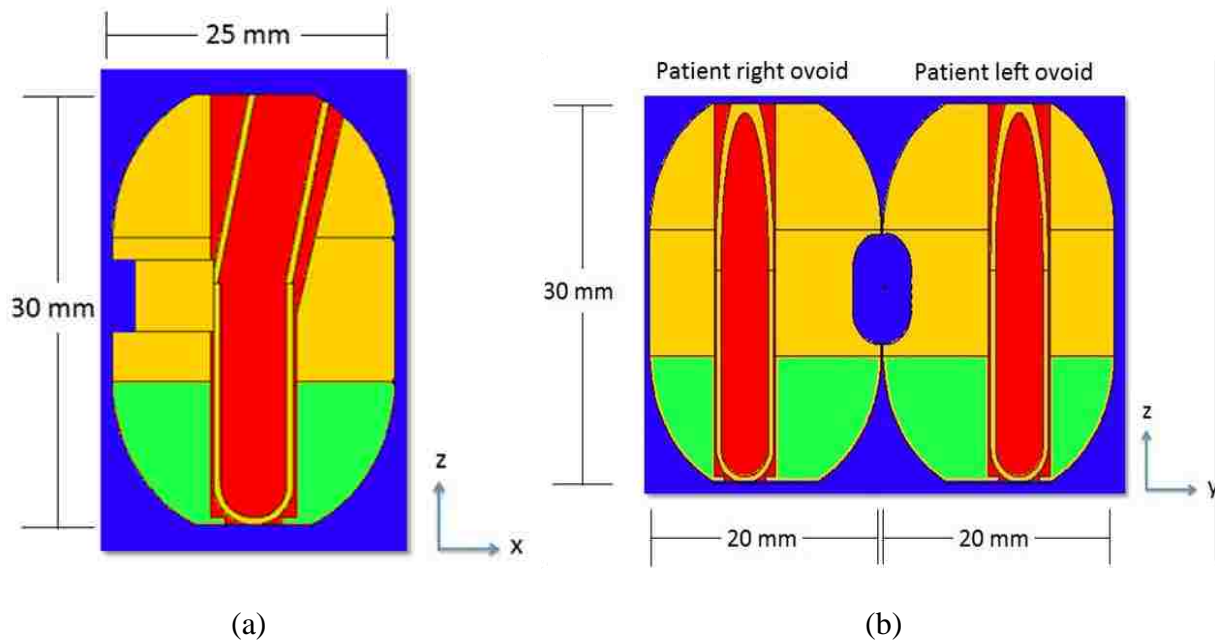


Figure 2.5: Two-dimensional plots of the modified CT-MR Fletcher ovoid applicator set using the MCNPX graphical plotter through a.) the ZX-plane bisecting the ovoid shaft, and b.) the ZY-plane bisecting the ovoid shafts in the left/ right ovoids. Colors show different materials where blue, yellow, green, and red are water, polysulfone, tungsten, and air, respectively.

To create the MC attenuation-correction dataset libraries, a mesh tally (F6: photons), 10 x 10 x 10 cm³ in size was used to tally energy deposition per particle within 1 mm³ voxels. A total of eight source-dwell indexes: 1500 mm, 1495 mm, 1490 mm, and 1485 mm (measured from the afterloader port) for both right and left ovoids, were simulated. The origin of each mesh tally

was positioned to coincide with the geometric center of the mHDR v2 Ir-192 source. All simulations were run for 260×10^6 histories to achieve a statistical uncertainty of less than 2% at the most distant elements of the tally grid. Due to the computing time required for simulations of this magnitude, a parallel-processing capable, super-computing cluster was used for these simulations. The Tezpur super-computing cluster (Louisiana State University High Performance Computing Department) is a 360 node cluster able to perform 15.3×10^{12} floating point operations per second. Since MC simulates and tracks every particle history independently, the histories can be grouped into several batches and executed in parallel. A single 260 million history simulation ($101 \times 101 \times 101$, 1 mm^3 tally voxels) ran parallel on 100 processors required approximately 10 hours. To test the hypothesis, the following two methods were employed to calculate the attenuation-correction matrices.

2.2.1 Method 1: Ovoid-Based Correction Factor, c_o

The ovoid-based correction factors, c_o , were calculated using:

$$c_o = \frac{d_o^{MC}(x, y, z)}{d_o^{TG43}(x, y, z)}, \quad (2.4)$$

where $d_o^{MC}(x, y, z)$ is dose rate per activity [$\text{Gy mCi}^{-1} \text{ hr}^{-1}$] to a voxel centered at (x, y, z) in the experimental coordinate system converted from MC-calculated energy deposition per particle using equation 2.1 and $d_o^{TG43}(x, y, z)$ is the dose rate per activity [$\text{Gy mCi}^{-1} \text{ hr}^{-1}$] to a voxel of an equivalent position, in the same coordinate system, as calculated by the TPS using AAPM Task Group 43 methodology [6]. The index, O , is equal to either 1 or 2, indicating the handedness of the ovoid, patient right or left, respectively. Both d_o^{MC} and d_o^{TG43} consist of the superposition individual dose distributions of multiple dwells in each colpostat and the origin of these matrices is defined to coincide with the most distal source-dwell-position (active) within the corresponding ovoid:

$$d_{O=1}^{MC}(x, y, z) = \sum_{s=1}^4 d_s^{MC}(x', y', z')$$

and

(2.5)

$$d_{O=2}^{MC}(x, y, z) = \sum_{s=5}^8 d_s^{MC}(x', y', z')$$

where $d_s^{MC}(x', y', z')$ is dose rate per activity to a voxel centered at (x', y', z') in the Monte Carlo coordinate system converted from MC-calculated energy deposition per particle using equation 2.1 for a single dwell-position. The index, s , corresponds to the dwell-position of the source within the ovoid (*i.e.* $s = 1$ (1500 mm), $s = 2$ (1495 mm), etc.). Dwells $1 < s < 4$ and $5 < s < 8$ are contained within the patient right and left ovoids, respectively. Provisions are made for clinical applications that utilize both three (dwell-positions: $s = 2$ (1495 mm), $s = 3$ (1490 mm), and $s = 4$ (1485 mm)) and four (dwell-positions: $s = 1$ (1500 mm), $s = 2$ (1495 mm), $s = 3$ (1490 mm), and $s = 4$ (1485 mm)) inter-colpostatic dwells as both are common practice (*i.e.* 3 vs. 4 distributions superimposed when calculating d_O^{MC}). $d_O^{TG43}(x, y, z)$, is the superposition of four dose distributions for a single ovoid. This superposition is performed within the Oncentra TPS and the origin of this distribution is defined to be in the geometrical center of the right or left ovoid as a function of O within the experimental coordinate system. For the calculation of both d_O^{MC} and d_O^{TG43} , source dwells were assumed to be coplanar, centered within the ovoid shaft, with the geometric center of each source located at its corresponding dwell-position index (*e.g.* 1500 mm).

2.2.2 Method 2: Source-Based Correction Factor, c_s

The source-based correction factors, c_s , were calculated using (Equation)

$$c_s = \frac{d_s^{MC}(x, y, z)}{d_s^{TG43}(x, y, z)},$$
(2.6)

where $d_s^{MC}(x, y, z)$ is dose rate per activity [$\text{Gy mCi}^{-1} \text{ hr}^{-1}$] to a voxel centered at (x, y, z) in the experimental coordinate system converted from MC-calculated energy deposition per particle

using equation 2.1 for a single dwell-position and $d_s^{TG43}(x, y, z)$ is the dose rate per activity [Gy mCi⁻¹ hr⁻¹] to a voxel of an equivalent position, in the same coordinate system, as calculated by the TPS using AAPM Task Group 43 methodology for a single dwell-position [6]. The index, s , is equal to values of 1 to 8, indicating the source position within of the ovoid (dwells $1 < s < 4$ and $5 < s < 8$ are contained within the patient right and left ovoids, respectively). Each d_s^{MC} dose distribution's origin is defined to coincide with the origin of the corresponding d_s^{TG43} .

2.2.3 Analysis Software Development

In-house software was developed using Matlab v7.8 (2007a, The MathWorks, Natick, MA) for all data processing. The software was written to facilitate importation, processing, and analyzing the dose data sets generated by the TPS, MC, and correction procedure (utilizing equations 2.3-2.6). The data sets were analyzed using a 3D distance-to-agreement algorithm, which is illustrated in Figure 2.5. The algorithm selects a corresponding point from two data sets and determines whether the percent error passes within the dose criteria (*i.e.* 2% tolerance). If this point is within the dose criterion, the algorithm continues to the next point in the data set. If the point is not within criteria, the algorithm searches for a point within the distance criterion (*i.e.* 2 mm) for a value which passes within the dose criteria (*i.e.* 2% tolerance). This is repeated for all points in the two data sets.

2.3 Aim 3: Application of 3D Correction Strategy to Patient Cases

2.3.1 DICOM

Digital Imaging and Communications in Medicine (DICOM) network protocol is a standard that is a framework for handling, storing, printing, and transmitting medical-imaging data [1]. The standard was developed in 1983 by the American College of Radiology (ACR) and the National Electrical Manufacturers Association (NEMA) with input from various vendors, academia, and industry groups. DICOM was developed as response to the need of a standard

method for transferring images and related information between devices from different companies. DICOM provides standardized formats for images, a common information model, application service definitions, and protocols for communication. DICOM is useful in storing and organizing radiotherapy plans because it groups information into data sets. For example, a DICOM file stores image data (*i.e.* CT image) and patient information (*i.e.* name, patient number, image type) within one file, so that the image can never be separated from the

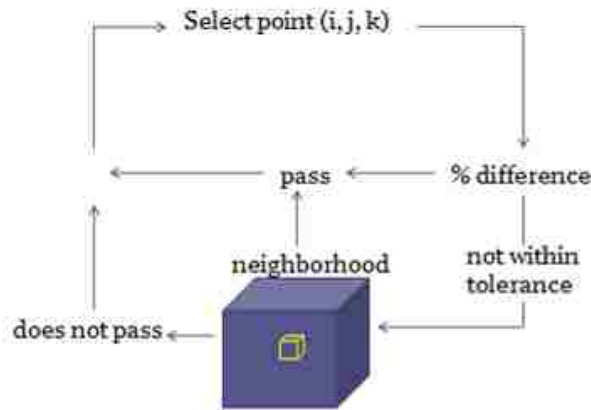


Figure 2.6: Illustration of 3D dose tolerance and distance-to-agreement algorithm. A point must pass the dose tolerance criteria or have another point within the distance criteria which is within the dose tolerance, in order for (x, y) to pass.

information by mistake. Oncentra uses the DICOM 3.0 standard for storage of the image data.

Oncentra exports three DICOM compliant files: (1) the DICOM Radiotherapy Plan (RP) file, (2) the DICOM Radiotherapy Dose (RD) file, and (3) the DICOM Radiotherapy Structures (RS).

2.3.2 Application of Correction Factors to TPS-Calculated Plans

2.3.2.1 Attenuation-Correction Factor Calculation for Method 1

The TPS corrected dose [Gy] to a point located at (X, Y, Z) in the patient coordinate system was calculated using:

$$D_{c_o}^{TPS}(X, Y, Z) = \sum_{O=1}^2 d_o^{TPS}(X, Y, Z) \cdot c_o(x, y, z), \quad (2.7)$$

where d_o^{TPS} is the superimposed ovoid-source surrogate dose distribution of either the left or right ovoid (O=1 represents left ovoid and O=2 represents right ovoid) generated using Oncentra TPS. The coordinate system of the ovoid-correction matrix, c_o , was translated using MATLAB to register and coincide with the TPS coordinate system (*i.e.* X, Y, Z) before it was applied. Two correction matrices were applied to correct the exported TPS plan.

2.3.2.2 Attenuation-Correction Factor Calculation for Method 2

The TPS corrected dose [Gy] to a point located at (X, Y, Z) in the patient coordinate system was calculated using:

$$D_{c_s}^{TPS}(X, Y, Z) = \sum_{S=1}^8 d_S^{TPS}(X, Y, Z) \cdot c_S(x, y, z), \quad (2.8)$$

where d_s^{TPS} is the source dose distribution of dwell index S (S=1-4 represents indexes within left ovoid and S=5-8 represents indexes within right ovoid) generated using Oncentra TPS. The coordinate system of the source-correction matrix, c_s , was translated using MATLAB to register and coincide with the TPS coordinate system (*i.e.* X, Y, Z) before it was applied. Eight correction matrices were applied to correct the exported TPS plan.

2.3.3 Case Selection

Three-dimensional planning for brachytherapy treatments requires modeling the patient anatomy utilizing a set of 2D images that represent a patient's anatomy in 3D, localizing the dwell-positions in 3D, calculating appropriate dwell-times, and finally simulating the dose distribution for the specified geometry. Treatment planning refers to the quantitative parts of the process by which the individualized patient treatment plan is determined.

Dwell-positions in a co-planar geometry were exported using Oncentra TPS, and several dwell-time combinations were investigated to test the hypothesis. This geometry was chosen

because (1) the same geometry for dwell-position coordinates could be specified in the MC coordinate system and (2) the voxel size was set to be equivalent to the MC models.

2.3.3.1 Maximum Adjacent Dwell-Time Gradient

Dwell-positions can be described according to their dwell-time as a relative difference **known as** the dwell-time weighting factor, w_n . The w_n was calculated by using:

$$w_n = \frac{t_n}{T_{total}}, \quad (2.9)$$

where t_n is the dwell-time at index “n” and T_{total} is the total dwell-time. The w_n ranges from zero to one (i.e. [0, 1]). A value of zero means that the dwell-time for that dwell-position is zero.

The adjacent dwell-time gradient, ∇_{dt} , was calculated for every dwell-position by using:

$$\nabla_{dt} = \left| w_n - w_{n+1} \right|_{n=1}^8 \quad (2.10)$$

This equation determines the difference between adjacent w_n . Calculations with a w_n of zero are ignored if that dwell index represents the distal or proximal end of the catheter.

Each comparison case was described by its maximum ∇_{dt} . Several ∇_{dt} (i.e. 0, 0.3, 0.6, 0.7) were used to analyze the effectiveness of both attenuation-correction factor methods. For every case, a comparison of the TG-43 calculation to the MC simulation was made utilizing the 3D DTA algorithm for both ovoid- and source- based attenuation correction factors.

2.3.4 Analysis

Several dwell-time weighting differences were used to test the hypothesis. Each plan was compared to its corresponding superimposed MC dose distribution to quantify the differences due to the presence of the applicator ovoids. Also, the dose distribution resulting from both MC models were compared to both corrected TPS plans (ovoid-based and source-based).

Comparisons were made by determining the percentage of points which agree within 2% or 2mm DTA.

Chapter 3 Results and Discussion

3.1 Aim 1: MC Modeling of a Nucletron ICBT CT-MR Fletcher Ovoid Applicator

3.1.1 Model Confirmation via Radiochromic Film

A comparison of radiochromic film (RCF) measurements and Monte Carlo (MC) simulated absolute dose in water for two perpendicular planes in water are shown in Figures 3.1 – 3.2. Three independent RCF measurements were averaged, for both the “rectum” surrogate and “disease” surrogate planes, and then spatially registered to the corresponding MC data set for comparison. To register these data sets, software written in Matlab which shifted the dataset by 1 mm in the up, down, left, and right direction. Since the water phantom setup did not allow for the RCF to be marked with respect to ovoid placement, registration was done visually in order to best match up the isodose lines. Regions containing dose values less than 3Gy were not included in RCF/MC comparisons per AAPM Task Group Report 55.

Qualitatively, one observes fair agreement of equivalent isodoses for compared data. Quantitatively, MCNPX tallied dose agreed to within $\pm 2\%$ or $\pm 2\text{mm}$ for 96% of the points on the film acting as the “disease” surrogate and to within $\pm 2\%$ or $\pm 2\text{mm}$ for 96% of the points on the film acting as the “rectum” surrogate. The average standard deviation of the three “disease” surrogate and “rectum” surrogate RCF measurement datasets are 11 ± 7.4 cGy and 9 ± 7.0 cGy, respectively. The “rectum” surrogate film had regional discrepancies at the high-dose gradient region near the center. This is possibly the result of the inverse square factor having a strong influence in regions close to the source. The center point of the film was the closest distance between the film plane and source. For MC, points farther from the center point of the mesh (*i.e.* simulated film) plane result in a larger distance to the source reduces statistical uncertainty. The “disease” surrogate film was 3.3 cm away from the source, in contrast to the 1.7 cm distance for the “rectum” plane, which results in less inverse-square influence. These

results indicate that the models of the mHDR v2 Ir-192 source and paired ovoid component of Nucletron's CT-MR compatible applicator MC model are robust enough to simulate dose distributions with sufficient accuracy within the context of this study.

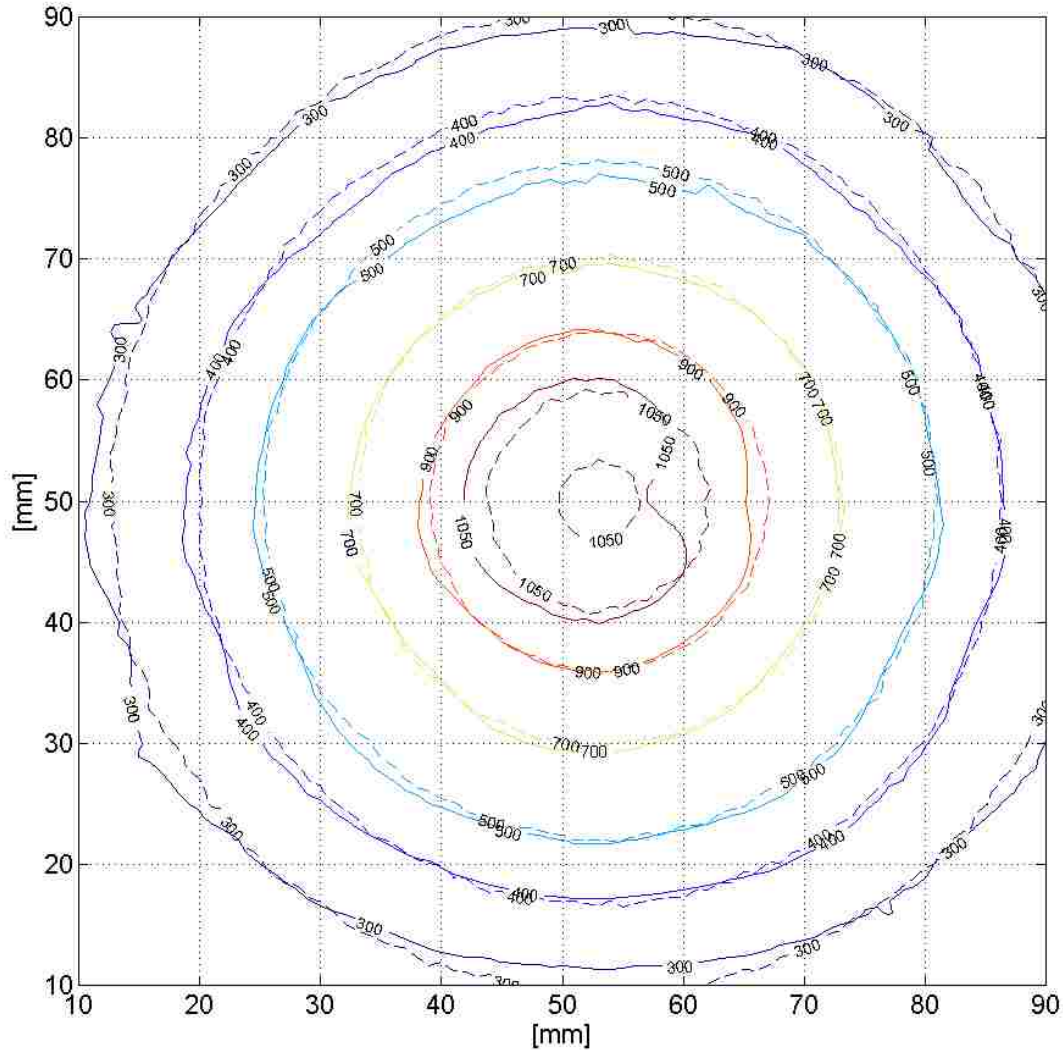


Figure 3.1: Anterior rectal wall MC/RCF isodose contour comparison. Comparison of MC (dashed) simulated and RCF (solid) measured dose, in cGy, for a plane located 1.7 cm distal to the distal surface of a single ovoid. This plane serves as a surrogate to the anterior rectal wall of a patient. The simulation and measurements are for three (3) dwell-positions indexed 1500, 1495, and 1490 mm from the afterloader exit port for dwell-times of 1.2 minutes per source for an activity of 8.32 Ci. Quantitatively, 96% of the comparison points are within +/- 2% or +/- 2mm.

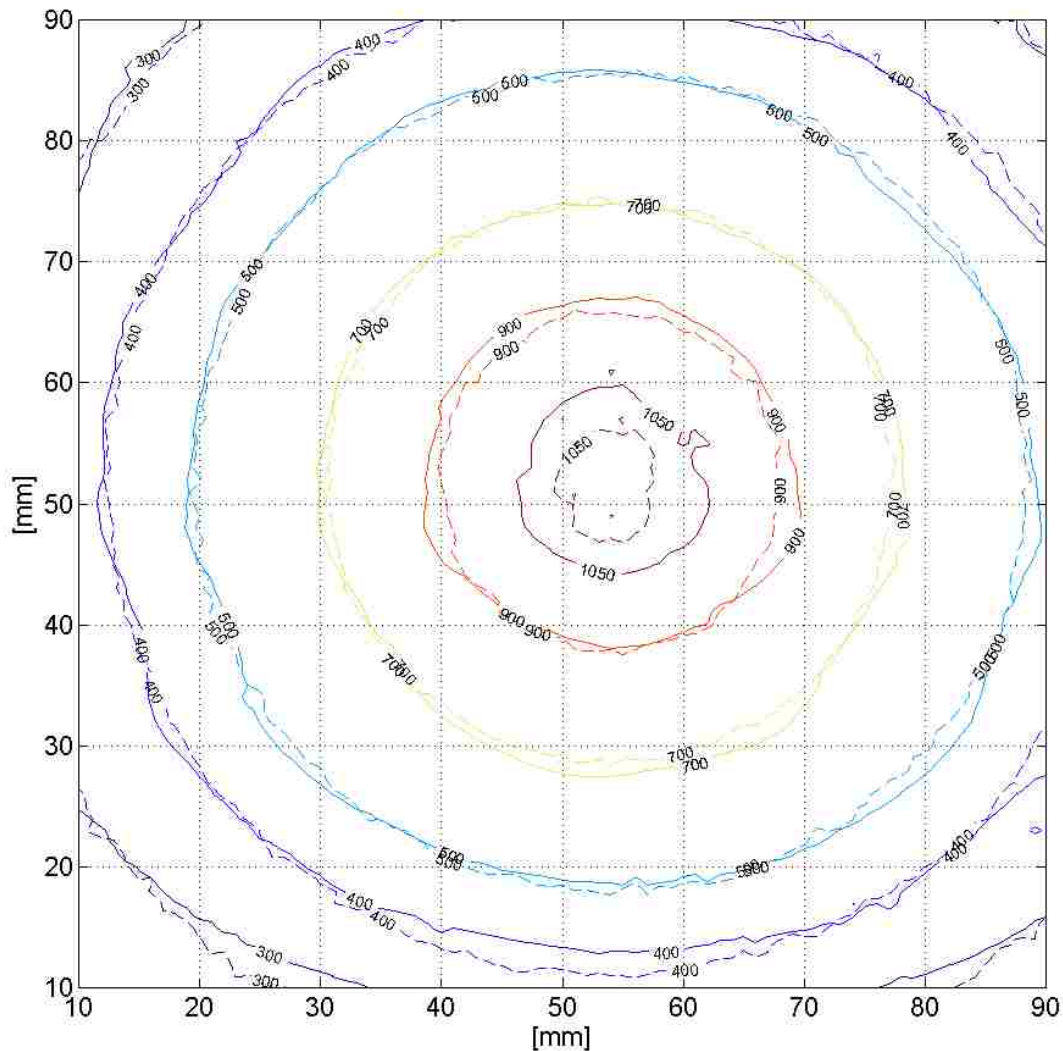


Figure 3.2: Lateral disease wall MC/RCF isodose contour comparison. Comparison of MC (dashed) simulated and RCF (solid) measured dose, in cGy, for a plane located 3.3 cm lateral to the long-axis of a single ovoid. This plane serves as a surrogate to the disease wall, lateral to the cervix, of a patient. The simulation and measurements are for three (3) dwell-positions indexed 1500, 1495, and 1490 mm from the afterloader exit port for dwell-times of 6.1 minutes per dwell for an activity of 8.32 Ci. Quantitatively, 96% of the comparison points are within +/- 2% or +/- 2mm.

3.2 Aim 2: Development of Ovoid and Source-Based Correction Factors

3.2.1 Nucletron MicroSelectron High-Dose Rate Ir-192 Source

Comparisons of MC-simulated isodose distribution and isodoses calculated using TG-43 methodology for a single mHDR v2 Ir-192 source in water with a source activity of 10 Ci and dwell-time of 100 seconds is shown in Figure 3.3. Observed in this figure are the qualitative differences in dose due to the different calculation methods and overlay of an Ir-192 source (not

to scale). Quantitatively, 99.6% of the comparison points are within +/- 2% or +/- 2mm between MC and TG-43 for a single source in water. The slight differences can be contributed to the high-dose, high-dose gradient region near the source. In the lateral direction (i.e. parallel to y axis), the isodose lines agree very well. The dose distribution along the longitudinal axis (i.e. parallel to z axis) of the Ir-192 source is intrinsically anisotropic due to self-attenuation throughout the high-density cylindrical Ir-192 core, asymmetric steel jacket construction, and steel cable attached to one end of the source. With respect to the orientation of the mHDR v2 Ir-192 source along its longitudinal axis, the forward direction for this comparison is $-z$ direction and the backward direction (along the braided steel cable) is $+z$ direction. The MC simulation predicts equivalent dose when compared to the dose distribution calculated using TG-43 calculations in the forward direction. Dose differences in the backward direction (*i.e.* with respect to the longitudinal axis) can be a result of (1) the mathematical modeling error associated with TG-43 methodology, (2) the MC photon transport code overestimating the anisotropy factor, or (3) attenuation due to the 5 mm braided steel cable attached to the source. Reviewing TG-43 source anisotropy factors utilized in the TPS, as expected, the dose distribution in the backward direction is relatively less than in the forward direction. Thus, AAPM TG-43 methodology accounts for an asymmetric anisotropy factor due to the asymmetric source construction.

3.2.2 Nucletron CT-MR Compatible Applicator

Comparisons of MC-simulated isodose distribution and isodoses calculated using TG-43 methodology for a single mHDR v2 Ir-192 source at multiple dwell indexes (*e.g.* dwell indexes 1500 mm, 1495 mm, 1490 mm, and 1485 mm) within a Nucletron CT-MR compatible applicator in water (source activity of 8 Ci and dwell-time of 200 seconds) are shown in Figures 3.4

through 3.5. Shown in Figure 3.6 illustrates the superimposed dose distributions which are used to create the ovoid- based correction matrix. Observed in these figures are the qualitative

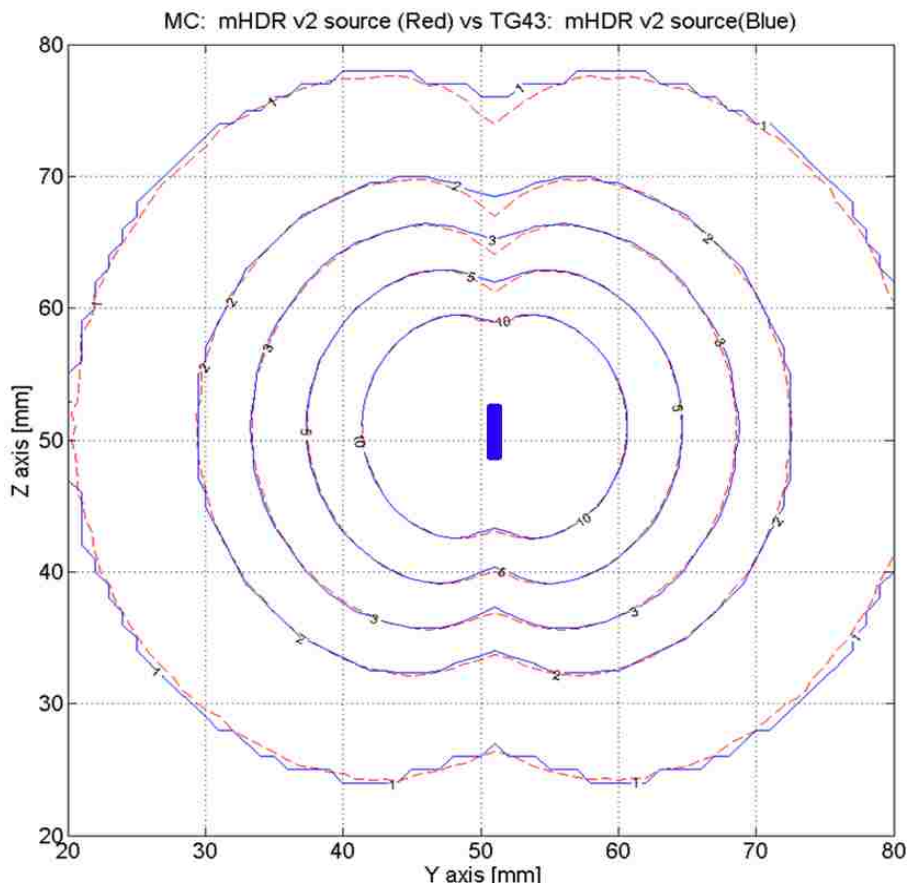
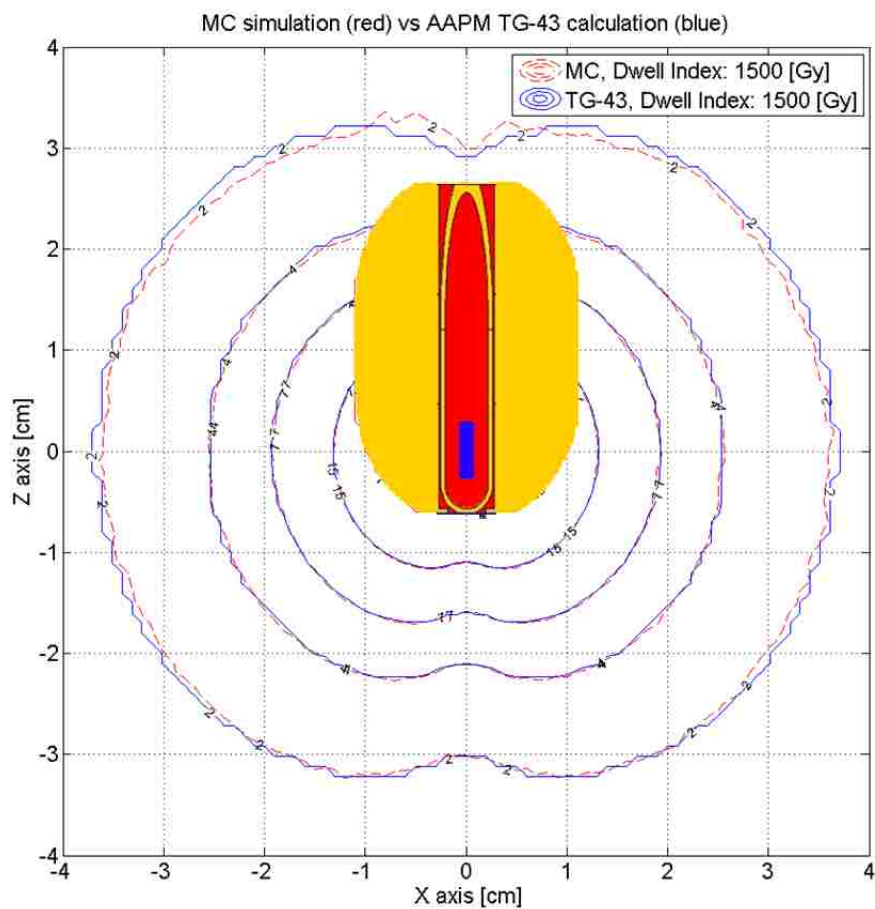
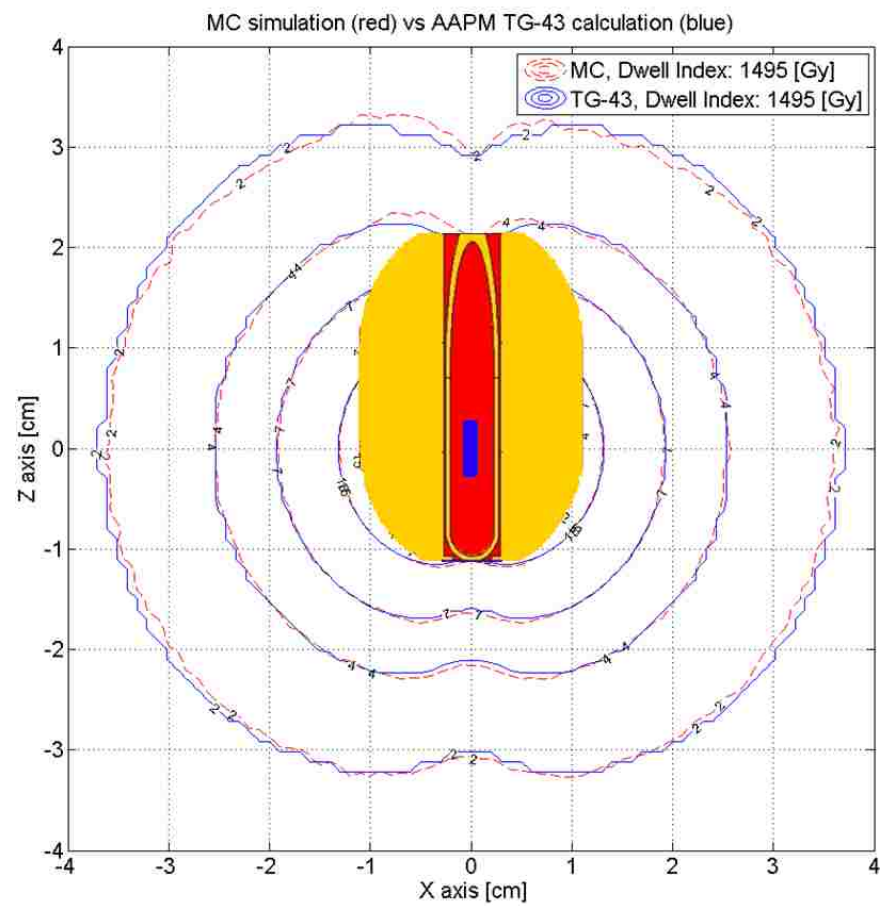


Figure 3.3: Comparison of MC (red dashed) and TG-43 (solid blue) dose distribution, in Gy, resulting from a single source in water with equivalent source activities and dwell-time. Quantitatively, 99.6% of the comparison points are within +/- 2% or +/- 2mm. The source is drawn to show perspective and is not drawn to scale.

differences in dose due to the perturbing effects of the ovoid accounted for in MC simulations (dashed red lines) and unaccounted for in TG-43 calculations (solid blue line) for a single 2D plane at each dwell index. Differences along the longitudinal axis of the source can be contributed to the air that is present within the ovoid shaft. Quantitatively, >99% of the comparison points are within +/- 2% or +/- 2mm for all comparisons. There are no appreciable differences between the MC simulations of each dwell index with an TG-43 calculation. The dose distribution is not significantly affected due to the presence of the CT-MR compatible applicator.

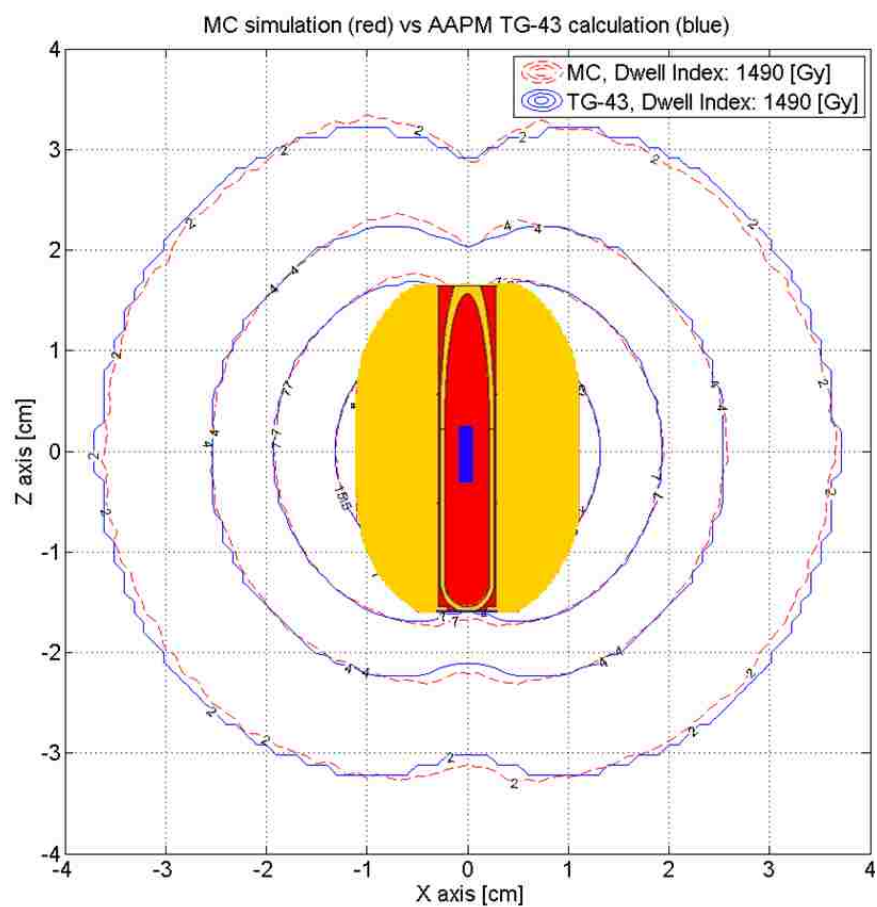


(a)

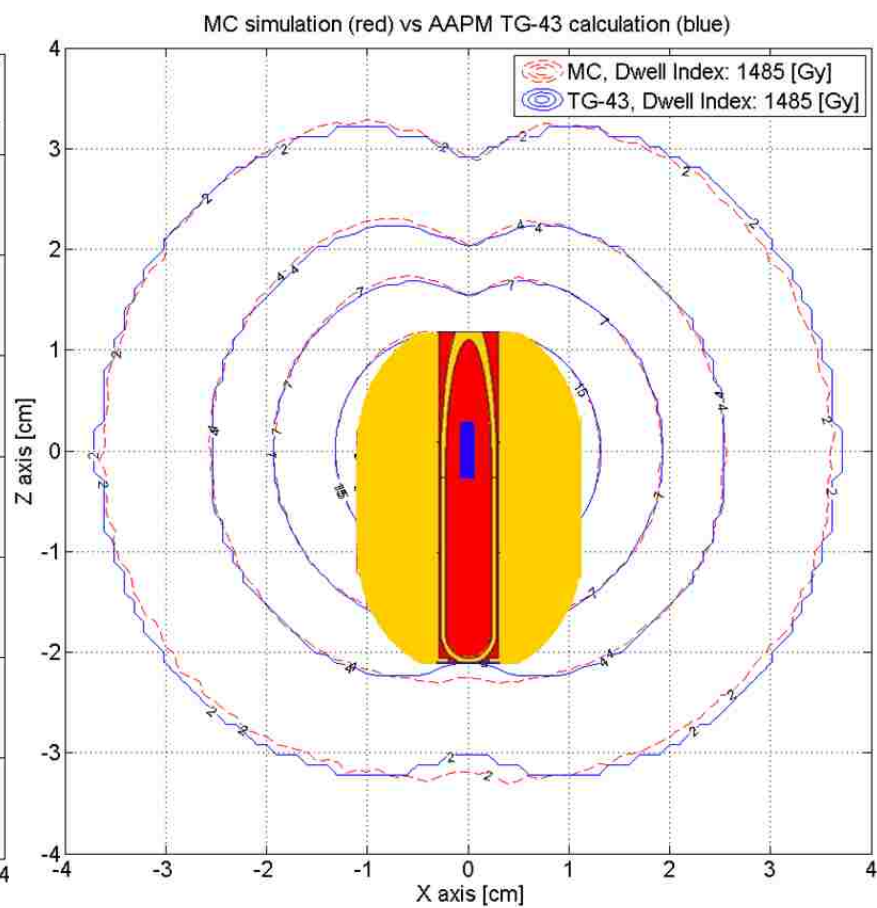


(b)

Figure 3.4(a-b): Comparison MC and TG-43 dose distribution for dwell index (a) 1500 mm and (b) 1495 mm, in Gy, within a plane bisecting the right ovoid, resulting from a single source with equivalent source activities and dwell-times. The source (blue cylinder, not to scale) is illustrated within the ovoid to give perspective of placement. These plots illustrate d_S^{MC} and d_S^{TG43} which are used to create the source-based correction matrix. Quantitatively, > 99% of the comparison points are within +/- 2% or +/- 2mm for both contour plots.



(a)



(b)

Figure 3.5(a-b): Comparison MC and TG-43 dose distribution for dwell index (a) 1490 mm and (b) 1485 mm, in Gy, within a plane bisecting the right ovoid, resulting from a single source with equivalent source activities and dwell-times. The source (blue cylinder, not to scale) is illustrated within the ovoid to give perspective of placement. These plots illustrate d_S^{MC} and d_S^{TG43} which are used to create the source-based correction matrix. Quantitatively, > 99% of the comparison points are within +/- 2% or +/- 2mm for both contour plots.

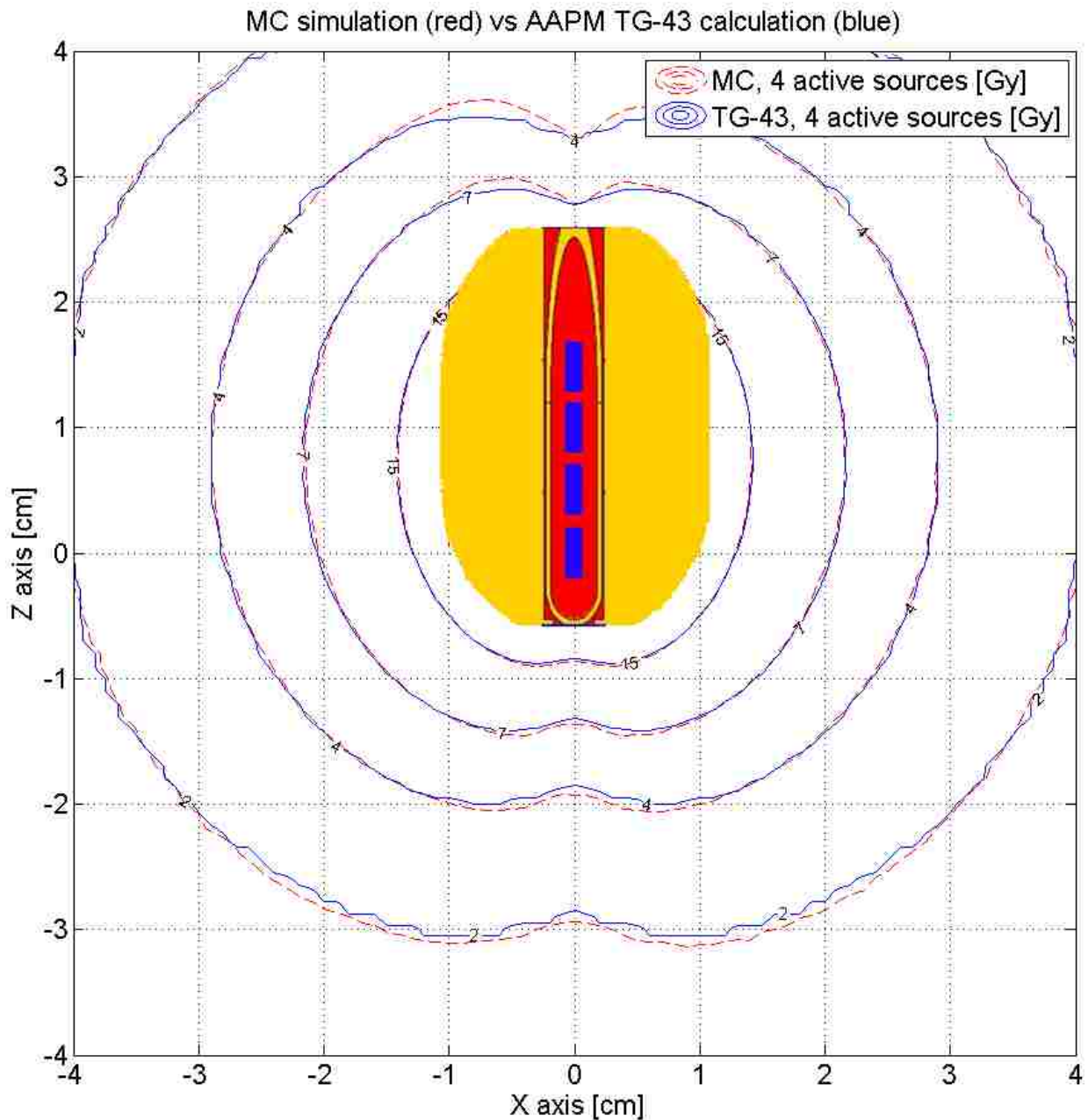


Figure 3.6: Comparison MC and TG-43 dose distribution for superimposed dwell indexes: 1500 mm, 1495 mm, 1490 mm, and 1485 mm, in Gy, within a plane bisecting the right ovoid, resulting from four source dwell-positions with equivalent source activities and dwell-times. The source (blue cylinders, not to scale) dwell-positions are illustrated within the ovoid to give perspective of placements. These plots illustrate d_o^{MC} and d_o^{TG43} which are used to create the ovoid-based correction matrix. Quantitatively, 99% of the comparison points are within +/- 2% or +/- 2mm.

3.2.3 MC Applicator Modified to Include High-Z Inhomogeneities

Differences between dose distributions resulting from the CT-MR compatible Fletcher ovoid applicator in water and TG-43 calculation for a single source in water agreed within the uncertainty of the MC simulation, a modification to include inhomogeneities within the MC model was introduced. This high-Z modification was included in this study to test the robustness of the correction scheme. Comparisons of MC-simulated isodose distribution and isodoses calculated using TG-43 methodology for a single mHDR v2 Ir-192 source at multiple dwell indexes (*e.g.* dwell indexes 1500 mm, 1495 mm, 1490 mm, and 1485 mm) within the MC model modified to include a high-Z inhomogeneities (source activity of 10 Ci and dwell-time of 300 seconds) are shown in Figures 3.7 through 3.8. These figures show the isodose distribution varies depending on which dwell-position is active. Figure 3.9 is the superimposed dose distributions (*i.e.* all active dwell-positions) which are used to create the ovoid- based correction matrix. Observed in these figures are the qualitative differences in dose due to the perturbing effects of the tungsten shield introduced in the MC simulations (dashed red lines) and unaccounted for in TG-43 calculations (solid blue line) for a single 2D plane.

Quantitatively, < 17.1%, 39.9%, 81.8%, and 89.0% of the comparison points are within +/- 2% or +/- 2mm for dwell index 1500 mm, 1495 mm, 1490 mm, and 1485 mm, respectively. The superimposed dose distribution had an agreement of 21.8% of the comparison points agreeing within +/- 2% or +/- 2mm. The dose distribution is significantly affected due to the presence of the tungsten shield. Dose distributions resulting from dwell-positions near the tungsten shield (*i.e.* dwell indexes: 1500 mm, 1495 mm) are affected the most out of the four dwell-positions. This is due to the Ir-192 source being contained within the high-Z metal. Primary photons, thus scatter radiation, in the path of tungsten are significantly reduced because of the high-Z attenuation.

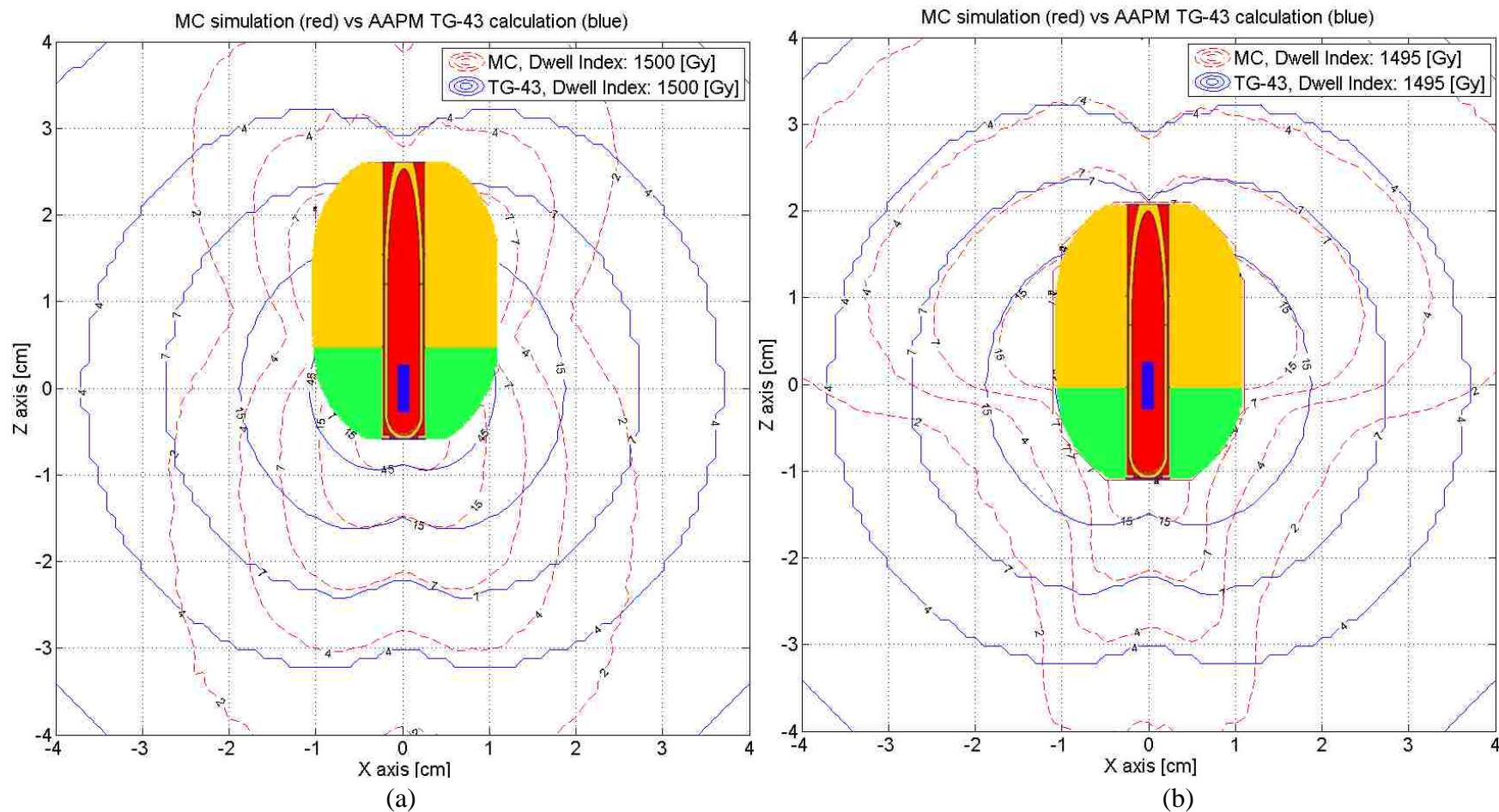
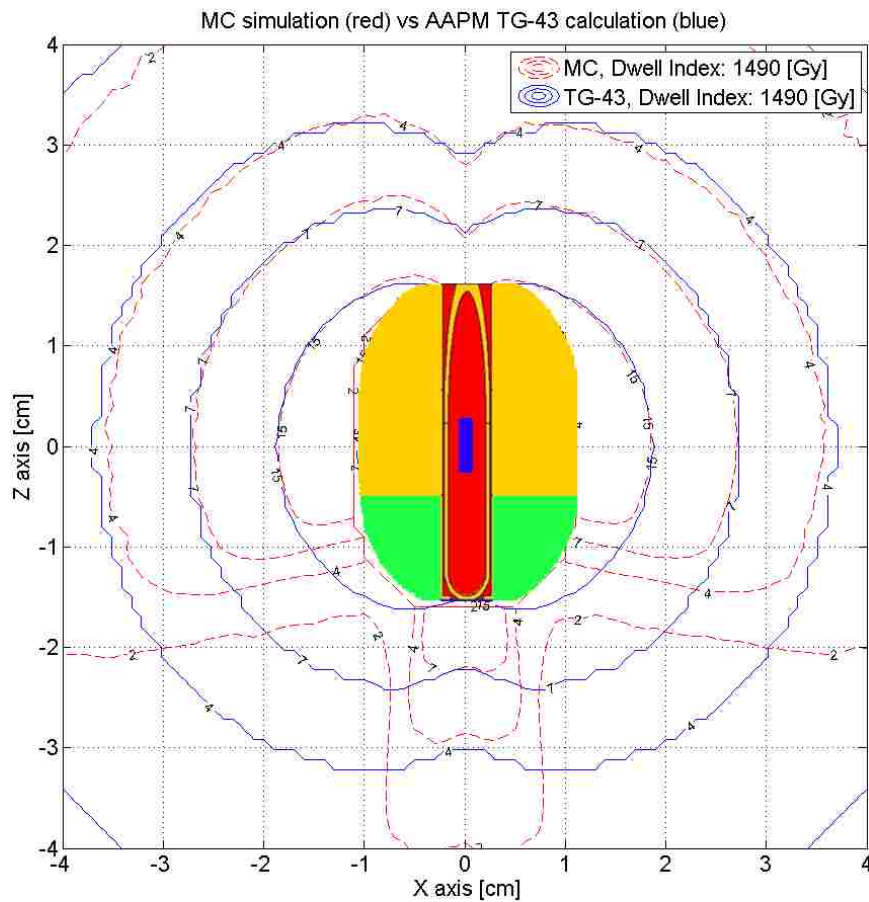
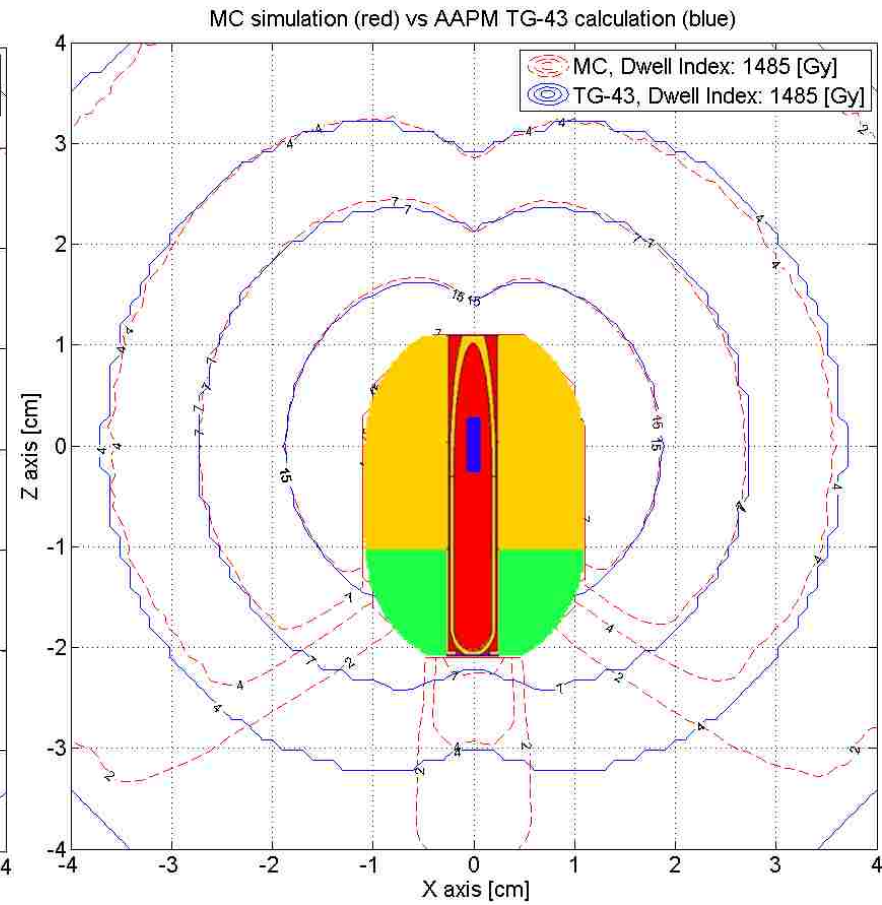


Figure 3.7(a-b): Comparison MC and TG-43 dose distribution for dwell index (a) 1500 mm and (b) 1495 mm, in Gy, within a plane bisecting the right ovoid, resulting from a single source with equivalent source activities and dwell-times. The source (blue cylinder, not to scale) is illustrated within the ovoid to give perspective of placement. The distal end (green) of the ovoid was modified to be tungsten with a density of 18 g/cm^3 . These plots illustrate d_S^{MC} and d_S^{TG43} which are used to create the source-based correction matrix. Quantitatively, 17.1% and 39.9% of the comparison points are within $\pm 2\%$ or $\pm 2\text{mm}$ for dwell index 1500 mm and 1495 mm, respectively.



(a)



(b)

Figure 3.8(a-b): Comparison MC and TG-43 dose distribution for dwell index (a) 1490 mm and (b) 1485 mm, in Gy, within a plane bisecting the right ovoid, resulting from a single source with equivalent source activities and dwell-times. The source (blue cylinder, not to scale) is illustrated within the ovoid to give perspective of placement. The distal end (green) of the ovoid was modified to be tungsten with a density of 18 g/cm^3 . These plots illustrate d_S^{MC} and d_S^{TG43} which are used to create the source-based correction matrix. Quantitatively, 81.8% and 89.0% of the comparison points are within +/- 2% or +/- 2mm for dwell index 1490 mm and 1485 mm, respectively.

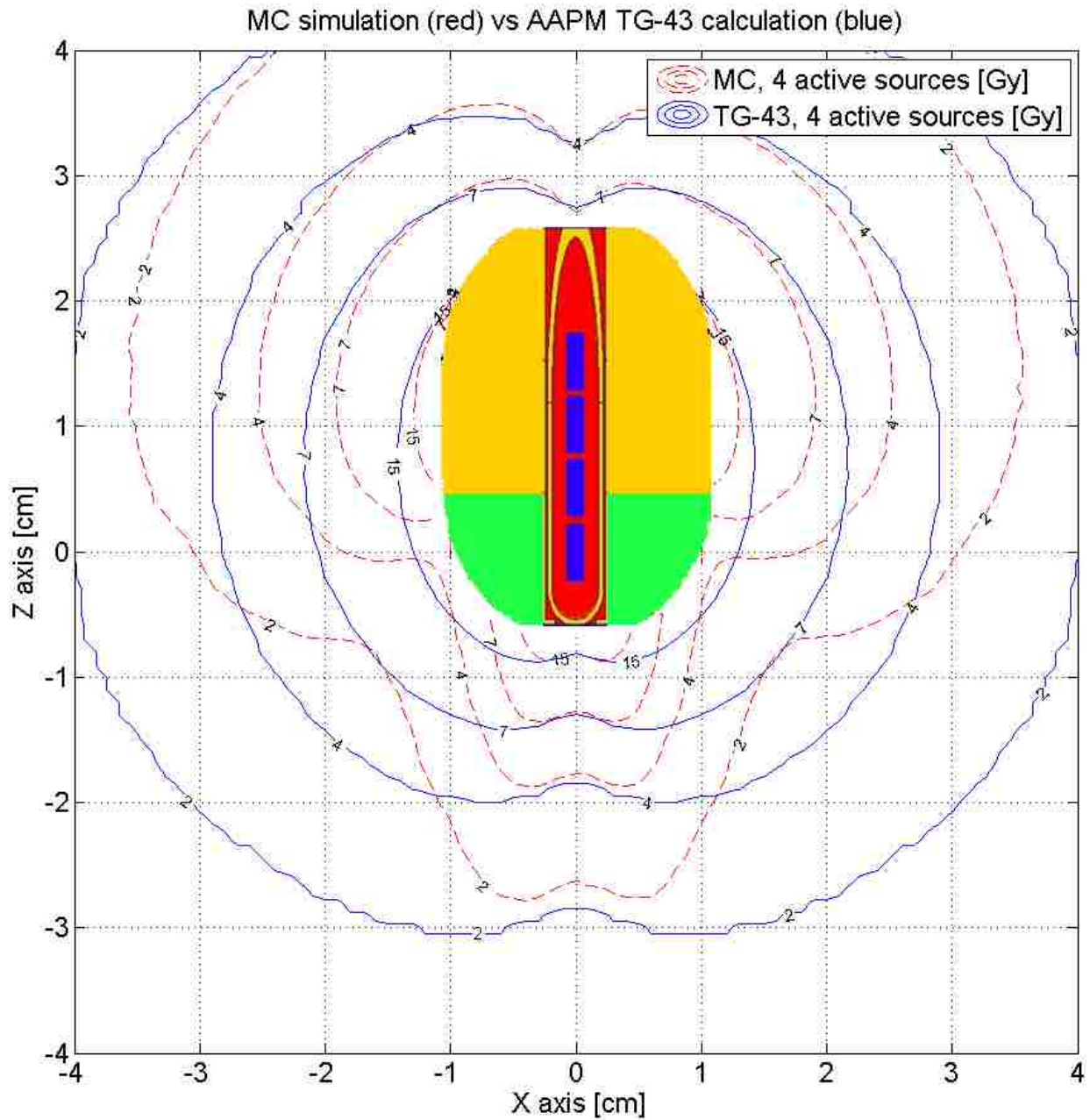


Figure 3.9: Comparison MC and TG-43 dose distribution for superimposed dwell indexes: 1500 mm, 1495 mm, 1490 mm, and 1485 mm, in Gy, within a plane bisecting the right ovoid, resulting from four source dwell-positions with equivalent source activities and dwell-times. The source (blue cylinders, not to scale) is illustrated within the ovoid to give perspective of placements. The distal end (green) of the ovoid was modified to be tungsten with a density of 18 g/cm³. These plots illustrate d_o^{MC} and d_o^{TG43} which are used to create the ovoid-based correction matrix. Quantitatively, 21.8 % of the comparison points are within +/- 2% or +/- 2mm.

3.3 Aim 3: Application of Source- and Ovoid-Based 3D Correction Strategies

3.3.1 Nucletron CT-MR compatible Fletcher Ovoid Applicator

Two coplanar ovoids were simulated with all four (4) dwell-positions per ovoid lying in the same plane. Points lying within the ovoid, for both MC simulations and TG-43 calculations, are not considered in comparison metrics as the dosimetry within the ovoids are of no clinical significance. Dwell-time combinations were varied to test whether different dwell-time gradients affect the efficiency of either correction scheme. Each plan was referenced according to the maximum dwell-time gradient (*i.e.* 0%, 5%, 10%, etc.) in the combination of dwell-times. A clinically applicable source activity of 8.7 Ci was used for all simulations.

3.3.1.1 No Dwell-Time Gradient

All dwell-times were equivalent and were set to 50 seconds. Comparisons of MC-simulated isodose distributions and isodoses calculated using TG-43 methodology is shown in Figure 3.10. The CT-MR compatible Fletcher ovoid illustration is to convey the size and placement of the ovoid pair. Although the plane bisects the source dwell-positions, the source is not illustrated. Observed in this figure are the qualitative differences in dose due to the perturbing effects of the ovoids accounted for in MC simulations (dashed red lines) and unaccounted for in TG-43 calculations (solid blue line) for a single 2D plane. Quantitatively, 99.8% of the comparison points are within +/- 2% or +/- 2mm. The differences between the two isodoses are within the uncertainty of the MC.

Comparisons of MC-simulated isodose distributions and isodoses calculated using TG-43 methodology that has been corrected using an ovoid-based correction factor is shown in Figure 3.11a. Observed in this figure are the qualitative differences in dose for MC simulations (dashed red lines) and ovoid-based corrected TG-43 plan (solid blue line) for a single 2D plane. Quantitatively, 100% of the comparison points are within +/- 2% or +/- 2mm. There are no appreciable differences between the MC simulation and ovoid-based corrected TG-43 plan.

Next, comparisons for MC-simulated isodose distributions and isodoses calculated using TG-43 methodology that has been corrected using a source-based correction factor is shown in Figures 3.11b. This figure illustrates the qualitative differences in dose for MC simulations (dashed red lines) and source-based corrected TG-43 plan (solid blue line) for a single 2D plane. Quantitatively, 100% of the comparison points are within +/- 2% or +/- 2mm. Again, there are no appreciable differences between the MC simulation and source-based corrected TG-43 plan.

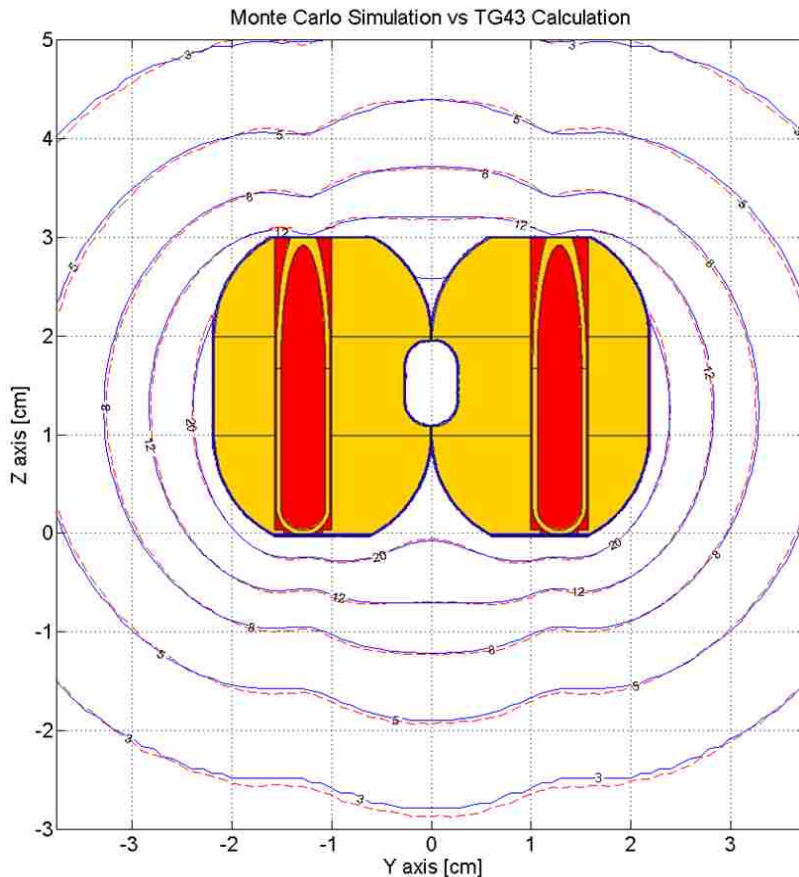
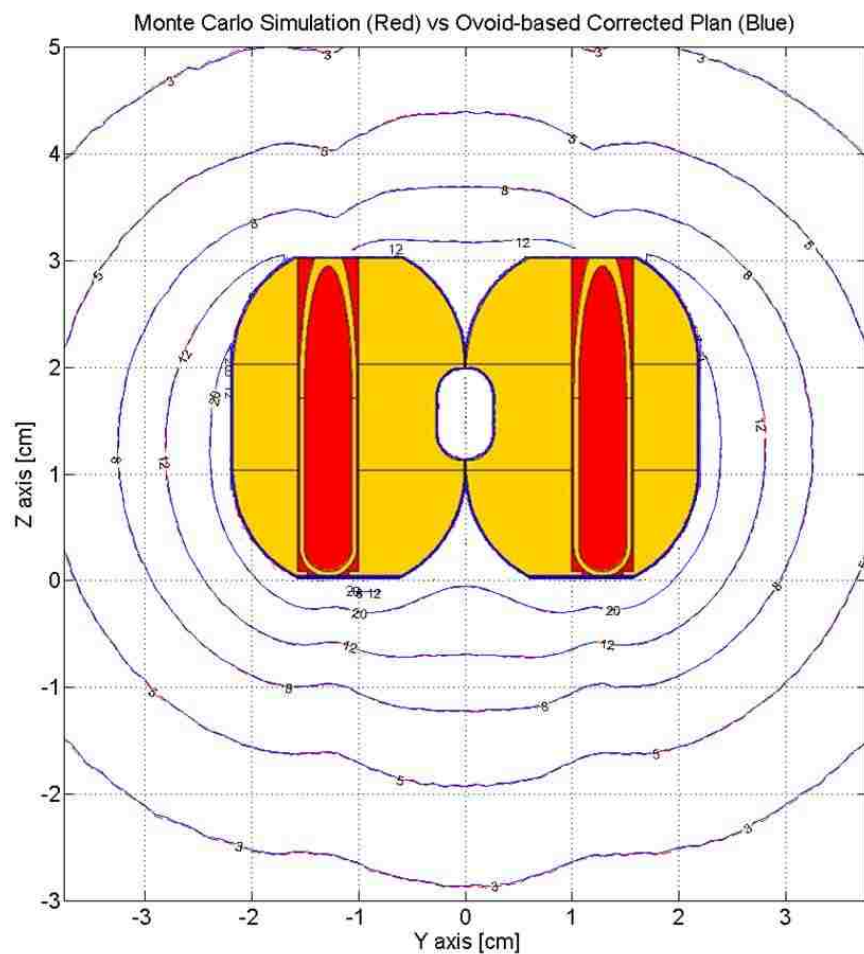
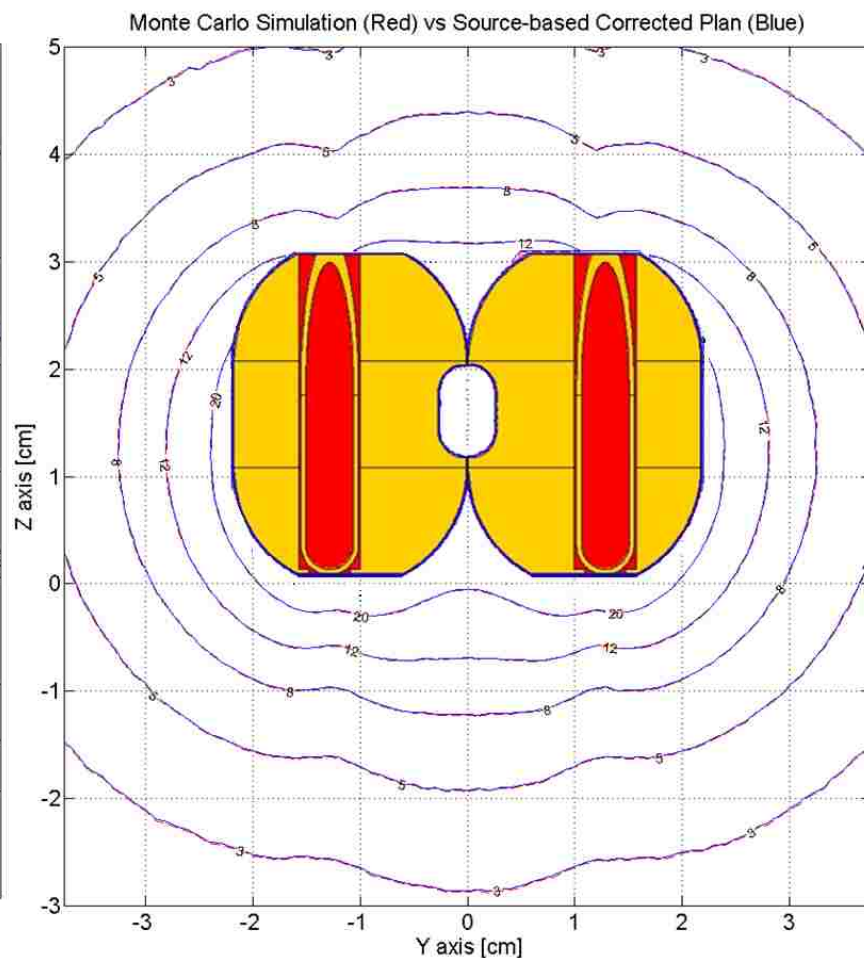


Figure 3.10: Comparison of MC simulation of a mHDR v2 Ir-192 source contained in a CT-MR compatible Fletcher ovoid applicator (red) vs. TG-43 calculations for a source in water (blue). Maximum adjacent dwell-time gradient is zero. Both ovoids are illustrated to show the plane and size of the ovoids. Shown here are absolute dose comparisons, in Gy, for 8 dwell-positions (four per ovoid, dwell-position indices of 1500, 1495, 1490, 1485 mm for each ovoid). Quantitatively, 99.8% of the comparison points are within +/- 2% or +/- 2mm.



(a)



(b)

Figure 3.11(a-b): Comparison of MC simulation of a mHDR v2 Ir-192 source contained in a CT-MR compatible Fletcher ovoid applicator vs. TG-43 corrected plans that account for applicator heterogeneities. Maximum adjacent dwell-time gradient is zero. Shown here are 2D planes bisecting the ovoid pair comparing full MC calculations (red) and isodoses calculated using (a) ovoid-based and (b) source-based corrected TG-43 plan (blue), in Gy, for 8 dwell-positions (four per ovoid, dwell-position indices: 1500, 1495, 1490, 1485 mm for each ovoid). Quantitatively, 100% of the comparison points are within $\pm 2\%$ or ± 2 mm for both comparisons.

3.3.1.2 Dwell-Time Gradient of 30%

The dwell-times, keeping the same plan as previous, were manually set to 5 seconds for dwell index 1500mm, 7.5 seconds for dwell index 1495mm, 45 seconds for dwell index 1490mm, and 67.5 seconds for dwell index 1485mm for both ovoids. The maximum dwell-time gradient for this combination of dwell-times is 30%.

Comparison of MC-simulated isodose distributions and isodoses calculated using TG-43 methodology is shown in Figure 3.12. The CT-MR compatible Fletcher ovoid illustration is to convey the size and placement of the ovoid pair. Although the plane bisects the source dwell-positions, and the source is only at a single location at any given time, the source is not illustrated. Observed in this figure are the qualitative differences in dose due to the perturbing effects of the ovoids accounted for in MC simulations (dashed red lines) and unaccounted for in TG-43 calculations (solid blue line) for a single 2D plane. Quantitatively, 99.7% of the comparison points are within +/- 2% or +/- 2mm. The differences between the two isodoses are within the uncertainty of the MC.

Comparisons of MC-simulated isodose distributions and isodoses calculated using TG-43 methodology that has been corrected using an ovoid-based correction factor is shown in Figure 3.13a. Observed in this figure are the qualitative differences in dose for MC simulations (dashed red lines) and ovoid-based corrected TG-43 plan (solid blue line) for a single 2D plane. Quantitatively, 99.9% of the comparison points are within +/- 2% or +/- 2mm. There are no appreciable differences between the MC simulation and ovoid-based corrected TG-43 plan.

Next, comparisons for MC-simulated isodose distributions and isodoses calculated using TG-43 methodology that has been corrected using a source-based correction factor is shown in Figures 3.13b. This figure illustrates the qualitative differences in dose for MC simulations (dashed red lines) and source-based corrected TG-43 plan (solid blue line) for a single 2D plane.

Quantitatively, 100% of the comparison points are within +/- 2% or +/- 2mm. Again, there are no appreciable differences between the MC simulation and source-based corrected TG-43 plan.

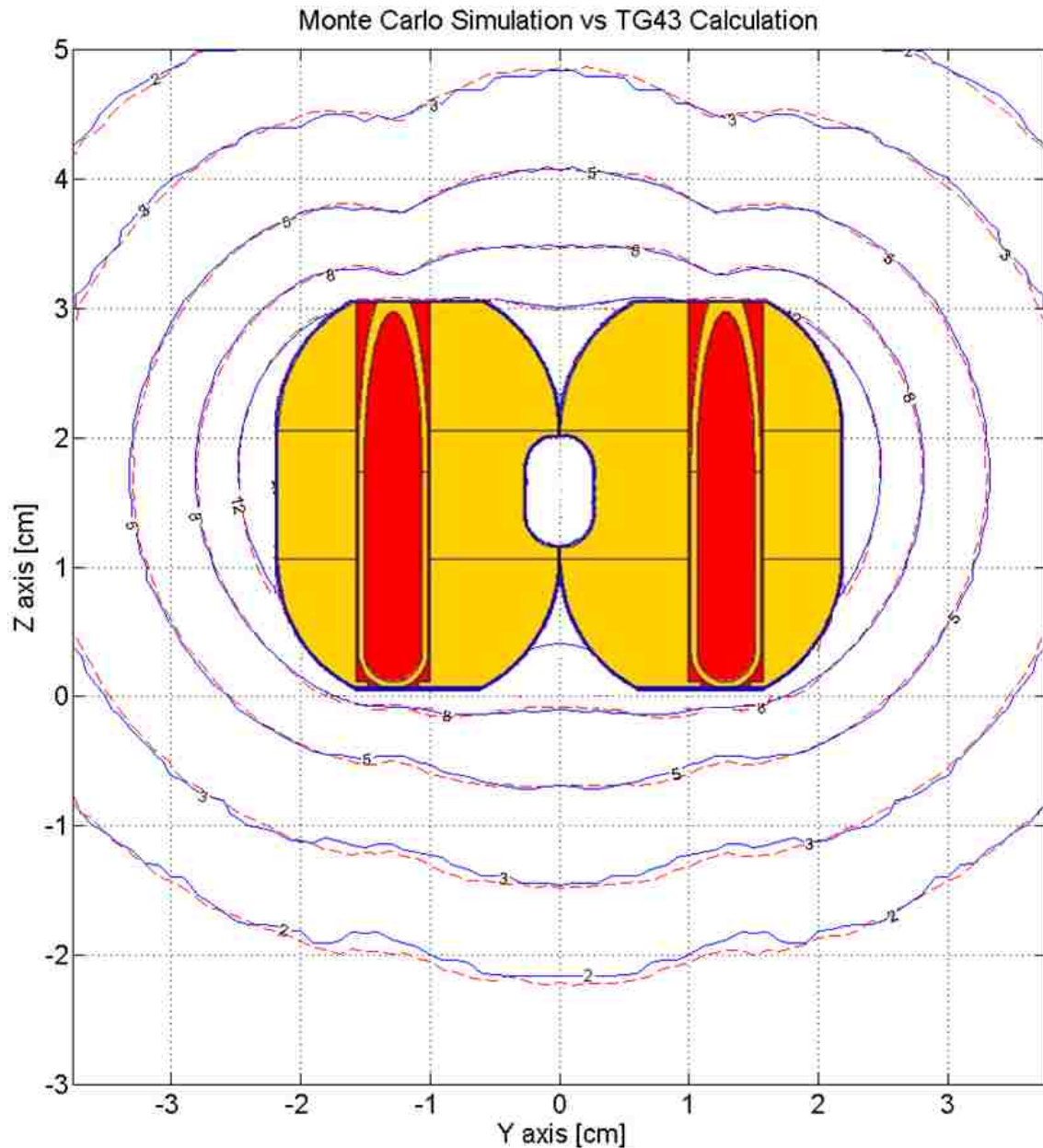


Figure 3.12: Comparison of MC simulation of a mHDR v2 Ir-192 source contained in a CT-MR compatible Fletcher ovoid applicator (red) vs. TG-43 calculations for a source in water (blue). Maximum adjacent dwell-time gradient is 30%. Both ovoids are illustrated to show the plane and size of the ovoids. Shown here are absolute dose comparisons, in Gy, for 8 dwell-positions (four per ovoid, dwell-position indices of 1500, 1495, 1490, 1485 mm for each ovoid). Quantitatively, 99.7% of the comparison points are within +/- 2% or +/- 2mm.

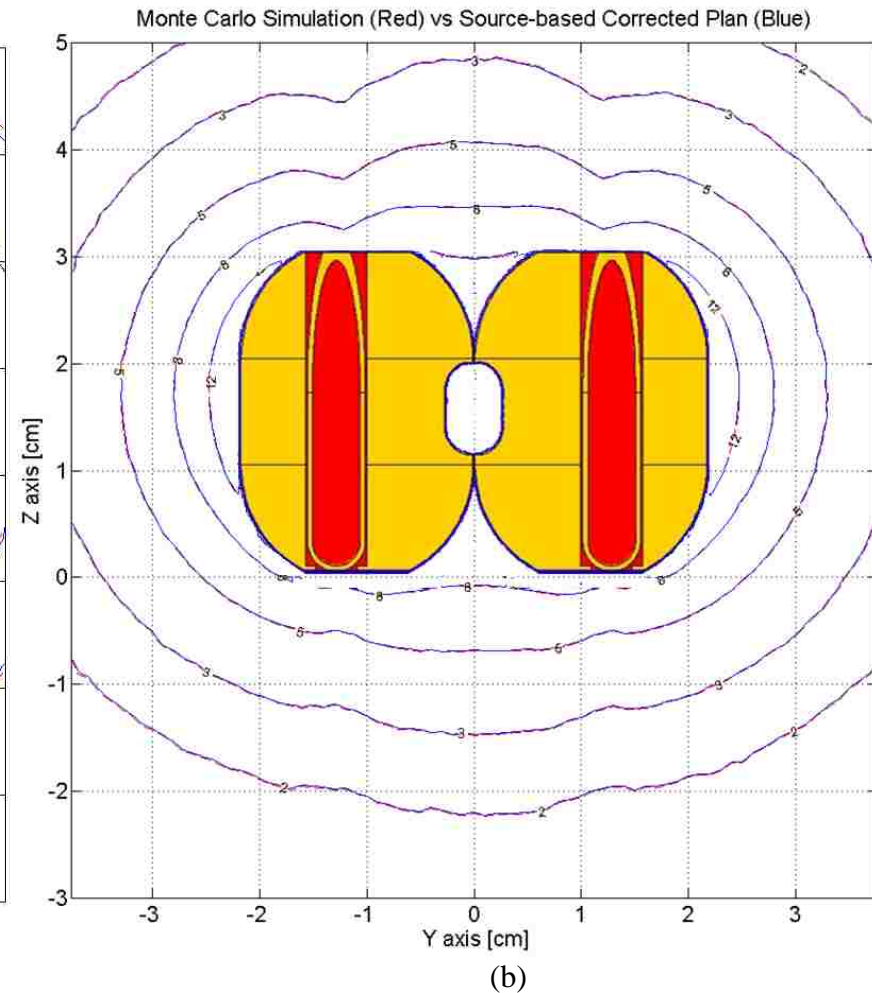
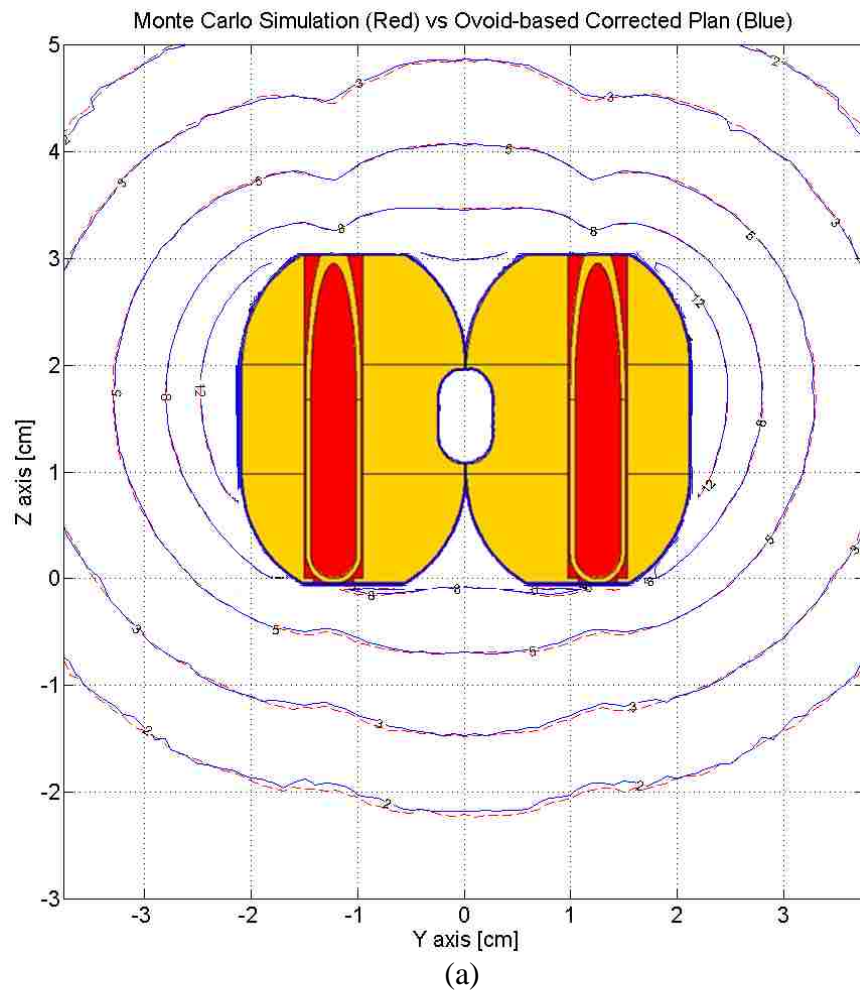


Figure 3.13: Comparison of MC simulation of a mHDR v2 Ir-192 source contained in a CT-MR compatible Fletcher ovoid applicator vs. TG-43 corrected plans of a source in water. Maximum adjacent dwell-time gradient is 30%. Shown here are 2D planes bisecting the ovoid pair comparing full MC calculations (red) and isodoses calculated using (a) ovoid-based and (b) source-based corrected TG-43 plan (blue), in Gy, for 8 dwell-positions (four per ovoid, dwell-position indices: 1500, 1495, 1490, 1485 mm for each ovoid). Quantitatively, 99.9% and 100% of the comparison points are within $\pm 2\%$ or $\pm 2\text{mm}$ for the ovoid-based and source-based corrected TG-43 plan, respectively.

3.3.1.3 Dwell-Time Gradient of 60%

The dwell-times, keeping the same plan as previous, were changed to 5 seconds for dwell index 1500mm, 5 seconds for dwell index 1495mm, 35 seconds for dwell index 1490mm, and 155 seconds for dwell index 1485mm for the left ovoid. The right ovoid dwell-times were changed to 155 seconds for dwell index 1500mm, 35 seconds for dwell index 1495mm, 5 seconds for dwell index 1490mm, and 5 seconds for dwell index 1485mm. The maximum dwell-time gradient for this combination is 60%.

Comparison of MC-simulated isodose distributions and isodoses calculated using TG-43 methodology is shown in Figure 3.14. The CT-MR compatible Fletcher ovoid illustration is to convey the size and placement of the ovoid pair. Although the plane bisects the source dwell-positions, and the source is only at a single location at any given time, the source is not illustrated. Observed in this figure are the qualitative differences in dose due to the perturbing effects of the ovoids accounted for in MC simulations (dashed red lines) and unaccounted for in TG-43 calculations (solid blue line) for a single 2D plane. Quantitatively, 99.0% of the comparison points are within +/- 2% or +/- 2mm. The differences between the two isodoses are within the uncertainty of the MC.

Comparisons of MC-simulated isodose distributions and isodoses calculated using TG-43 methodology that has been corrected using an ovoid-based correction factor is shown in Figure 3.15a. Observed in this figure are the qualitative differences in dose for MC simulations (dashed red lines) and ovoid-based corrected TG-43 plan (solid blue line) for a single 2D plane. Quantitatively, 99.7% of the comparison points are within +/- 2% or +/- 2mm. There are no appreciable differences between the MC simulation and ovoid-based corrected TG-43 plan.

Next, comparisons for MC-simulated isodose distributions and isodoses calculated using TG-43 methodology that has been corrected using a source-based correction factor is shown in

Figures 3.15b. This figure illustrates the qualitative differences in dose for MC simulations (dashed red lines) and source-based corrected TG-43 plan (solid blue line) for a single 2D plane. Quantitatively, 100% of the comparison points are within +/- 2% or +/- 2mm. Again, there are no appreciable differences between the MC simulation and source-based corrected TG-43 plan.

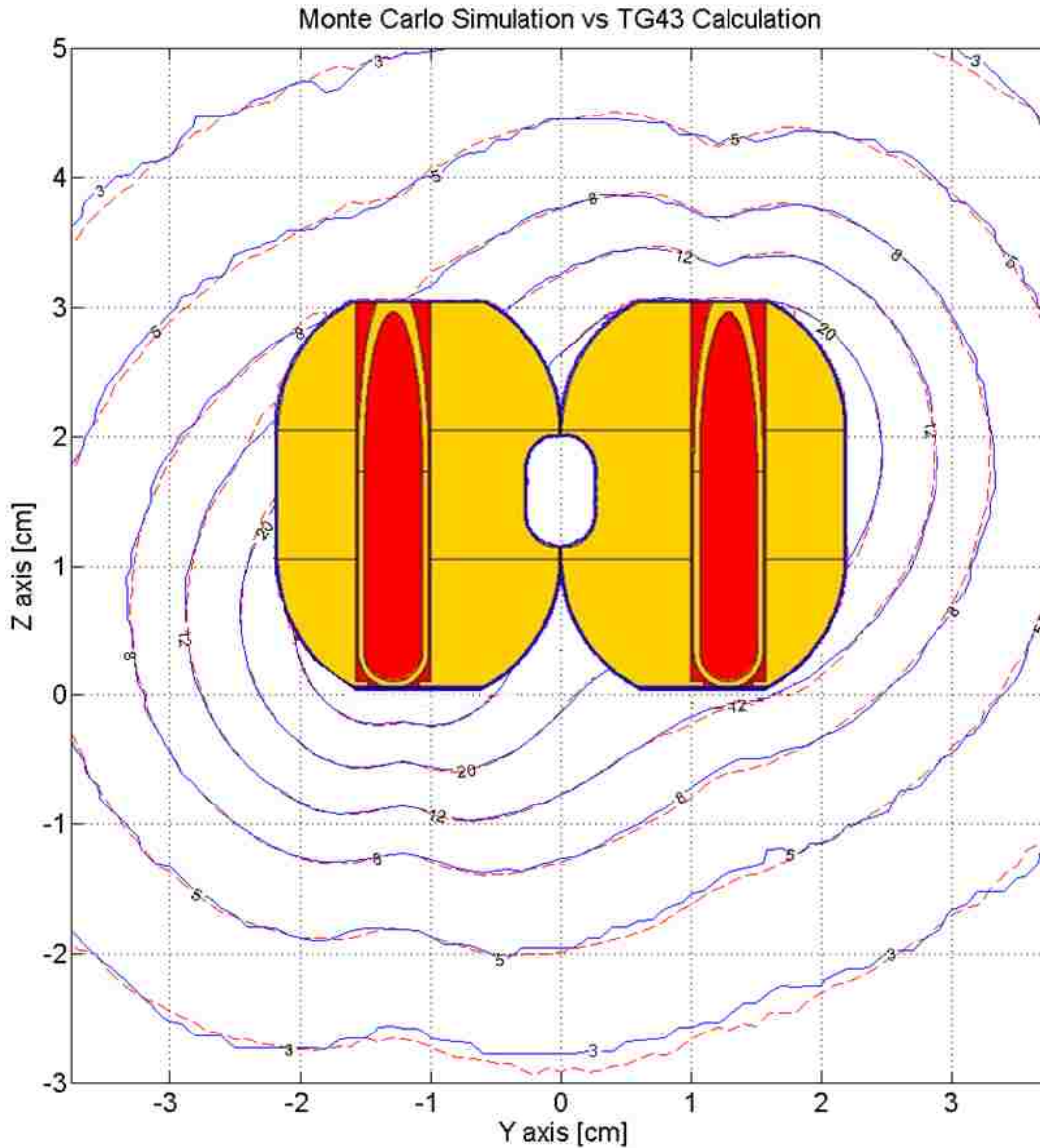


Figure 3.14: Comparison of MC simulation of a mHDR v2 Ir-192 source contained in a CT-MR compatible Fletcher ovoid applicator (red) vs. TG-43 calculations for a source in water (blue). Maximum adjacent dwell-time gradient is 60%. Both ovoids are illustrated to show the plane and size of the ovoids. Shown here are absolute dose comparisons, in Gy, for 8 dwell-positions (four per ovoid, dwell-position indices of 1500, 1495, 1490, 1485 mm for each ovoid). Quantitatively, 99.0% of the comparison points are within +/- 2% or +/- 2mm.

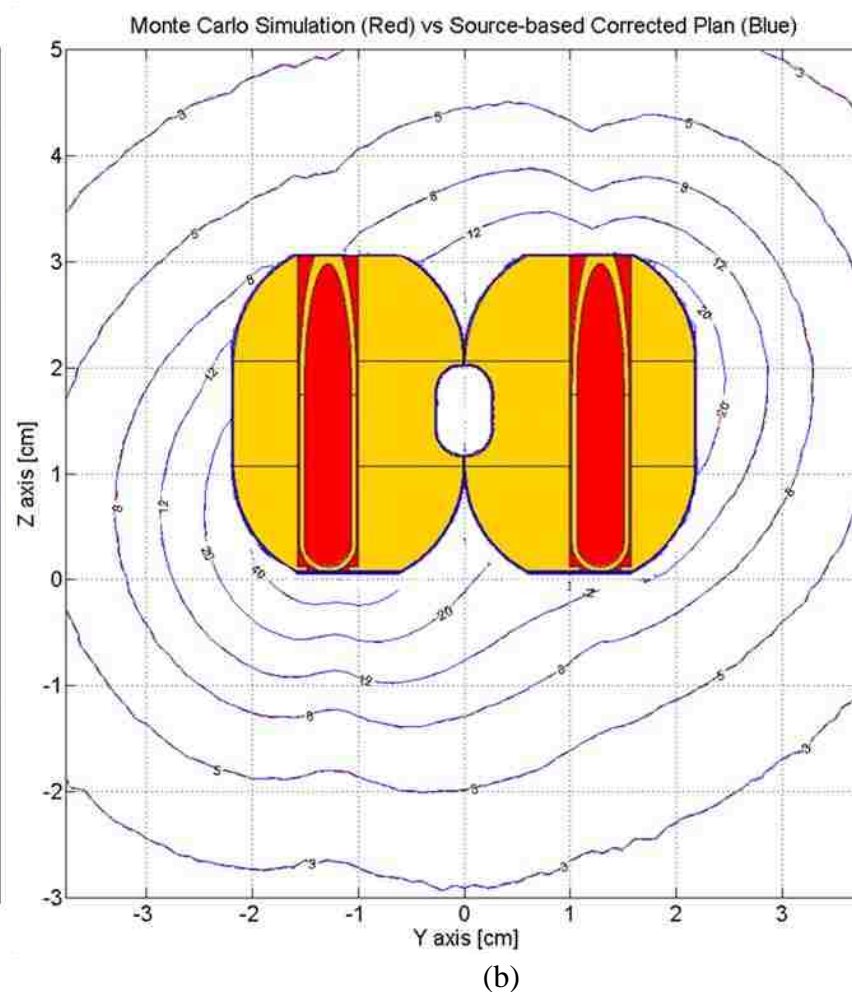
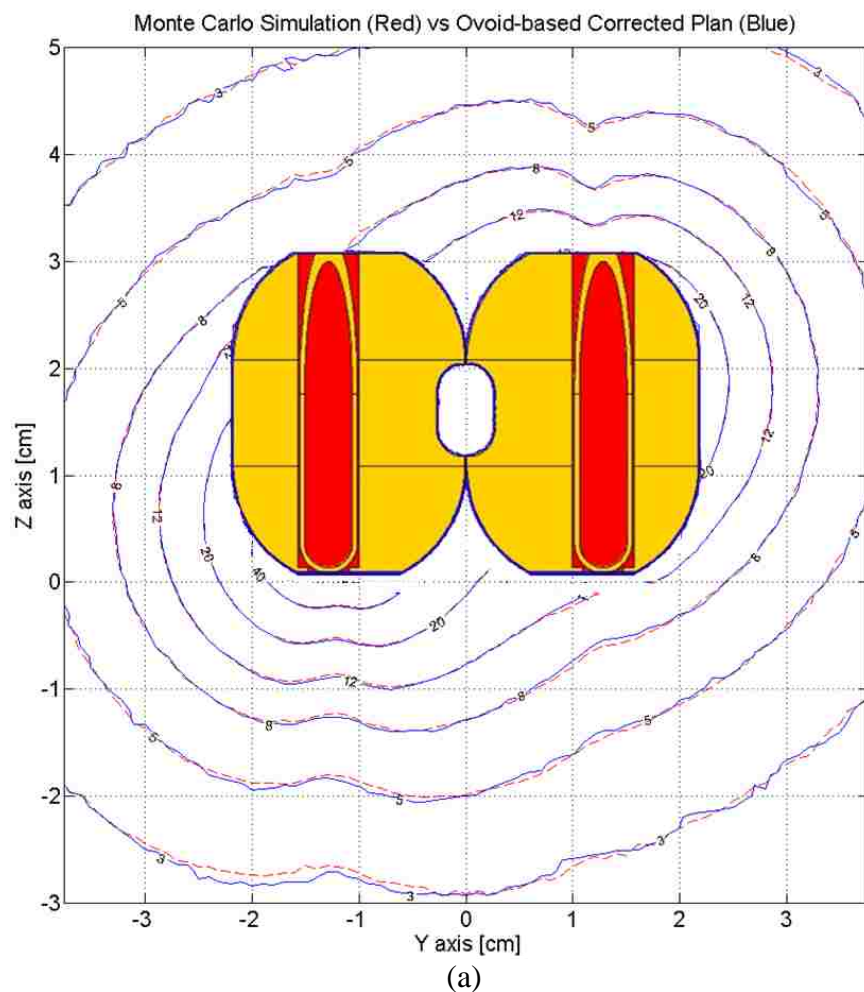


Figure 3.15(a-b): Comparison of MC simulation of a mHDR v2 Ir-192 source contained in a CT-MR compatible Fletcher ovoid applicator vs. TG-43 corrected plans of a source in water. Maximum adjacent dwell-time gradient is 60%. Shown here are 2D planes bisecting the ovoid pair comparing full MC calculations (red) and isodoses calculated using (a) ovoid-based and (b) source-based corrected TG-43 plan (blue), in Gy, for 8 dwell-positions (four per ovoid, dwell-position indices: 1500, 1495, 1490, 1485 mm for each ovoid). Quantitatively, 99.7% and 100% of the comparison points are within $\pm 2\%$ or $\pm 2\text{mm}$ for the ovoid-based and source-based corrected TG-43 plan, respectively.

3.3.1.4 Dwell-Time Gradient of 70%

The dwell-times, keeping the same plan, were changed to 25 seconds for dwell index 1500mm, 35 seconds for dwell index 1495mm, 2 seconds for dwell index 1490mm, and 150 seconds for dwell index 1485mm for the left ovoid. All dwell-times in the right ovoid were set to 25 seconds. The maximum dwell-time weighting difference for this set is thus 70%.

Comparison of MC-simulated isodose distributions and isodoses calculated using TG-43 methodology is shown in Figure 3.16. The CT-MR compatible Fletcher ovoid illustration is to convey the size and placement of the ovoid pair. Although the plane bisects the source dwell-positions, and the source is only at a single location at any given time, the source is not illustrated. Observed in this figure are the qualitative differences in dose due to the perturbing effects of the ovoids accounted for in MC simulations (dashed red lines) and unaccounted for in TG-43 calculations (solid blue line) for a single 2D plane. Quantitatively, 99.6% of the comparison points are within +/- 2% or +/- 2mm. The differences between the two isodoses are within the uncertainty of the MC.

Comparisons of MC-simulated isodose distributions and isodoses calculated using TG-43 methodology that has been corrected using an ovoid-based correction factor is shown in Figure 3.17a. Observed in this figure are the qualitative differences in dose for MC simulations (dashed red lines) and ovoid-based corrected TG-43 plan (solid blue line) for a single 2D plane. Quantitatively, 99.9% of the comparison points are within +/- 2% or +/- 2mm. There are no appreciable differences between the MC simulation and ovoid-based corrected TG-43 plan.

Next, comparisons for MC-simulated isodose distributions and isodoses calculated using TG-43 methodology that has been corrected using a source-based correction factor is shown in Figures 3.17b. This figure illustrates the qualitative differences in dose for MC simulations (dashed red lines) and source-based corrected TG-43 plan (solid blue line) for a single 2D plane.

Quantitatively, 100% of the comparison points are within +/- 2% or +/- 2mm. Again, there are no appreciable differences between the MC simulation and source-based corrected TG-43 plan.

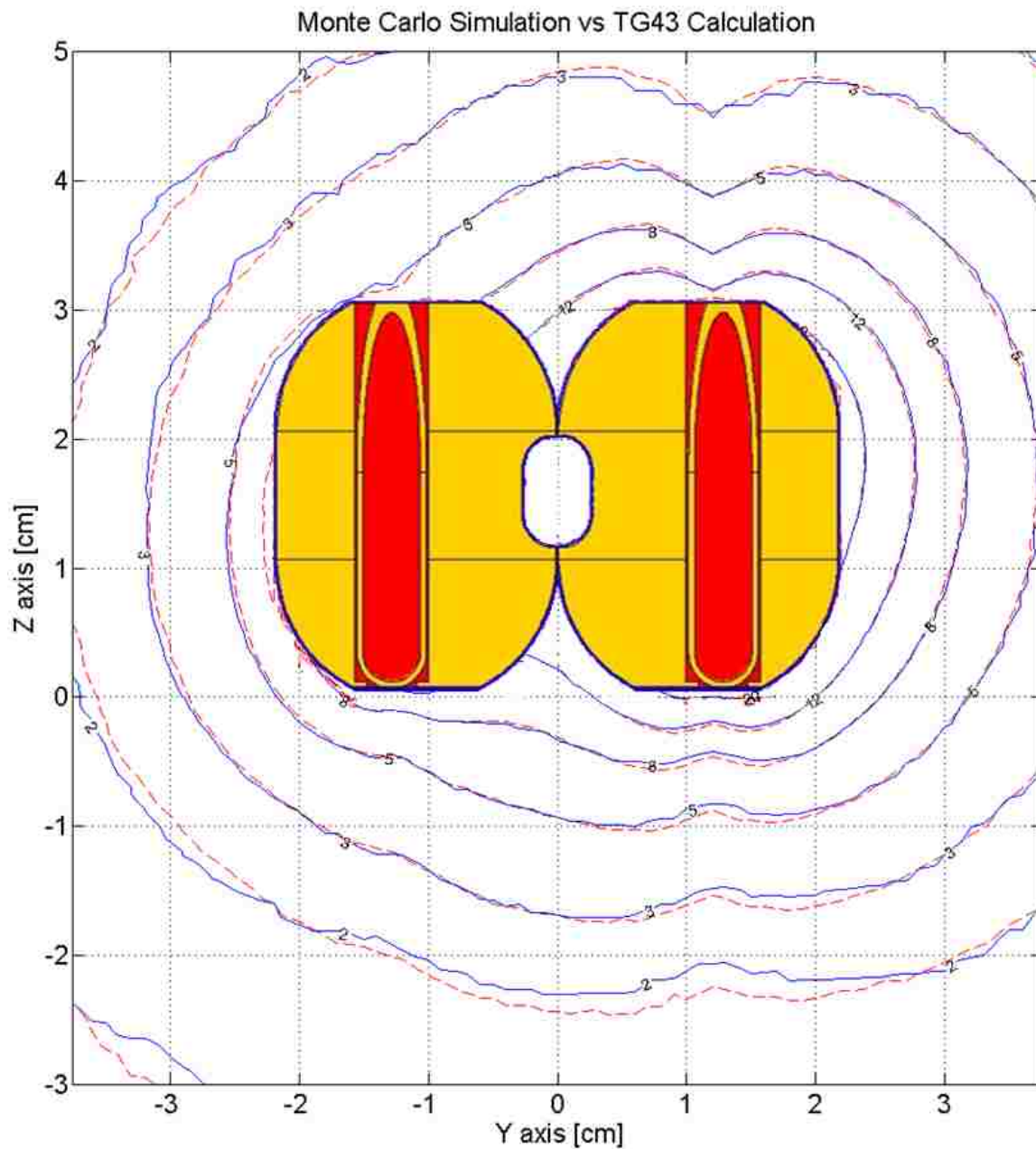
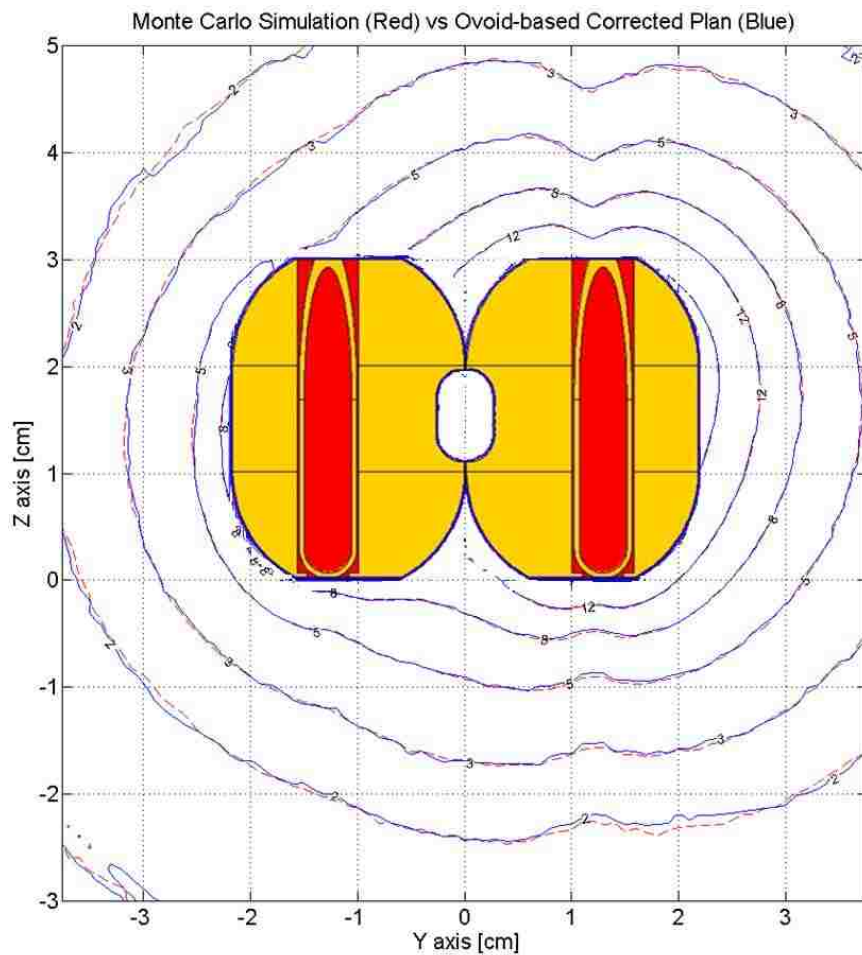
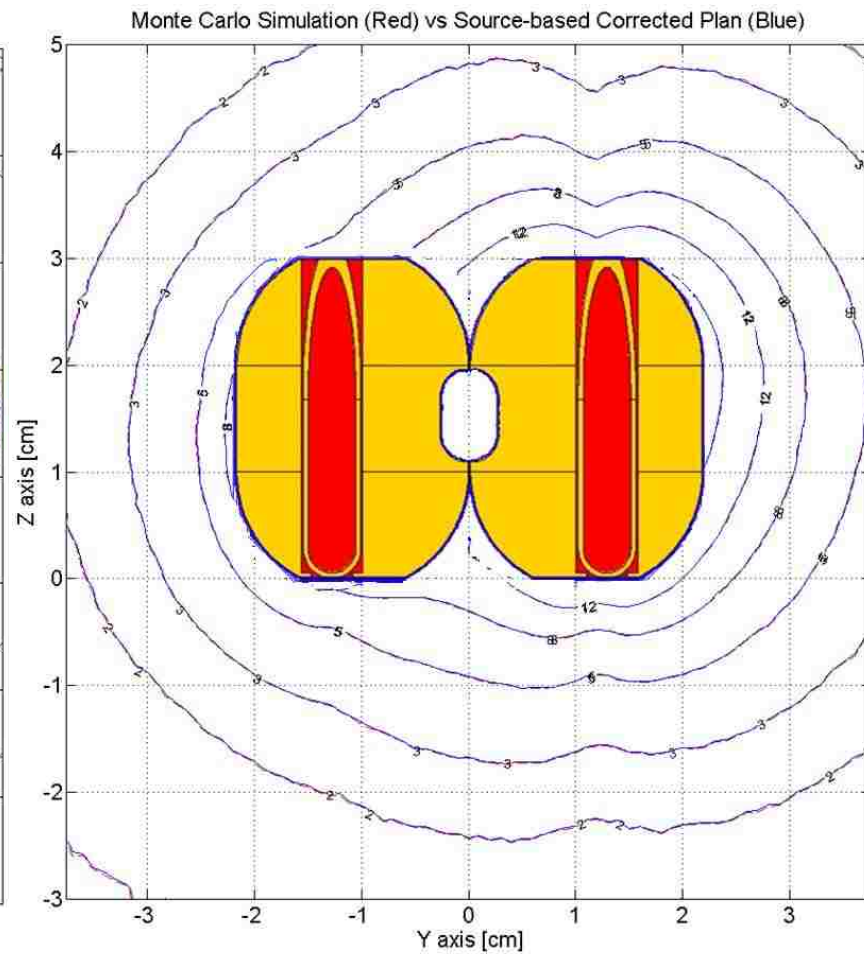


Figure 3.16: Comparison of MC simulation of a mHDR v2 Ir-192 source contained in a CT-MR compatible Fletcher ovoid applicator (red) vs. TG-43 calculations for a source in water (blue). Maximum adjacent dwell-time gradient is 70%. Both ovoids are illustrated to show the plane and size of the ovoids. Shown here are absolute dose comparisons, in Gy, for 8 dwell-positions (four per ovoid, dwell-position indices of 1500, 1495, 1490, 1485 mm for each ovoid). Quantitatively, 99.6% of the comparison points are within +/- 2% or +/- 2mm.



(a)



(b)

Figure 3.17: Comparison of MC simulation of a mHDR v2 Ir-192 source contained in a CT-MR compatible Fletcher ovoid applicator vs. TG-43 corrected plans of a source in water. Maximum adjacent dwell-time gradient is 70%. Shown here are 2D planes bisecting the ovoid pair comparing full MC calculations (red) and isodoses calculated using (a) ovoid-based and (b) source-based corrected TG-43 plan (blue), in Gy, for 8 dwell-positions (four per ovoid, dwell-position indices: 1500, 1495, 1490, 1485 mm for each ovoid). Quantitatively, 99.9% and 100% of the comparison points are within $\pm 2\%$ or $\pm 2\text{mm}$ for the ovoid-based and source-based corrected TG-43 plan, respectively.

3.3.2 MC Applicator Modified to Include High-Z Inhomogeneities

The distal end of the ovoid material was converted to tungsten. Points lying within the ovoids, for both MC simulations and AAPM TG-43 calculations, are not considered in comparison metrics as the dosimetry within the ovoids are of no clinical significance. Dwell-time combinations were varied so that different maximum dwell-time gradients were compared to test the hypothesis. A clinically applicable source activity of 8.7 Ci was used for all comparisons.

3.3.1.1 No Dwell-Time Gradient

All dwell-times were equivalent and set to 50 seconds. Comparisons of MC-simulated isodose distributions and isodoses calculated using TG-43 methodology is shown in Figure 3.18. The CT-MR compatible Fletcher ovoid illustration is to convey the size and placement of the ovoid pair. Although the plane bisects the source dwell-positions, the source is not illustrated. Observed in this figure are the qualitative differences in dose due to the perturbing effects of the ovoids accounted for in MC simulations (dashed red lines) and unaccounted for in TG-43 calculations (solid blue line) for a single 2D plane. Quantitatively, 13.2% of the comparison points are within +/- 2% or +/- 2mm.

Comparisons of MC-simulated isodose distributions and isodoses calculated using TG-43 methodology that has been corrected using an ovoid-based correction factor is shown in Figure 3.19a. Observed in this figure are the qualitative differences in dose for MC simulations (dashed red lines) and ovoid-based corrected TG-43 plan (solid blue line) for a single 2D plane. Quantitatively, 100% of the comparison points are within +/- 2% or +/- 2mm. There are no appreciable differences between the MC simulation and ovoid-based corrected TG-43 plan.

Next, comparisons for MC-simulated isodose distributions and isodoses calculated using TG-43 methodology that has been corrected using a source-based correction factor is shown in Figures 3.11b. This figure illustrates the qualitative differences in dose for MC simulations

(dashed red lines) and source-based corrected TG-43 plan (solid blue line) for a single 2D plane. Quantitatively, 100% of the comparison points are within +/- 2% or +/- 2mm. Again, there are no appreciable differences between the MC simulation and source-based corrected TG-43 plan.

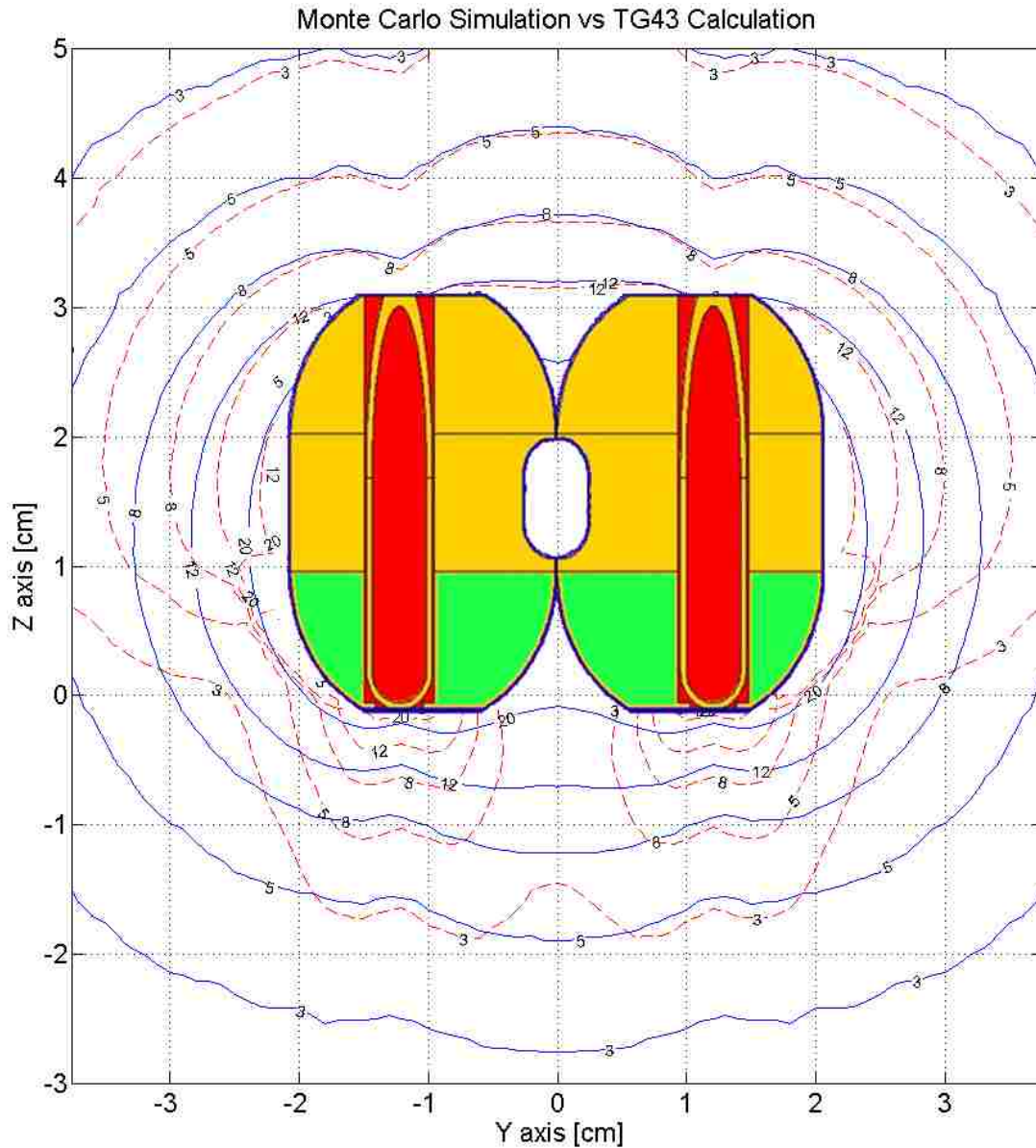


Figure 3.18: Comparison of MC simulation of a mHDR v2 Ir-192 source contained in a modified CT-MR compatible Fletcher ovoid applicator to include a high-Z shield (red) vs. TG-43 calculations for a source in water (blue). Maximum adjacent dwell-time gradient is zero. Both ovoids are illustrated to show the plane and size of the ovoids. Shown here are absolute dose comparisons, in Gy, for 8 dwell-positions (four per ovoid, dwell-position indices of 1500, 1495, 1490, 1485 mm for each ovoid). Quantitatively, 13.2% of the comparison points are within +/- 2% or +/- 2mm.

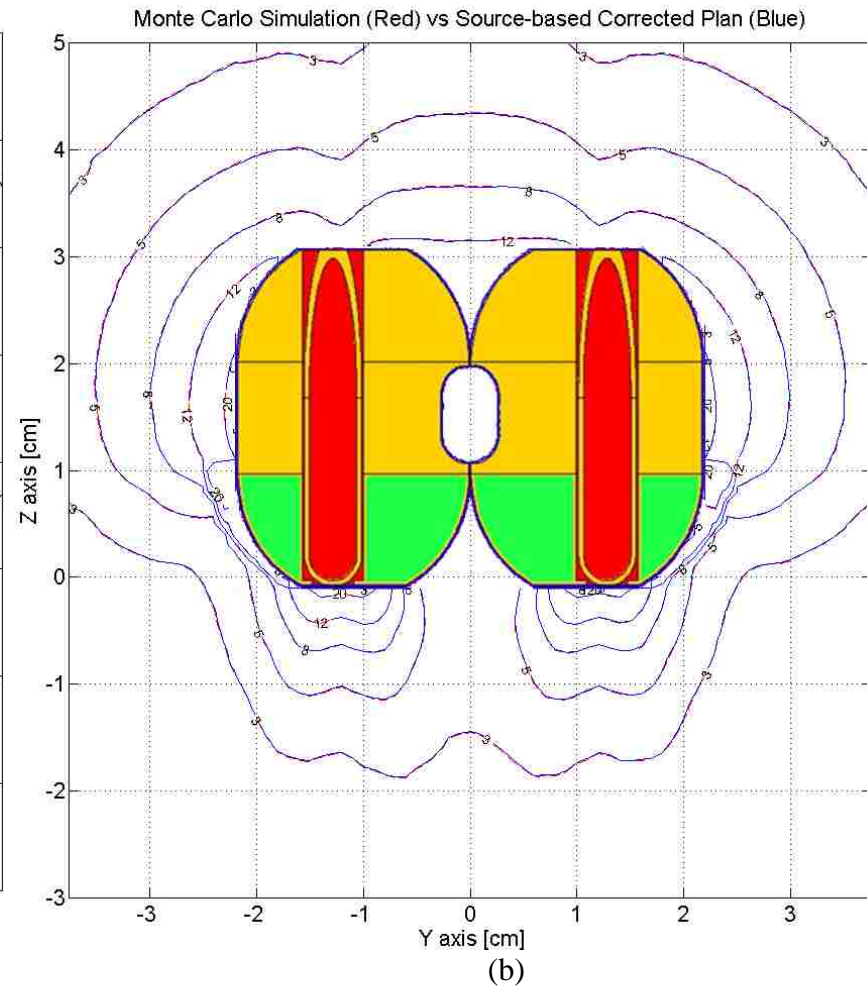
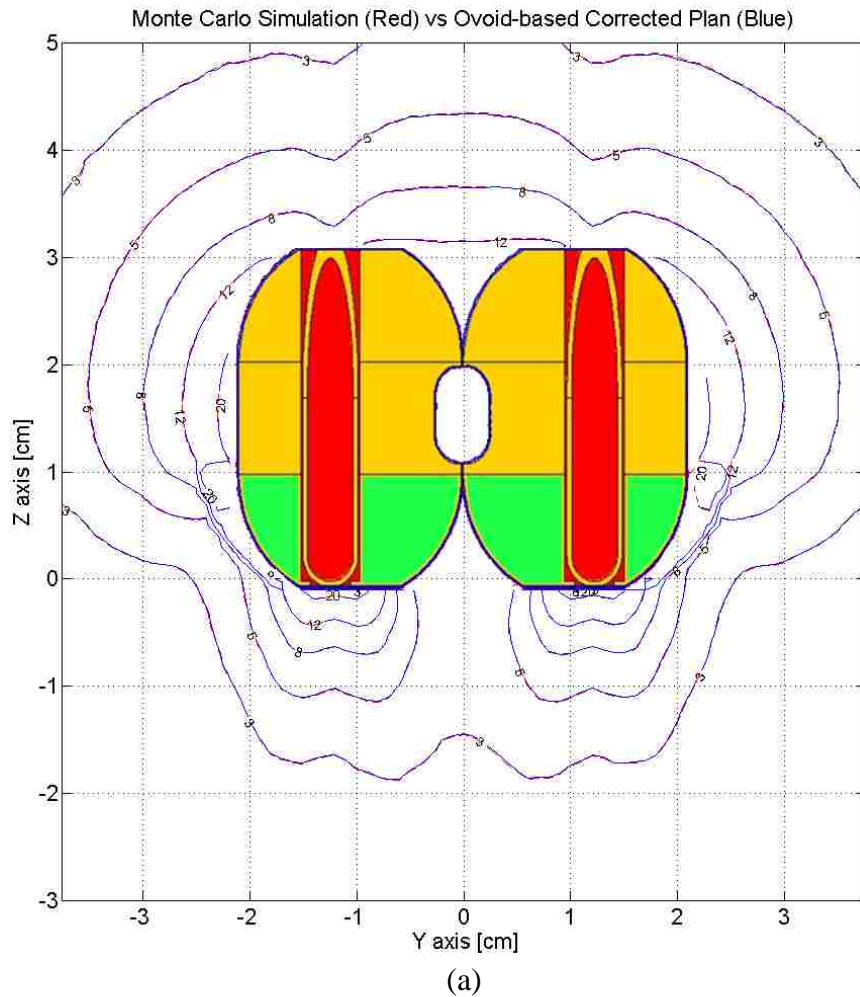


Figure 3.19(a-b): Comparison of MC simulation of a mHDR v2 Ir-192 source contained in a modified CT-MR compatible Fletcher ovoid applicator to include high-Z shield vs. TG-43 corrected plans of a source in water. Maximum adjacent dwell-time gradient is zero. Shown here are 2D planes bisecting the ovoid pair comparing full MC calculations (red) and isodoses calculated using (a) ovoid-based and (b) source-based corrected TG-43 plan (blue), in Gy, for 8 dwell-positions (four per ovoid, dwell-position indices: 1500, 1495, 1490, 1485 mm for each ovoid). Quantitatively, 100% of the comparison points are within $\pm 2\%$ or $\pm 2\text{mm}$ for both comparisons.

3.3.1.2 Dwell-Time Gradient of 5%

The dwell-times, keeping the same plan, were manually set to 55 seconds for dwell index 1500mm, 55 seconds for dwell index 1495mm, 45 seconds for dwell index 1490mm, and 45 seconds for dwell index 1485mm for both ovoids. This dwell-time combination results in a maximum dwell-time weighting difference for this set is thus 5%.

Comparison of MC-simulated isodose distributions and isodoses calculated using TG-43 methodology is shown in Figure 3.20. The CT-MR compatible Fletcher ovoid illustration is to convey the size and placement of the ovoid pair. Although the plane bisects the source dwell-positions, and the source is only at a single location at any given time, the source is not illustrated. Observed in this figure are the qualitative differences in dose due to the perturbing effects of the ovoids accounted for in MC simulations (dashed red lines) and unaccounted for in TG-43 calculations (solid blue line) for a single 2D plane. Quantitatively, 26.6% of the comparison points are within +/- 2% or +/- 2mm.

Comparisons of MC-simulated isodose distributions and isodoses calculated using TG-43 methodology that has been corrected using an ovoid-based correction factor is shown in Figure 3.21a. Observed in this figure are the qualitative differences in dose for MC simulations (dashed red lines) and ovoid-based corrected TG-43 plan (solid blue line) for a single 2D plane. Quantitatively, 99.2% of the comparison points are within +/- 2% or +/- 2mm. There are no appreciable differences between the MC simulation and ovoid-based corrected TG-43 plan.

Next, comparisons for MC-simulated isodose distributions and isodoses calculated using TG-43 methodology that has been corrected using a source-based correction factor is shown in Figures 3.21b. This figure illustrates the qualitative differences in dose for MC simulations (dashed red lines) and source-based corrected TG-43 plan (solid blue line) for a single 2D plane.

Quantitatively, 100% of the comparison points are within +/- 2% or +/- 2mm. Again, there are no appreciable differences between the MC simulation and source-based corrected TG-43 plan.

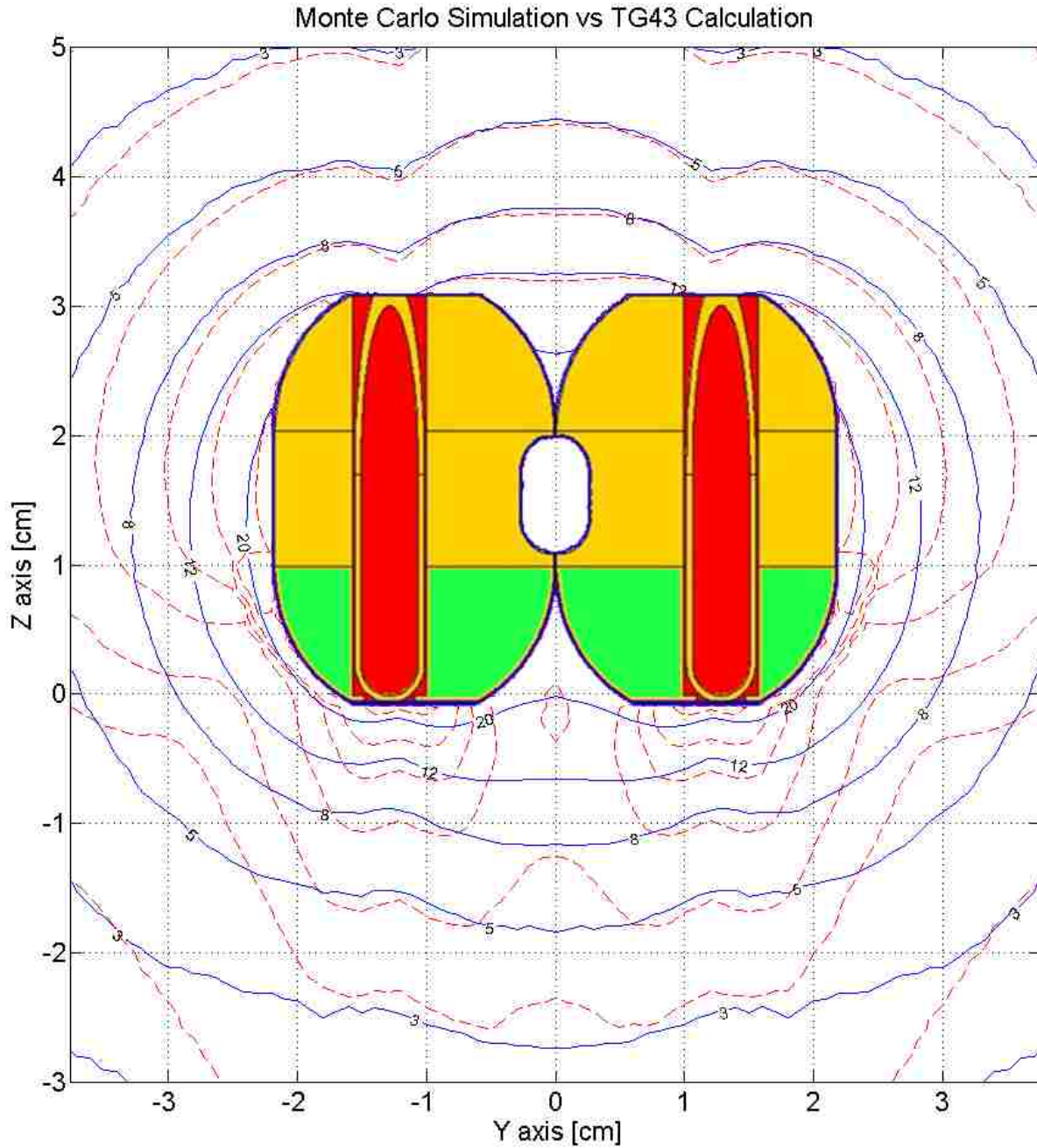


Figure 3.20: Comparison of MC simulation of a mHDR v2 Ir-192 source contained in a modified CT-MR compatible Fletcher ovoid applicator to include a high-Z shield (red) vs. TG-43 calculations for a source in water (blue). Maximum adjacent dwell-time gradient is 5%. Both ovoids are illustrated to show the plane and size of the ovoids. Shown here are absolute dose comparisons, in Gy, for 8 dwell-positions (four per ovoid, dwell-position indices of 1500, 1495, 1490, 1485 mm for each ovoid). Quantitatively, 26.6% of the comparison points are within +/- 2% or +/- 2mm.

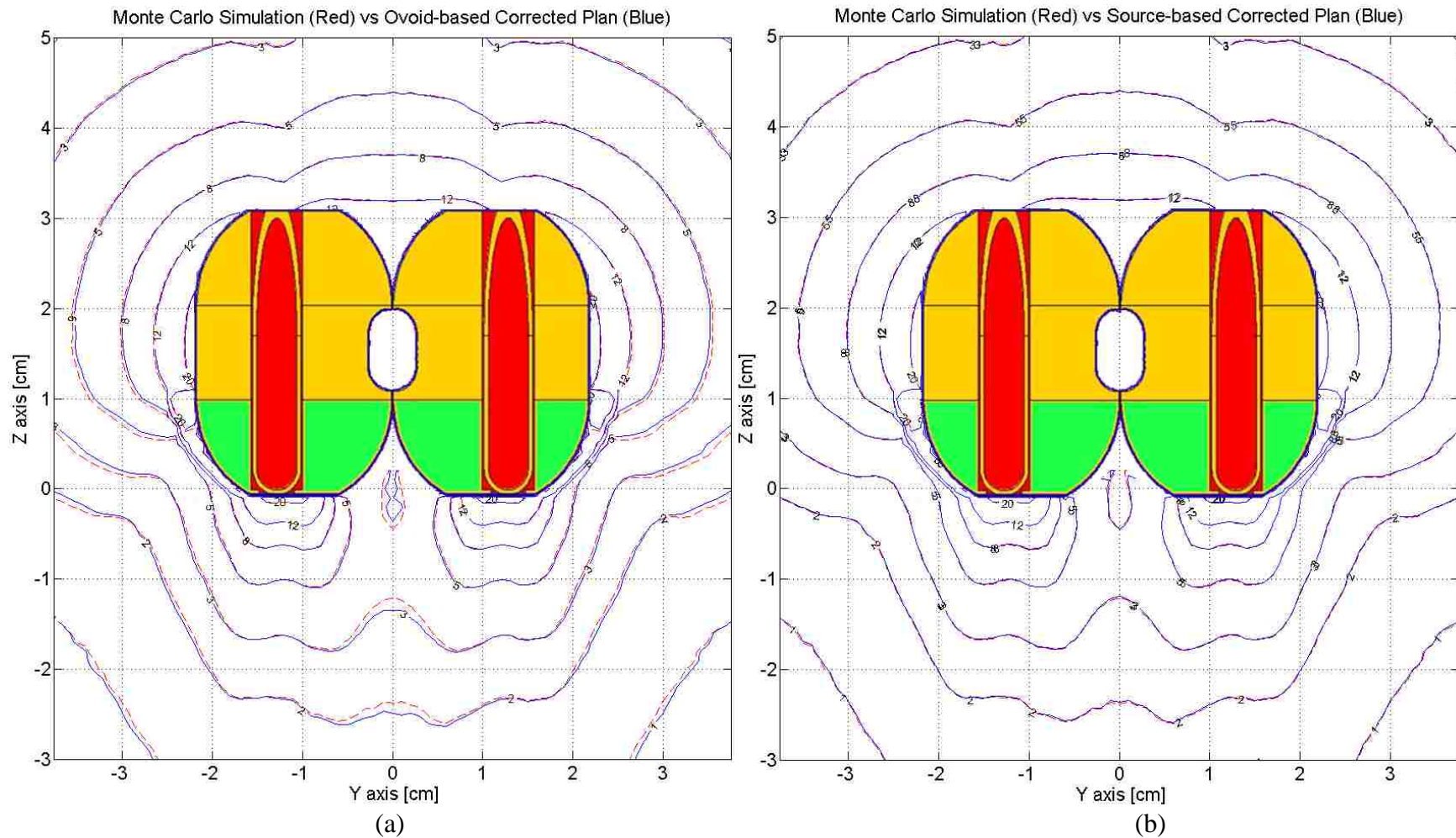


Figure 3.21: Comparison of MC simulation of a mHDR v2 Ir-192 source contained in a modified CT-MR compatible Fletcher ovoid applicator to include high-Z shield vs. TG-43 corrected plans of a source in water. Maximum adjacent dwell-time gradient is 5%. Shown here are 2D planes bisecting the ovoid pair comparing full MC calculations (red) and isodoses calculated using (a) ovoid-based and (b) source-based corrected TG-43 plan (blue), in Gy, for 8 dwell-positions (four per ovoid, dwell-position indices: 1500, 1495, 1490, 1485 mm for each ovoid). Quantitatively, 99.2% and 100% of the comparison points are within $\pm 2\%$ or $\pm 2\text{mm}$ for the ovoid-based and source-based corrected TG-43 plan, respectively.

3.3.1.2 Dwell-Time Gradient of 10%

The dwell-times were manually set to 60 seconds for dwell index 1500mm, 60 seconds for dwell index 1495mm, 40 seconds for dwell index 1490mm, and 40 seconds for dwell index 1485mm for both ovoids. The maximum dwell-time gradient for this combination is 10%.

Comparison of MC-simulated isodose distributions and isodoses calculated using TG-43 methodology is shown in Figure 3.22. The CT-MR compatible Fletcher ovoid illustration is to convey the size and placement of the ovoid pair. Although the plane bisects the source dwell-positions, and the source is only at a single location at any given time, the source is not illustrated. Observed in this figure are the qualitative differences in dose due to the perturbing effects of the ovoids accounted for in MC simulations (dashed red lines) and unaccounted for in TG-43 calculations (solid blue line) for a single 2D plane. Quantitatively, 30.1% of the comparison points are within +/- 2% or +/- 2mm.

Comparisons of MC-simulated isodose distributions and isodoses calculated using TG-43 methodology that has been corrected using an ovoid-based correction factor is shown in Figure 3.23a. Observed in this figure are the qualitative differences in dose for MC simulations (dashed red lines) and ovoid-based corrected TG-43 plan (solid blue line) for a single 2D plane. Quantitatively, 96.3% of the comparison points are within +/- 2% or +/- 2mm.

Next, comparisons for MC-simulated isodose distributions and isodoses calculated using TG-43 methodology that has been corrected using a source-based correction factor is shown in Figures 3.23b. This figure illustrates the qualitative differences in dose for MC simulations (dashed red lines) and source-based corrected TG-43 plan (solid blue line) for a single 2D plane. Quantitatively, 100% of the comparison points are within +/- 2% or +/- 2mm. There are no appreciable differences between the MC simulation and source-based corrected TG-43 plan.

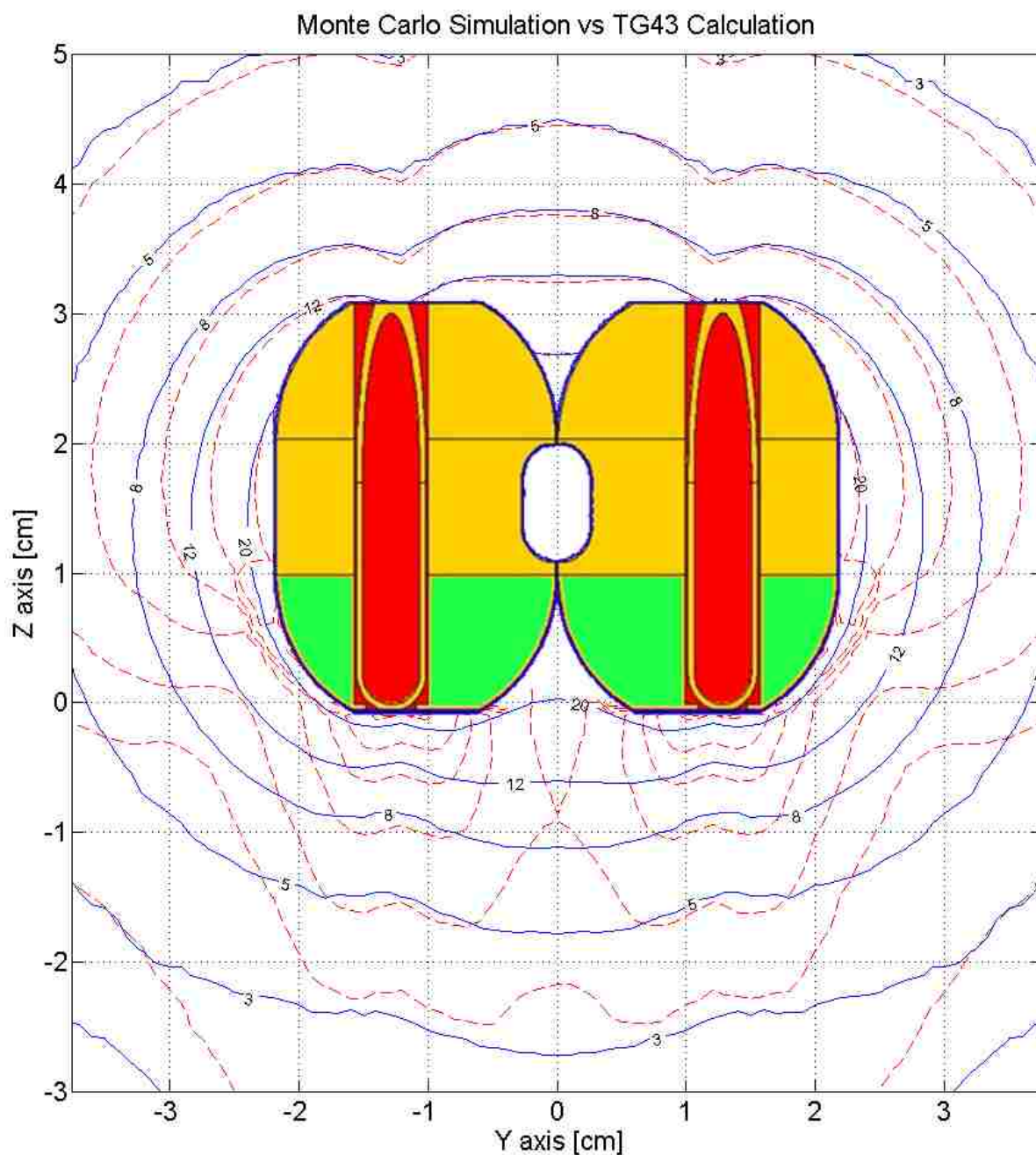


Figure 3.22: Comparison of MC simulation of a mHDR v2 Ir-192 source contained in a modified CT-MR compatible Fletcher ovoid applicator to include a high-Z shield (red) vs. TG-43 calculations for a source in water (blue). Maximum adjacent dwell-time gradient is 10%. Both ovoids are illustrated to show the plane and size of the ovoids. Shown here are absolute dose comparisons, in Gy, for 8 dwell-positions (four per ovoid, dwell-position indices of 1500, 1495, 1490, 1485 mm for each ovoid). Quantitatively, 30.1% of the comparison points are within $\pm 2\%$ or $\pm 2\text{mm}$.

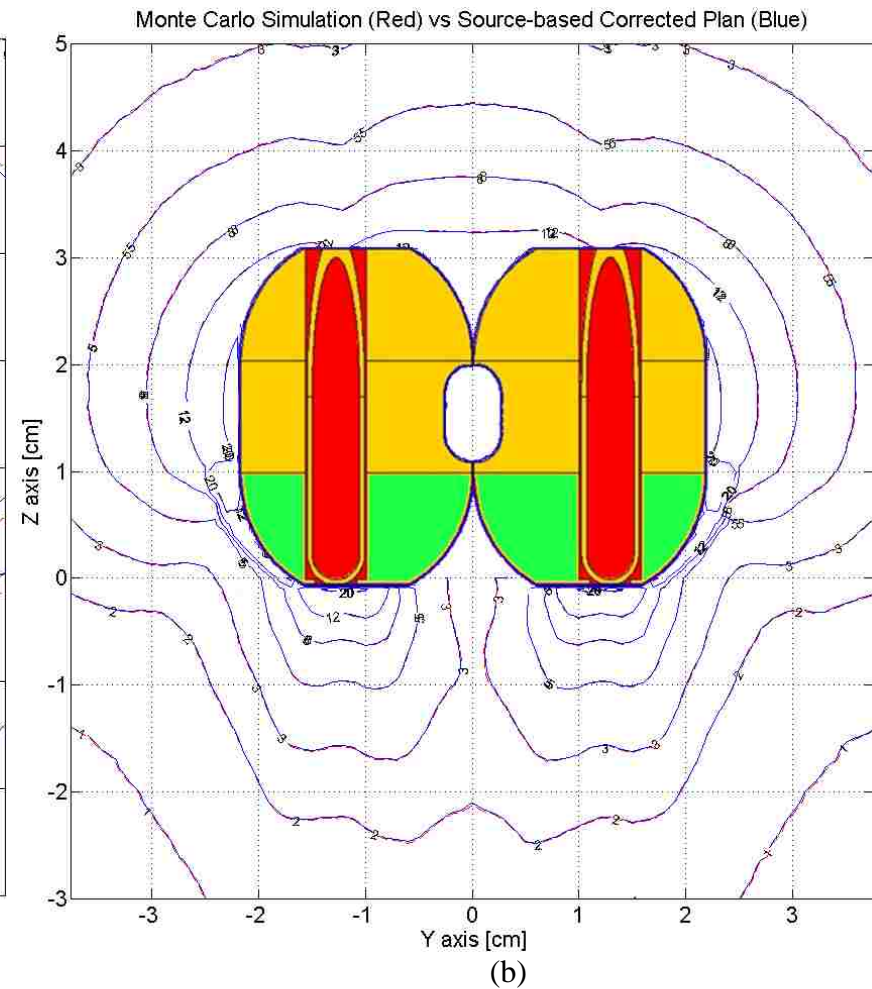
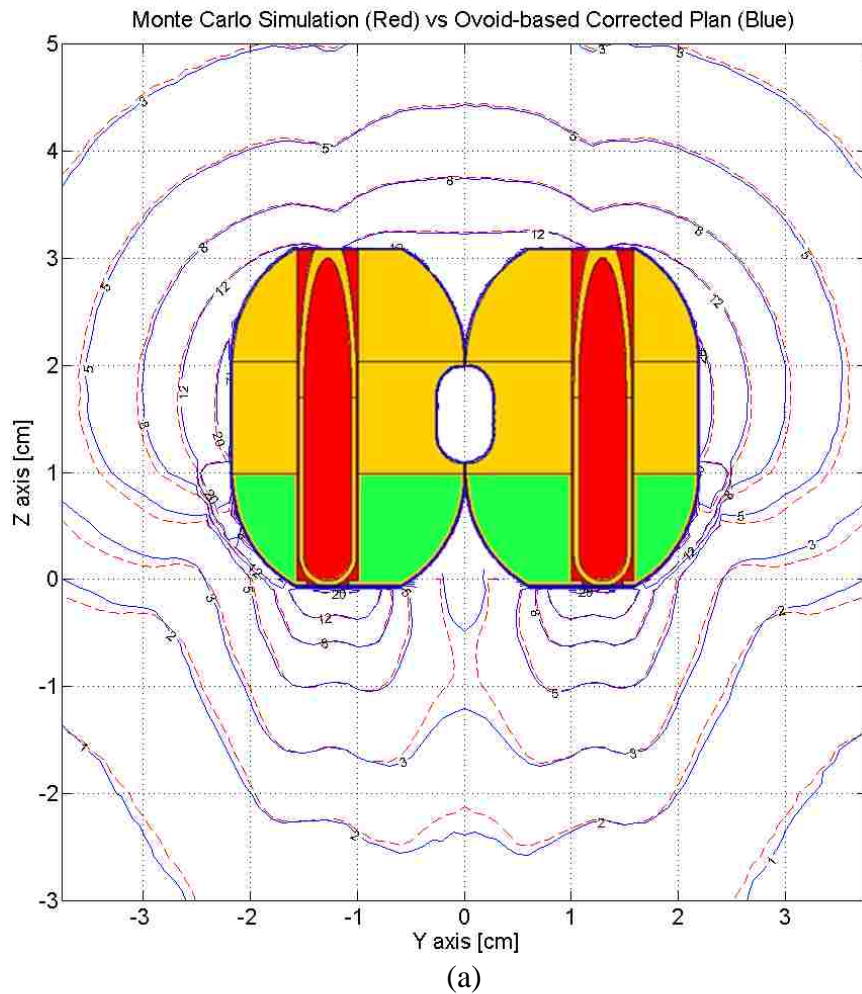


Figure 3.23(a-b): Comparison of MC simulation of a mHDR v2 Ir-192 source contained in a modified CT-MR compatible Fletcher ovoid applicator to include high-Z shield vs. TG-43 corrected plans of a source in water. Maximum adjacent dwell-time gradient is 10%. Shown here are 2D planes bisecting the ovoid pair comparing full MC calculations (red) and isodoses calculated using (a) ovoid-based and (b) source-based corrected TG-43 plan (blue), in Gy, for 8 dwell-positions (four per ovoid, dwell-position indices: 1500, 1495, 1490, 1485 mm for each ovoid). Quantitatively, 96.3% and 100% of the comparison points are within +/- 2% or +/- 2mm for the ovoid-based and source-based corrected TG-43 plan, respectively.

3.3.1.2 Dwell-Time Gradient of 15%

The dwell-times, keeping the same plan, were manually set to 5 seconds for dwell index 1500mm, 7.5 seconds for dwell index 1495mm, 45 seconds for dwell index 1490mm, and 67.5 seconds for dwell index 1485mm for both ovoids. The maximum dwell-time gradient for this combination is 30%.

Comparison of MC-simulated isodose distributions and isodoses calculated using TG-43 methodology is shown in Figure 3.24. The CT-MR compatible Fletcher ovoid illustration is to convey the size and placement of the ovoid pair. Although the plane bisects the source dwell-positions, and the source is only at a single location at any given time, the source is not illustrated. Observed in this figure are the qualitative differences in dose due to the perturbing effects of the ovoids accounted for in MC simulations (dashed red lines) and unaccounted for in TG-43 calculations (solid blue line) for a single 2D plane. Quantitatively, 34.4% of the comparison points are within +/- 2% or +/- 2mm.

Comparisons of MC-simulated isodose distributions and isodoses calculated using TG-43 methodology that has been corrected using an ovoid-based correction factor is shown in Figure 3.25a. Observed in this figure are the qualitative differences in dose for MC simulations (dashed red lines) and ovoid-based corrected TG-43 plan (solid blue line) for a single 2D plane. Quantitatively, 85.9% of the comparison points are within +/- 2% or +/- 2mm.

Next, comparisons for MC-simulated isodose distributions and isodoses calculated using TG-43 methodology that has been corrected using a source-based correction factor is shown in Figures 3.25b. This figure illustrates the qualitative differences in dose for MC simulations (dashed red lines) and source-based corrected TG-43 plan (solid blue line) for a single 2D plane. Quantitatively, 100% of the comparison points are within +/- 2% or +/- 2mm. There are no appreciable differences between the MC simulation and source-based corrected TG-43 plan.

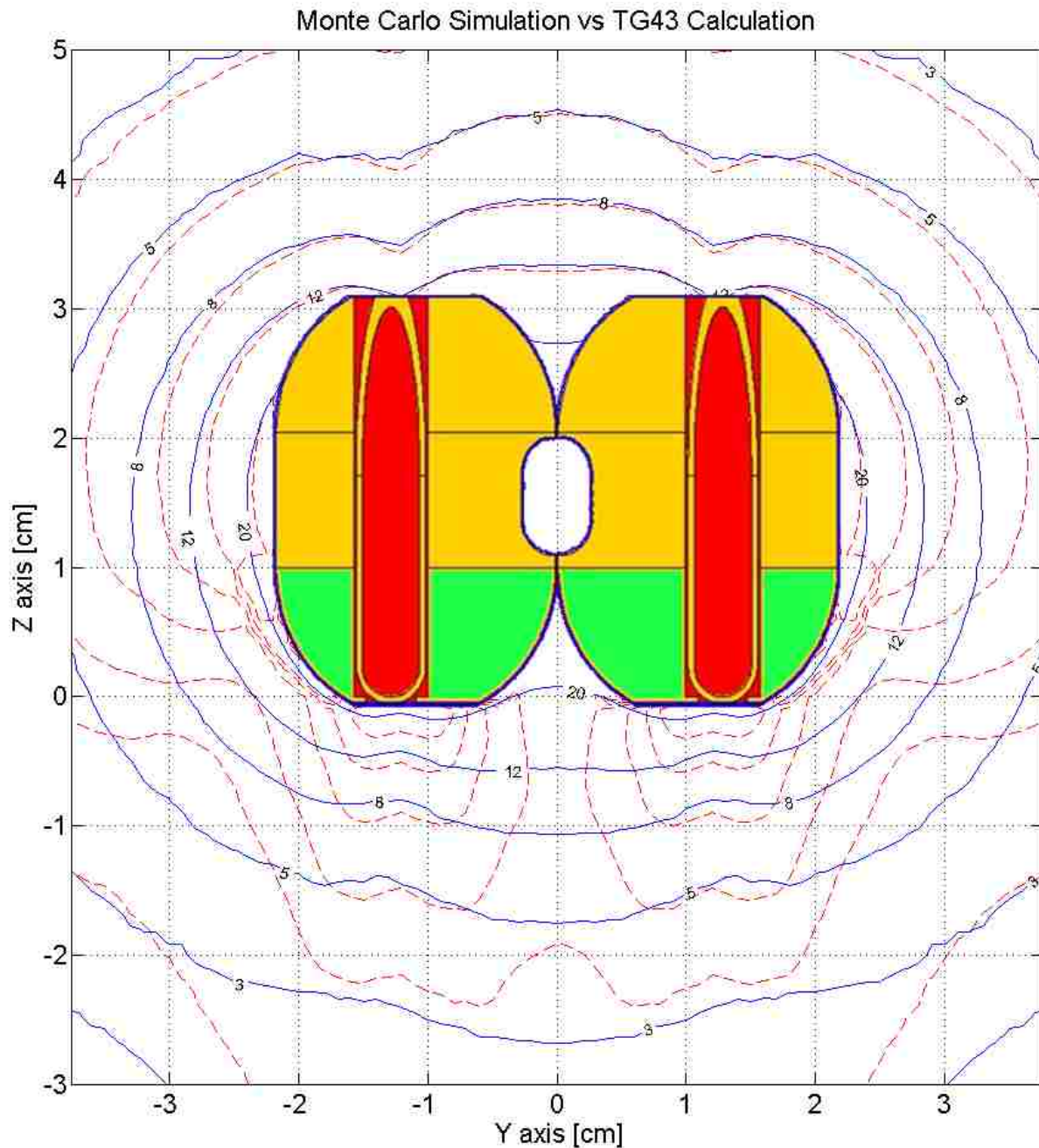
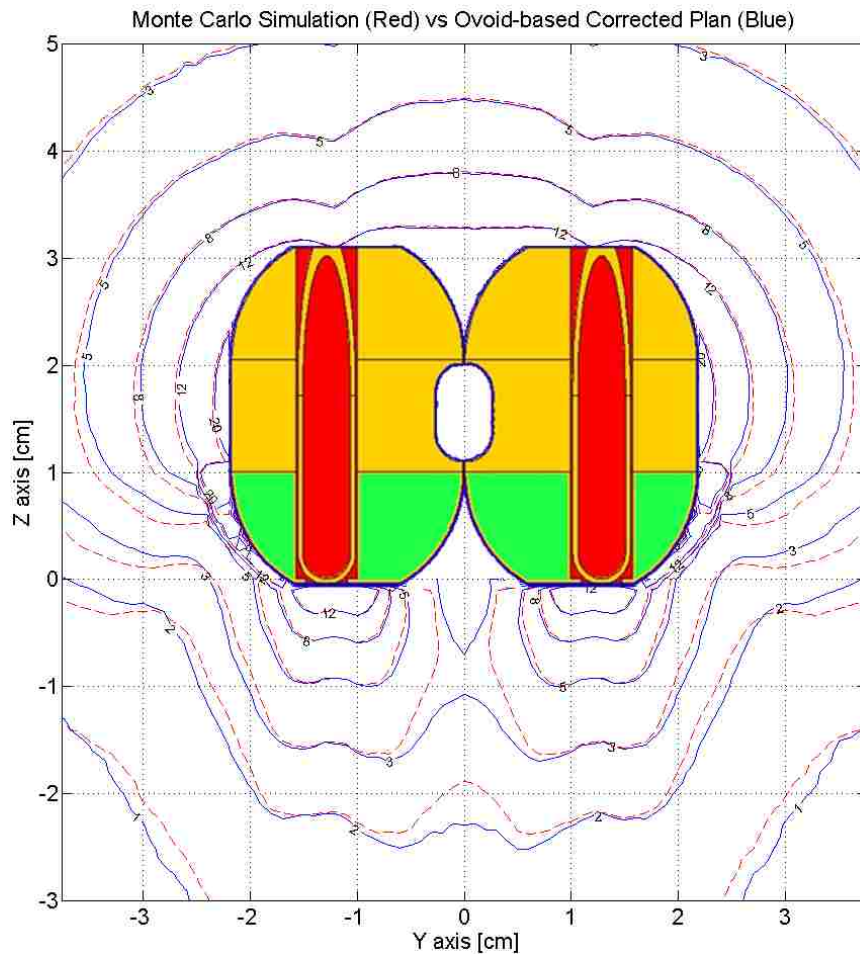
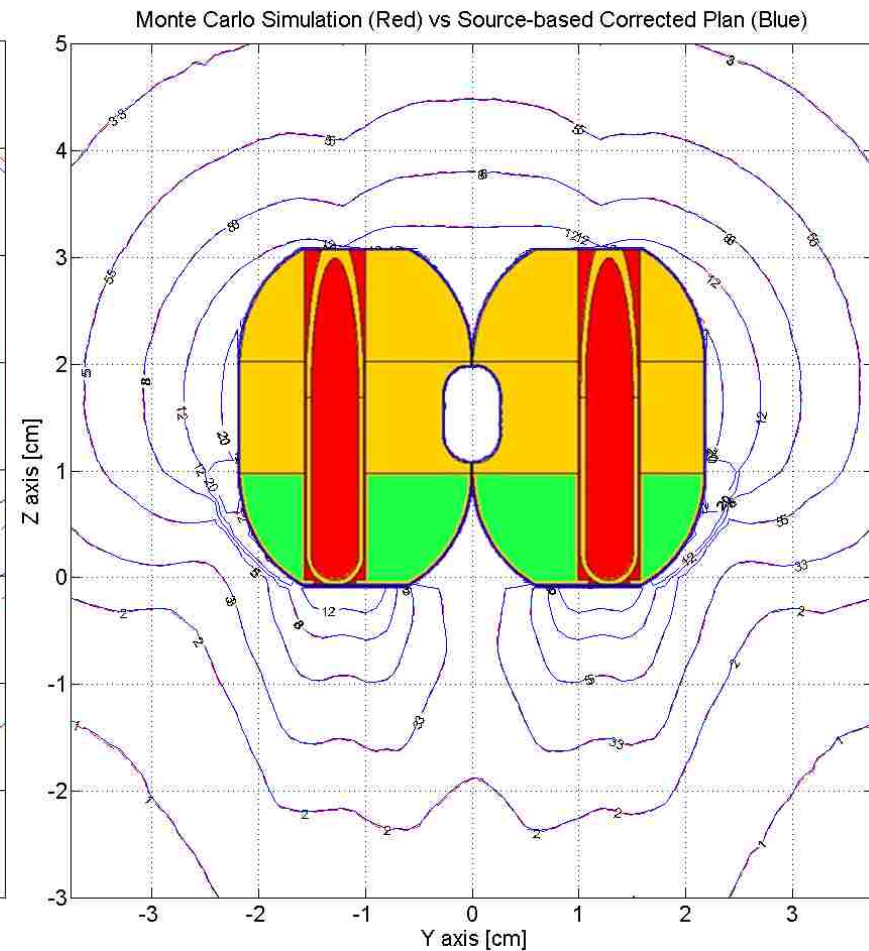


Figure 3.24: Comparison of MC simulation of a mHDR v2 Ir-192 source contained in a modified CT-MR compatible Fletcher ovoid applicator to include a high-Z shield (red) vs. TG-43 calculations for a source in water (blue). Maximum adjacent dwell-time gradient is 15%. Both ovoids are illustrated to show the plane and size of the ovoids. Shown here are absolute dose comparisons, in Gy, for 8 dwell-positions (four per ovoid, dwell-position indices of 1500, 1495, 1490, 1485 mm for each ovoid). Quantitatively, 34.4% of the comparison points are within +/- 2% or +/- 2mm.



(a)



(b)

Figure 3.25: Comparison of MC simulation of a mHDR v2 Ir-192 source contained in a CT modified CT-MR compatible Fletcher ovoid applicator to include high-Z shield vs. TG-43 corrected plans of a source in water. Maximum adjacent dwell-time gradient is 15%. Shown here are 2D planes bisecting the ovoid pair comparing full MC calculations (red) and isodoses calculated using (a) ovoid-based and (b) source-based corrected TG-43 plan (blue), in Gy, for 8 dwell-positions (four per ovoid, dwell-position indices: 1500, 1495, 1490, 1485 mm for each ovoid). Quantitatively, 85.9% and 100% of the comparison points are within $\pm 2\%$ or ± 2 mm for the ovoid-based and source-based corrected TG-43 plan, respectively.

3.3.1.2 Dwell-Time Gradient of 30%

The dwell-times, keeping the same plan, were manually set to 5 seconds for dwell index 1500mm, 7.5 seconds for dwell index 1495mm, 45 seconds for dwell index 1490mm, and 67.5 seconds for dwell index 1485mm for both ovoids. The maximum dwell-time weighting difference for this combination is 30%.

Comparison of MC-simulated isodose distributions and isodoses calculated using TG-43 methodology is shown in Figure 3.26. The CT-MR compatible Fletcher ovoid illustration is to convey the size and placement of the ovoid pair. Although the plane bisects the source dwell-positions, and the source is only at a single location at any given time, the source is not illustrated. Observed in this figure are the qualitative differences in dose due to the perturbing effects of the ovoids accounted for in MC simulations (dashed red lines) and unaccounted for in TG-43 calculations (solid blue line) for a single 2D plane. Quantitatively, 66.9% of the comparison points are within +/- 2% or +/- 2mm.

Comparisons of MC-simulated isodose distributions and isodoses calculated using TG-43 methodology that has been corrected using an ovoid-based correction factor is shown in Figure 3.27a. Observed in this figure are the qualitative differences in dose for MC simulations (dashed red lines) and ovoid-based corrected TG-43 plan (solid blue line) for a single 2D plane. Quantitatively, 34.2% of the comparison points are within +/- 2% or +/- 2mm.

Next, comparisons for MC-simulated isodose distributions and isodoses calculated using TG-43 methodology that has been corrected using a source-based correction factor is shown in Figures 3.27b. This figure illustrates the qualitative differences in dose for MC simulations (dashed red lines) and source-based corrected TG-43 plan (solid blue line) for a single 2D plane. Quantitatively, 100% of the comparison points are within +/- 2% or +/- 2mm. There are no appreciable differences between the MC simulation and source-based corrected TG-43 plan.

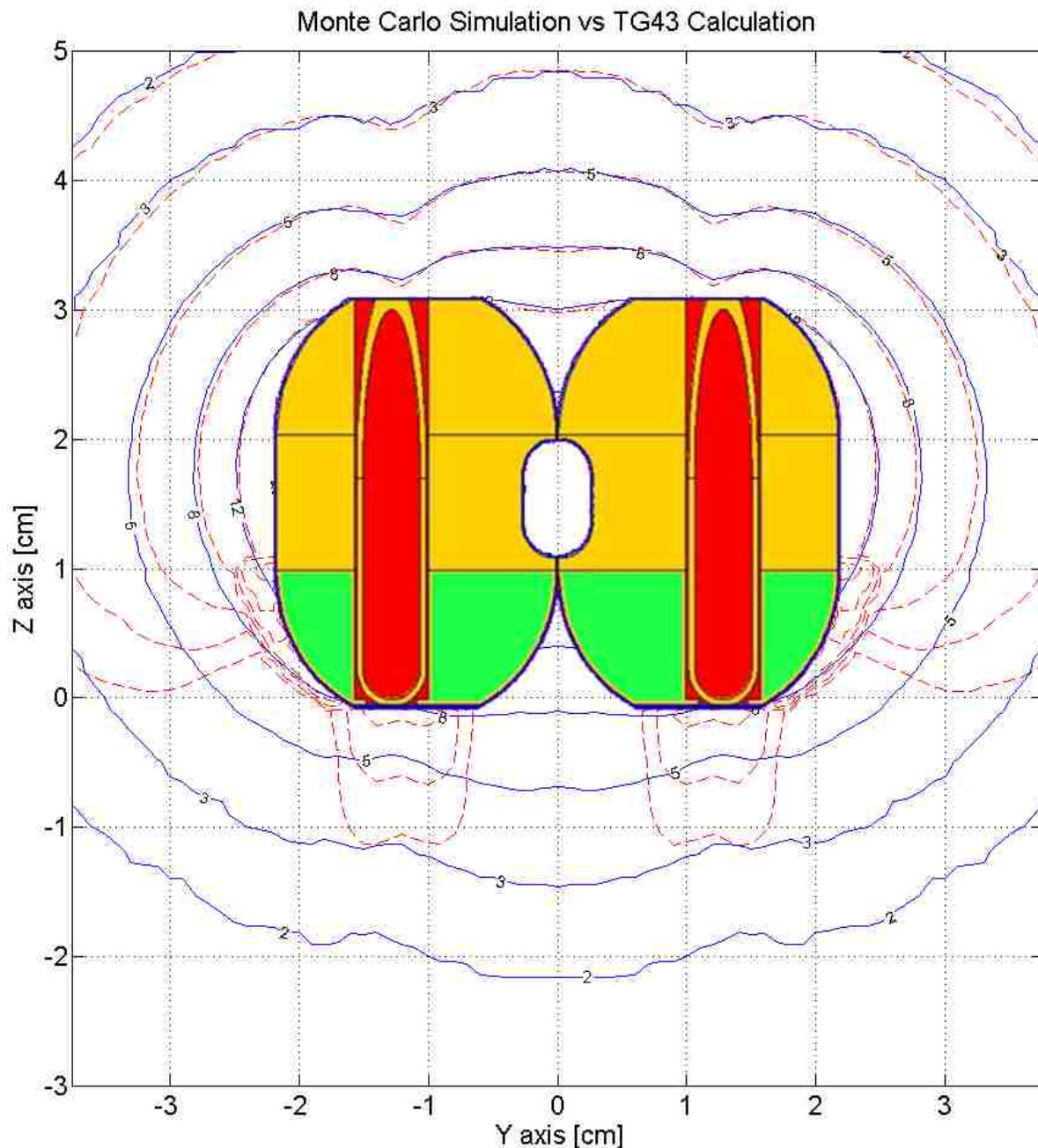


Figure 3.26: Comparison of MC simulation of a mHDR v2 Ir-192 source contained in a modified CT-MR compatible Fletcher ovoid applicator to include a high-Z shield (red) vs. TG-43 calculations for a source in water (blue). Maximum adjacent dwell-time gradient is 30%. Both ovoids are illustrated to show the plane and size of the ovoids. Shown here are absolute dose comparisons, in Gy, for 8 dwell-positions (four per ovoid, dwell-position indices of 1500, 1495, 1490, 1485 mm for each ovoid). Quantitatively, 66.9% of the comparison points are within +/- 2% or +/- 2mm.

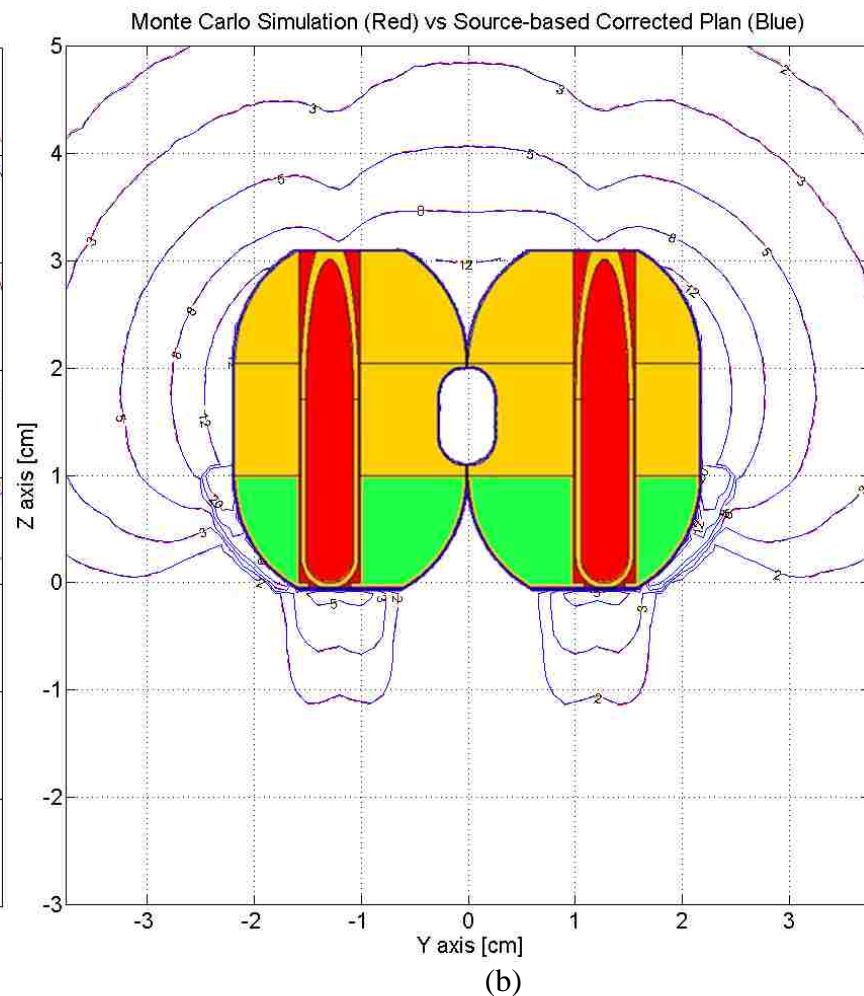
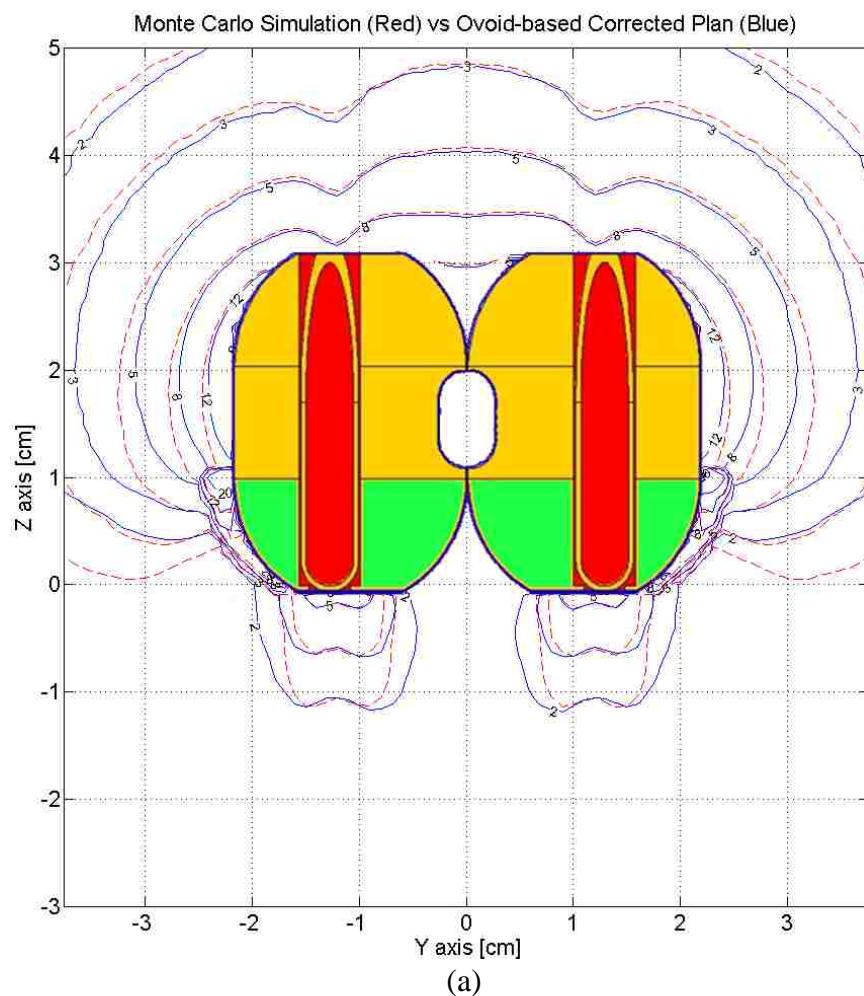


Figure 3.27: Comparison of MC simulation of a mHDR v2 Ir-192 source contained in a modified CT-MR compatible Fletcher ovoid applicator to include high-Z shield vs. TG-43 corrected plans of a source in water. Maximum adjacent dwell-time gradient is 30%. Shown here are 2D planes bisecting the ovoid pair comparing full MC calculations (red) and isodoses calculated using (a) ovoid-based and (b) source-based corrected TG-43 plan (blue), in Gy, for 8 dwell-positions (four per ovoid, dwell-position indices: 1500, 1495, 1490, 1485 mm for each ovoid). Quantitatively, 34.2% and 100% of the comparison points are within $\pm 2\%$ or $\pm 2\text{mm}$ for the ovoid-based and source-based corrected TG-43 plan, respectively.

3.3.1.3 Dwell-time Gradient of 60%

The dwell-times, keeping the same plan, were changed to 5 seconds for dwell index 1500mm, 5 seconds for dwell index 1495mm, 35 seconds for dwell index 1490mm, and 155 seconds for dwell index 1485mm for the left ovoid. The right ovoid dwell-times are the same as the left, but the order of the dwell indices is flipped. The maximum dwell-time gradient for this combination is 60%.

Comparison of MC-simulated isodose distributions and isodoses calculated using TG-43 methodology is shown in Figure 3.28. The CT-MR compatible Fletcher ovoid illustration is to convey the size and placement of the ovoid pair. Although the plane bisects the source dwell-positions, and the source is only at a single location at any given time, the source is not illustrated. Observed in this figure are the qualitative differences in dose due to the perturbing effects of the ovoids accounted for in MC simulations (dashed red lines) and unaccounted for in TG-43 calculations (solid blue line) for a single 2D plane. Quantitatively, 10.5% of the comparison points are within +/- 2% or +/- 2mm. .

Comparisons of MC-simulated isodose distributions and isodoses calculated using TG-43 methodology that has been corrected using an ovoid-based correction factor is shown in Figure 3.29a. Observed in this figure are the qualitative differences in dose for MC simulations (dashed red lines) and ovoid-based corrected TG-43 plan (solid blue line) for a single 2D plane. Quantitatively, 56.8% of the comparison points are within +/- 2% or +/- 2mm.

Next, comparisons for MC-simulated isodose distributions and isodoses calculated using TG-43 methodology that has been corrected using a source-based correction factor is shown in Figures 3.29b. This figure illustrates the qualitative differences in dose for MC simulations (dashed red lines) and source-based corrected TG-43 plan (solid blue line) for a single 2D plane.

Quantitatively, 100% of the comparison points are within +/- 2% or +/- 2mm. There are no appreciable differences between the MC simulation and source-based corrected TG-43 plan.

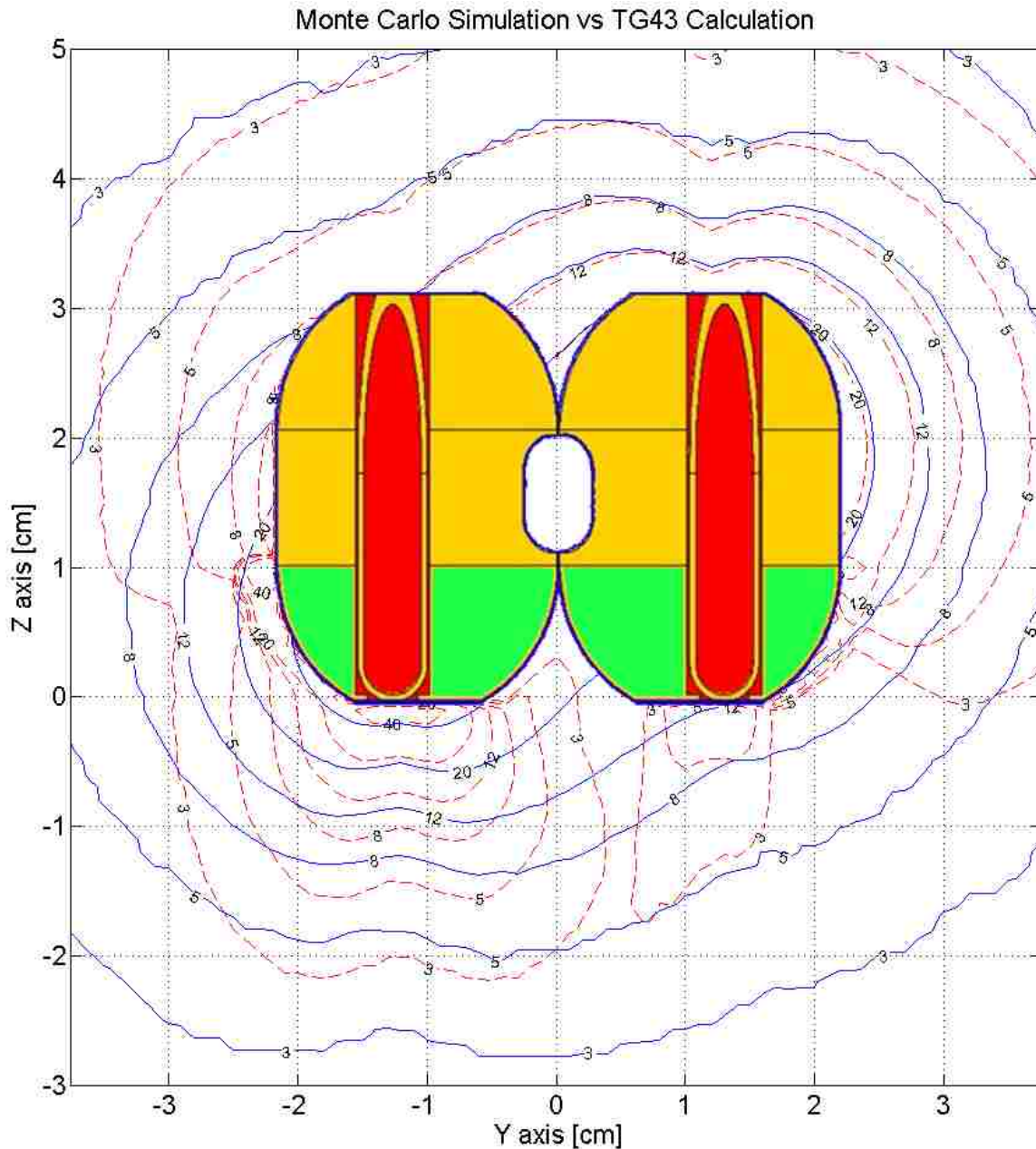


Figure 3.28: Comparison of MC simulation of a mHDR v2 Ir-192 source contained in a modified CT-MR compatible Fletcher ovoid applicator to include a high-Z shield (red) vs. TG-43 calculations for a source in water (blue). Maximum adjacent dwell-time gradient is 60%. Both ovoids are illustrated to show the plane and size of the ovoids. Shown here are absolute dose comparisons, in Gy, for 8 dwell-positions (four per ovoid, dwell-position indices of 1500, 1495, 1490, 1485 mm for each ovoid). Quantitatively, 10.5% of the comparison points are within +/- 2% or +/- 2mm.

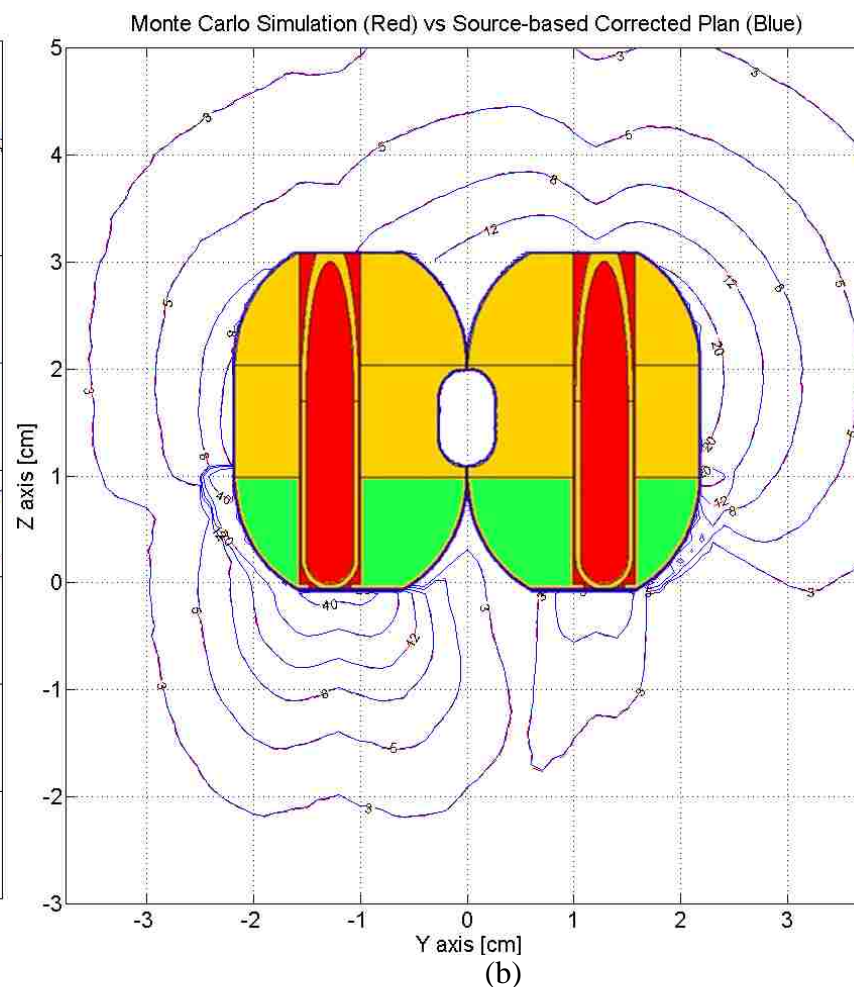
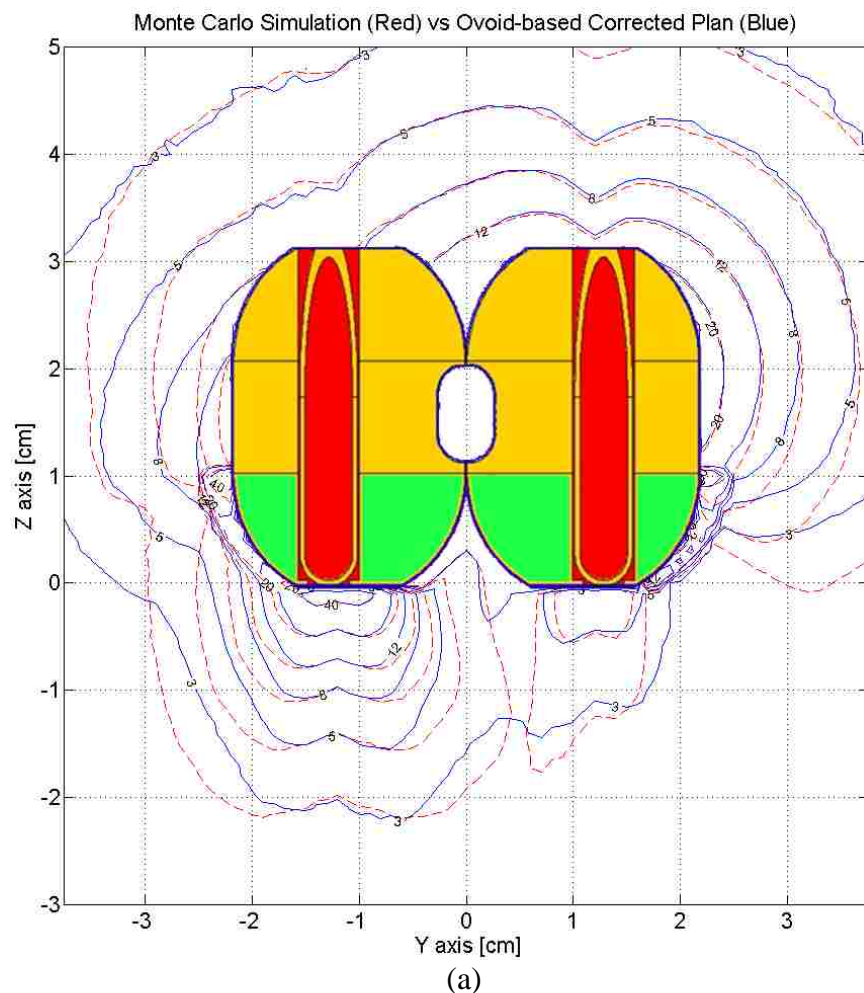


Figure 3.29(a-b): Comparison of MC simulation of a mHDR v2 Ir-192 source contained in a modified CT-MR compatible Fletcher ovoid applicator to include high-Z shield vs. TG-43 corrected plans of a source in water. Maximum adjacent dwell-time gradient is 60%. Shown here are 2D planes bisecting the ovoid pair comparing full MC calculations (red) and isodoses calculated using (a) ovoid-based and (b) source-based corrected TG-43 plan (blue), in Gy, for 8 dwell-positions (four per ovoid, dwell-position indices: 1500, 1495, 1490, 1485 mm for each ovoid). Quantitatively, 56.8% and 100% of the comparison points are within $\pm 2\%$ or $\pm 2\text{mm}$ for the ovoid-based and source-based corrected TG-43 plan, respectively.

3.3.3 Summary of Results

Table 3.1 lists the agreement (percent dose and DTA) for comparisons of MC simulated and TG-43 calculated 3D dose distributions utilizing a comparison dose cut-off of 50 cGy isodose line. These results indicate that a TG-43 isodose calculation of a mHDR v2 Ir-192 source in water agrees within the uncertainty of the MC simulation for any combination of dwell-time gradients. Although ovoid- and source- based corrected plans had better agreement than TG-43 calculations with full MC datasets, the TG-43 calculations agree within the MC uncertainty. For every dwell-time combination, the source- based corrected plan agreed 100% with the full MC dataset.

Table 3.1: Agreement of MC simulation with TG-43 data set, Ovoid-correction plan, and Source-correction plan. Agreement metric: 2% or 2mm.

∇	MC versus:	Agreement (2%/2mm)
0%	TG-43	99.8%
	Ovoid-Correction plan	100%
	Source-Correction plan	100%
30%	TG-43	99.7%
	Ovoid-Correction plan	99.9%
	Source-Correction plan	100%
60%	TG-43	99.0%
	Ovoid-Correction plan	99.7%
	Source-Correction plan	100%
70%	TG-43	99.6%
	Ovoid-Correction plan	99.9%
	Source-Correction plan	100%

Table 3.2 lists the agreement for comparisons between the simulations from the modified MC model which includes high-Z inhomogeneities. This high-Z shield alteration to the CT-MR compatible Fletcher ovoid model was to test the robustness of the correction schemes for dose distributions that were relatively different to TG-43 dose calculations of a single source in water. This modification was studied since the MC simulations of a single source within the CT-MR compatible Fletcher ovoid agreed within the MC uncertainty with the TG-43 calculations of a

source in water. As expected, there was not a single MC simulation that agreed within criteria when compared to the full MC dataset. There is relatively higher agreement with the plan having a ∇_{dt} equal to 30. This can be a contributed to the dwell-time combination being utilized for this comparison. This plan has the highest dwell-times at the dwell-positions farther from the shields and relatively low dwell-times near the shields. The source- based corrected plans agreed 100% with the full MC simulations. Agreement was not affected on the difference between the TG-43 calculations compared to MC. It seems as if the limiting factor for agreement was due to the maximum ∇_{dt} . Once the maximum ∇_{dt} was above 10%, the ovoid- based correction scheme began to fail.

Table 3.2: Agreement of modified MC model simulation with TG-43 data set, Ovoid-correction plan, and Source-correction plan. Agreement metric: 2% or 2mm.

∇	MC versus:	Agreement (2%/2mm)
0%	TG-43	13.2%
	Ovoid-Correction plan	100%
	Source-Correction plan	100%
5%	TG-43	26.6%
	Ovoid-Correction plan	99.2%
	Source-Correction plan	100%
10%	TG-43	30.1%
	Ovoid-Correction plan	96.3%
	Source-Correction plan	100%
15%	TG-43	34.4%
	Ovoid-Correction plan	85.9%
	Source-Correction plan	100%
30%	TG-43	67.0%
	Ovoid-Correction plan	59.1%
	Source-Correction plan	100%
60%	TG-43	10.5%
	Ovoid-Correction plan	56.8%
	Source-Correction plan	100%

3.4 Discussions

Dose perturbations resulting from the ICBT CT-MR compatible Fletcher applicator set were relatively small and agreed to TG-43 calculations for a source in water within the uncertainty of the MC simulations (>99% points within +/-2% dose or 2mm DTA). This is due to the main ovoid heterogeneity being polyphenylsulfone with a density very similar to water. This makes the entire MC model fairly homogeneous. Thus, a correction scheme is not necessary.

The “shielded” ovoid applicator set did not agree to TG-43 calculations for a source in water. This MC model was introduced to test the robustness of both correction schemes (ovoid- or source-based). Dose perturbations were due to a significant ovoid heterogeneity. The tungsten shield in this study is relatively larger than clinically-available ovoid shields. Correction factors were applied to TPS exported plans by developing software written in Matlab. Once the DICOM compatible files were compiled into a Matlab format, the software extracted treatment parameters such as dwell-times, dwell-coordinates, source activity, dose grid size, and dose grid axis indexes. These parameters were then applied to the MC simulation to generate an equivalent treatment plan.

Plans generated by Oncentra TPS with a maximum dwell-time gradient less than 10% can be corrected utilizing either the ovoid-based or source-based correction methods to agree with full simulated Monte Carlo datasets to within +/- 2% or +/- 2mm DTA. Although, dwell-time combinations utilized in this study with a maximum dwell-time gradient above 10% is a threshold for the ovoid- based correction scheme to correct the TG-43 calculation. The source-based correction method consistently results in 100% agreement between a corrected plan and the equivalent MC generated plan.

For brachytherapy plans with equivalent dwell-times, as typically found with plans generated using the Manchester system, either correction scheme is appropriate. Treatment plans that generate a “patient” specific dose distribution, rather than the dose distribution inherent to the tandem and ovoid applicator (*i.e.* pear shape), to cover the disease need to utilize the source-based correction method. A “patient” specific dose distribution is commonly generated utilizing the GEC ESTRO dose specification.

It should be noted that this correction scheme requires a CT dataset that does not contain high-Z artifacts. This criterion is made possible only with Nucletron’s Anatomically Adaptive Applicator. Currently, investigations are being made that by using a MVCT (as opposed to a kVCT) scan, high-Z artifacts can be reduced significantly.

Chapter 4 Conclusions

4.1 Summary of Results

This study was able to confirm the absolute dose distributions calculated by MCNPX for a CT-MR compatible ICBT applicator. We demonstrated that our MC modeling of a paired ovoid set (without surrogate shield) is accurate and robust enough to simulate dose distributions with sufficient accuracy within the context of this study.

Ovoid- and source-based correction factors were created for a clinically utilized ovoid paired set (with and without shield surrogate) for four dwell positions per ovoid with a 5mm step-size. In all, there were two ovoid- based correction factors for each ovoid (left and right) and eight source- based correction factors for each individual dwell positions.

Plans calculated utilizing Oncentra were corrected to include dose perturbations from the “shielded” ovoid set. The ovoid- based correction factors improved TG-43 calculated plans with maximum dwell-time gradients of less than 10%. The source- based correction scheme consistently generated results that agreed 100% with the full MC simulation.

4.2 Evaluation of Hypothesis

“A 3D Monte Carlo-simulated dose distribution of the ovoid contribution to a cervical intracavitary brachytherapy (ICBT) treatment administered via Nucletron’s Fletcher CT-MR ovoid applicator (Nucletron Corporation, Veenendaal, The Netherlands), modeled with and without a rectal shield surrogate, will agree, within criteria, with the dose distribution resulting from an equivalent treatment calculated using AAPM Task Group-43 (TG-43) methodology when corrected for heterogeneities using pre-calculated MC correction factors applied (a) to individual source dwell-positions and (b) individual ovoids acting as multi-source surrogates for varying adjacent dwell-time gradients (∇_{dt}). Criteria are defined as agreement within +/- 2% or +/- 2 mm distance-to-agreement.”

The results of this research support part of the hypothesis that applicator correction factors calculated for individual source, as opposed to ovoid, positions are required to predict intracavitary brachytherapy dose distributions that agree with Monte Carlo simulations to within 2% dose or 2mm DTA for dwell-time gradients greater than 10%. However, for dwell-time gradients below 10%, either correction scheme (ovoid- or source- based) will result in a dose distribution that agrees within criteria.

4.3 Future Work

Since dose grids larger than $7 \times 7 \times 7 \text{cm}$ (1mm^3 resolution) are too large to process using the Gridconv auxiliary MCNPX program [11], another method should be sought out to convert the MC output to a format that can be integrated into the process utilized in this study. A larger MC dose grid on the order of 16cm^3 should be processed in order to account for translation of the sources in a $10 \times 10 \times 10 \text{cm}^3$ dose grid. This will allow for the corrected dose distribution to be added to the tandem contribution of the ICBT procedure without losing dose information beyond the distal end of the tandem.

The method presented in this study utilizing MATLAB does not allow for a multi-frame DICOM file to be generated. Another strategy should be sought out so that the corrected dose distribution can be imported to Oncentra in DICOM format for plan analysis.

Nucletron's next generation TPS utilizes Collapsed Cone Convolution to calculate patient-specific dose distributions. Although the CCC algorithm cannot handle large perturbations in dose due to high-Z heterogeneities like those introduced by intra-ovoid shielding. The methods presented in this work can be used to correct these dose distributions for the effect of ovoid shielding, thus providing an accurate representation of dose delivered to a patient undergoing ICBT.

References

1. Khan, F.M., *The physics of radiation therapy*. 3rd ed. 2003, Philadelphia: Lippincott Williams & Wilkins. 1 v. (various pagings), 16 p. of plates.
2. Gerbaulet, A., et al., *The GEC ESTRO Handbook of Brachytherapy*. 2002.
3. Datta, N.R., et al., *Problems in reporting doses and volumes during multiple high-dose-rate intracavitary brachytherapy for carcinoma cervix as per ICRU Report 38: a comparative study using flexible and rigid applicators*. *Gynecol Oncol*, 2003. **91**(2): p. 285-92.
4. Gao, M., et al., *3D CT-based volumetric dose assessment of 2D plans using GEC-ESTRO guidelines for cervical cancer brachytherapy*. *Brachytherapy*, 2010. **9**(1): p. 55-60.
5. Nag, S., et al., *The American Brachytherapy Society recommendations for high-dose-rate brachytherapy for carcinoma of the cervix*. *Int J Radiat Oncol Biol Phys*, 2000. **48**(1): p. 201-11.
6. Nath, R., et al., *Dosimetry of interstitial brachytherapy sources: recommendations of the AAPM Radiation Therapy Committee Task Group No. 43*. *American Association of Physicists in Medicine*. *Med Phys*, 1995. **22**(2): p. 209-34.
7. Price, M.J., et al., *Dosimetric evaluation of the Fletcher-Williamson ovoid for pulsed-dose-rate brachytherapy: a Monte Carlo study*. *Phys Med Biol*, 2005. **50**(21): p. 5075-87.
8. Kapur, A., et al., *Monte Carlo calculations of electron beam output factors for a medical linear accelerator*. *Phys Med Biol*, 1998. **43**(12): p. 3479-94.
9. Daskalov, G.M., E. Loffler, and J.F. Williamson, *Monte Carlo-aided dosimetry of a new high dose-rate brachytherapy source*. *Med Phys*, 1998. **25**(11): p. 2200-8.
10. Rivard, M.J., J.L. Venselaar, and L. Beaulieu, *The evolution of brachytherapy treatment planning*. *Med Phys*, 2009. **36**(6): p. 2136-53.
11. Waters, L.S., *MCNPX User's Manual Version 2.6.0*. 2008. **Los Alamos, NM: Los Alamos National Laboratory**.
12. Williamson, J.F. and A.S. Meigooni, *Quantitative dosimetry methods in brachytherapy*. in *Brachytherapy Physics*., 1995. **Medical Physics Publishing, Madison, WI**.
13. Price, M.J., et al., *Dose perturbation due to the polysulfone cap surrounding a Fletcher-Williamson colpostat*. *J Appl Clin Med Phys*, 2010. **11**(1): p. 3146.
14. Price, M.J. and F. Mourtada, *A 3D Forward Treatment Planning Algorithm using Pre-calculated Monte Carlo Data Sets for HDR/PDR Tandem and Ovoid Intracavitary Systems* in *American Brachytherapy Society Annual Meeting*. May 2007: Chicago, IL.

15. Rivard, M.J., et al., *An approach to using conventional brachytherapy software for clinical treatment planning of complex, Monte Carlo-based brachytherapy dose distributions*. Med Phys, 2009. **36**(6): p. 1968-75.
16. Price, M.J., et al., *The Imaging and Dosimetric Capabilities of a Novel CT/MR-Suitable, Anatomically Adaptive, Shielded HDR/PDR Intracavitary Brachytherapy Applicator for the Treatment of Cervical Cancer*. Med Phys, 2008. **35**: p. 2855-2856.
17. Price, M.J., et al., *Monte Carlo model for a prototype CT-compatible, anatomically adaptive, shielded intracavitary brachytherapy applicator for the treatment of cervical cancer*. Med Phys, 2009. **36**(9): p. 4147-55.
18. Glasgow, G.P. and L.T. Dillman, *Specific gamma-ray constant and exposure rate constant of ^{192}Ir* . Med Phys, 1979. **6**(1): p. 49-52.
19. Williamson, J.F. and Z. Li, *Monte Carlo aided dosimetry of the microelectron pulsed and high dose-rate ^{192}Ir sources*. Med Phys, 1995. **22**(6): p. 809-19.
20. Karaiskos, P., et al., *Monte Carlo dosimetry of a new ^{192}Ir pulsed dose rate brachytherapy source*. Med Phys, 2003. **30**(1): p. 9-16.
21. Ballester, F., et al., *Evaluation of high-energy brachytherapy source electronic disequilibrium and dose from emitted electrons*. Med Phys, 2009. **36**(9): p. 4250-6.
22. Niroomand-Rad, A., et al., *Radiochromic film dosimetry: recommendations of AAPM Radiation Therapy Committee Task Group 55*. American Association of Physicists in Medicine. Med Phys, 1998. **25**(11): p. 2093-115.
23. Tiago A. Ferreira and W. Rasband. *The ImageJ User Guide. Version 1.43*. 2010; Available from: <http://rsb.info.nih.gov/ij/docs/user-guide.pdf>.

Appendix 1 Process Digitized Film (.tiff images) and Calculate Standard Deviation

```
% This processes .tiff images and calculates the average standard deviation
% and the standard deviation of the standard deviation...
% Input: 3 processed (scanned) RCF datasets as .tiff images
% Import films
D1 = double(imread('disease1001.tif'));
D2 = double(imread('disease2001.tif'));
D3 = double(imread('disease3001.tif'));
% Red channel
gFilmOne1=D1(:,:,1);
gFilmOne2=D2(:,:,1);
gFilmOne3=D3(:,:,1);
% Smooth
gFilmOne1=wiener2(gFilmOne1);
gFilmOne2=wiener2(gFilmOne2);
gFilmOne3=wiener2(gFilmOne3);
% Crop.. index specified by location on flat-bed scanner
gFilmOne1crop=gFilmOne1(150:580,150:580);
gFilmOne2crop=gFilmOne2(150:580,150:580);
gFilmOne3crop=gFilmOne3(150:580,150:580);
% Resolution
info = imfinfo('disease1001.tif');
xresolution = info.XResolution;
yresolution = info.YResolution;
xres_setting = (2.54)/xresolution;
yres_setting = (2.54)/yresolution;
% Interpolate to 1mm^3
[rowsfilm colsfilm] = size(gFilmOne1crop);
xx = 0 : xres_setting : xres_setting * (rowsfilm - 1);
yy = 0 : yres_setting : yres_setting * (colsfilm - 1);
xend = floor(xres_setting * (rowsfilm - 1));
yend = floor(yres_setting * (colsfilm - 1));
XI = 0:0.1:xend;
YI = 0:0.1:yend;
% Film 1
for i = 1:(11*10+1);
    for j = 1:(11*10+1);
        iFilmOne(j,i) = interp2(yy,xx,gFilmOne1crop,XI(i),YI(j),'*linear');
    end
end;
% Crop to 101 x 101 dose grid to match MC
gFilmOne1_interp = iFilmOne(1:101,11:111);
% Convert scanner values to absolute dose (calibration curve)
gF1 = arrayfun(@(x) 0.000000021448218*x.^2 - 0.002274568204140*x +...
    61.167641732761900, gFilmOne1_interp);
% Film 2
```

```

for i = 1:(11*10+1);
    for j = 1:(11*10+1);
        iFilmOne(j,i) = interp2(yy,xx,gFilmOne2crop,XI(i),YI(j),'*linear');
    end
end;
%Crop to 101 x 101 dose grid to match MC
gFilmOne2_interp = iFilmOne(1:101,11:111);
%Convert scanner values to absolute dose (calibration curve)
gF2 = arrayfun(@(x) 0.000000021448218*x.^2 - 0.002274568204140*x +...
    61.167641732761900, gFilmOne2_interp);
%Film 3
for i = 1:(11*10+1);
    for j = 1:(11*10+1);
        iFilmOne(j,i) = interp2(yy,xx,gFilmOne3crop,XI(i),YI(j),'*linear');
    end
end;
%Crop to 101 x 101 dose grid to match MC
gFilmOne3_interp = iFilmOne(1:101,11:111);
%Convert scanner values to absolute dose (calibration curve)
gF3 = arrayfun(@(x) 0.000000021448218*x.^2 - 0.002274568204140*x +...
    61.167641732761900, gFilmOne3_interp);
%average data sets
mean=(gF1+gF2+gF3)/3;
%Number of .tiff images
N=3;
sigma_map=zeros(101,101);
count=0;
%calculate sigma
for i = 1:101,
    for j = 1:101,
        x_mean=mean(i,j);
        x_i_1 = gF1(i,j);
        x_i_2 = gF2(i,j);
        x_i_3 = gF3(i,j);
        l = (x_i_1 - x_mean)^2;
        m = (x_i_2 - x_mean)^2;
        n = (x_i_3 - x_mean)^2;
        numerator = l+m+n;
        sigma_map(i,j)= sqrt(numerator/(N-1));
        count = count+sigma_map(i,j);
    end
end
sigma_map_mean = (sigma_map/sqrt(N));
%standard deviation of the average standard deviation
average_of_sigmas = count/(101*101);
summation=0;
for i = 1:101,
    for j = 1:101,

```

```
x_i=sigma_map_mean(i,j);  
x_mean = average_of_sigmas;  
  
difference=(x_i - x_mean)^2;  
  
    summation = summation+difference;  
end  
end  
standard_deviation_of_sigma = sqrt(summation/(101*101));
```

Appendix 2 Compile Dose Grid from a RD DICOM File

```
%Input:RD_DICOM (.dcm extension) from TPS
%DICOM scales the dose grid down, obtain scaling factor using dicominfo to
%scale back into actual values
    factor = dicominfo('filename.dcm');
    dosegridscaling = double(factor.DoseGridScaling);
%Dose grid dimensions
    frames = factor.NumberOfFrames;
    rows = factor.Rows;
    columns = factor.Columns;
%Create a matrix the same size as DICOM dose grid
    Empty = double(zeros(frames,rows,columns));
%Compile all 2D frames to develop 3D dose grid
    for i = 1:frames,
        b = double(dicomread('filename.dcm','frames',i));
        Empty(:,i,:) = b(101:-1:1, :, :) * dosegridscaling;
    end;
%Name Dose grid, and save it as .mat file
    RENAME = Empty;
    save('RENAME','RENAME');
%end
```

Appendix 3 Dose Tolerance and Distance to Agreement Algorithm

```
% Calculates the percentage of points that agree within percent tolerance
% of absolute dose or able to locate a valid point within specified distance.
% Input: 2 matrices the same size (measured, calculated)
% Resolution must be 1mm^3
% DTA specified in mm, Dose tolerance specified in percent (i.e. 2 %)
% Low limit threshold specified in same unit as dose grid values
measured = compare1;
calculated = compare2;
DTA = 3;
tolerance = 3;
limit = 3;
% Pass/fail matrix, same size as input
% Begins with all 10s, when a point passes, replaces it with value of 1.
% (i.e. points above 1 fail)
size1 = size(measured);
passfail = zeros(size1(1),size1(2),size1(3));
passfail = passfail + 10;
% tallies = 0 to begin
passtally = 0;
falsetally = 0;
totaltally = 0;
highlimit = 0;
lowlimit = 0;
blackbox = 0;
%Begin DTA algorithm
for i = 1:size1(1);
    for j = 1:size1(2);
        for k = 1:size1(3);
% Condition statements to kickout points below limit threshold,
% above high limit threshold, or within a blackbox (for this study,
% non-relative clinical points were set to negative values)
            if calculated(i,j,k) <= limit && calculated(i,j,k) >= 0,
                lowlimit = lowlimit + 1;
            else
                if measured(i,j,k) <= limit && measured(i,j,k) >= 0,
                    lowlimit = lowlimit + 1;
                else
                    if calculated(i,j,k) > 15 || measured(i,j,k) > 15 ,
                        highlimit = highlimit + 1;
                    else
                        if calculated(i,j,k) <= 0 || measured(i,j,k) <= 0,
                            blackbox = blackbox + 1;
                        else
% If point does not fall within condition statements above, it is used as a
% valid comparison point for agreement analysis.
                            totaltally = totaltally + 1;
                        end
                    end
                end
            end
        end
    end
end
```

```

% Check if corresponding pixel is within tolerance. If sufficient, no more
% comparisons are needed and the process starts over, otherwise.. continue
    if abs((((calculated(i, j, k) - measured(i, j, k))/(measured(i, j, k))*100)) <= tolerance,
        passfail(i,j,k) = 1;
        passtally = passtally + 1;
    else
%Begin "Neighborhood" search for value within tolerance
% Define indexes that construct neighborhood
    startrow = i - DTA;
    endrow = i + DTA;
    startcol = j - DTA;
    endcol = j + DTA;
    startheight = k - DTA;
    endheight = k + DTA;
% Boundary fix
    if startrow <= 0, startrow = i; end
    if endrow > size1(1), endrow = size1(1); end
    if startcol <= 0, startcol = j; end
    if endcol > size1(2), endcol = size1(2); end
    if startheight <= 0, startheight = k; end
    if endheight > size1(3), endheight = size1(3); end
%Neighborhood of pixels of measured with respect to calc(i, j, k).
    neighborhood = measured(startrow:endrow,startcol:endcol,startheight:endheight);
    numrows = endrow - startrow + 1;
    numcols = endcol - startcol + 1;
    numheight = endheight - startheight + 1;
% Minigrid is small version of pass/fail conditions
% Caution, kickout conditions are not evaluated for neighborhood search
    minigrid = zeros(numrows,numcols,numheight);
    Dosediff_criterion = zeros(numrows,numcols,numheight);
% Search neighborhood for a point that passes both criterions
    for r = 1:numrows;
        for s = 1:numcols;
            for t = 1:numheight;
                calcpt = calculated(i,j,k);
%Step pixels from end to start.
                rowstep = (r - (DTA + 1));
                colstep = (s - (DTA + 1));
                heightstep = (t - (DTA + 1));
                newrow = i - rowstep;
                newcol = j - colstep;
                newheight = k - heightstep;
%Check distance of neighborhood pixel.
                distance = sqrt(((i-newrow)^2 + (j-newcol)^2 + (k-newheight)^2));
%Check if corresponding pixel is within tolerance.
                Dosediff_criterion(r,s,t) = abs((((calcpt - neighborhood(r,s,t))...
                    /(neighborhood(r,s,t))*100));
                if (distance <= DTA) && (Dosediff_criterion(r,s,t) <= tolerance),

```

```

        minigrid(r,s,t) = 1;
    else
        minigrid(r,s,t) = 5;
    end;
end;
end;
end;
%End "Neighborhood" search for value within tolerance
    passfail(i, j, k) = min(min(min(minigrid)));
%If passfail point passes, add 1 to passtally, if not
%add one to falsetally
    if passfail(i,j,k) <= 1,
        passtally = passtally + 1;
    else
        falsetally = falsetally + 1;
    end;
end;
% End kickoff 'if' conditional statements
end;
end;
end;
end;
% End i,j,k loops
end;
end;
end;
passrate = floor((passtally/(passtally+falsetally))*100);
%Send passrate to command window
passrate

```

Appendix 4 Define Plan Parameters from RP, RD DICOM Files

```
% for a Plan Consisting of Two Ovoids with 6 out of 8 Active Dwell-Positions
%Dig for variables to build MC dose distribution
infoRP = dicominfo('RPT.dcm');
infoRD = dicominfo('RDT.dcm');
%Find right ovoid source coordinates
coordinateRT1 = infoRP.ApplicationSetupSequence.Item_1.ChannelSequence.Item_5.Brachy...
    ControlPointSequence.Item_2.ControlPoint3DPosition;
coordinateRT2 = infoRP.ApplicationSetupSequence.Item_1.ChannelSequence.Item_5.Brachy...
    ControlPointSequence.Item_4.ControlPoint3DPosition;
coordinateRT3 = infoRP.ApplicationSetupSequence.Item_1.ChannelSequence.Item_5.Brachy...
    ControlPointSequence.Item_6.ControlPoint3DPosition;
%listed as x, y, z
R1500 = [ (coordinateRT1(3)) (coordinateRT1(1)) -(coordinateRT1(2)) ];
R1495 = [ (coordinateRT2(3)) (coordinateRT2(1)) -(coordinateRT2(2)) ];
R1490 = [ (coordinateRT3(3)) (coordinateRT3(1)) -(coordinateRT3(2)) ];
%left
coordinateLT1 = infoRP.ApplicationSetupSequence.Item_1.ChannelSequence.Item_4.Brachy...
    ControlPointSequence.Item_2.ControlPoint3DPosition;
coordinateLT2 = infoRP.ApplicationSetupSequence.Item_1.ChannelSequence.Item_4.Brachy...
    ControlPointSequence.Item_4.ControlPoint3DPosition;
coordinateLT3 = infoRP.ApplicationSetupSequence.Item_1.ChannelSequence.Item_4.Brachy...
    ControlPointSequence.Item_6.ControlPoint3DPosition;
L1500 = [ (coordinateLT1(3)) (coordinateLT1(1)) -(coordinateLT1(2)) ];
L1495 = [ (coordinateLT2(3)) (coordinateLT2(1)) -(coordinateLT2(2)) ];
L1490 = [ (coordinateLT3(3)) (coordinateLT3(1)) -(coordinateLT3(2)) ];
%Decimal spot
R1500x = sign(coordinateRT1(3))*(abs(coordinateRT1(3)) - abs(fix(coordinateRT1(3))));
R1500y = sign(coordinateRT1(1))*(abs(coordinateRT1(1)) - abs(fix(coordinateRT1(1))));
R1500z = -sign(coordinateRT1(2))*(abs(coordinateRT1(2)) - abs(fix(coordinateRT1(2))));
R1495x = sign(coordinateRT2(3))*(abs(coordinateRT2(3)) - abs(fix(coordinateRT2(3))));
R1495y = sign(coordinateRT2(1))*(abs(coordinateRT2(1)) - abs(fix(coordinateRT2(1))));
R1495z = -sign(coordinateRT2(2))*(abs(coordinateRT2(2)) - abs(fix(coordinateRT2(2))));
R1490x = sign(coordinateRT3(3))*(abs(coordinateRT3(3)) - abs(fix(coordinateRT3(3))));
R1490y = sign(coordinateRT3(1))*(abs(coordinateRT3(1)) - abs(fix(coordinateRT3(1))));
R1490z = -sign(coordinateRT3(2))*(abs(coordinateRT3(2)) - abs(fix(coordinateRT3(2))));
%left
L1500x = sign(coordinateLT1(3))*(abs(coordinateLT1(3)) - abs(fix(coordinateLT1(3))));
L1500y = sign(coordinateLT1(1))*(abs(coordinateLT1(1)) - abs(fix(coordinateLT1(1))));
L1500z = sign(coordinateLT1(2))*(abs(coordinateLT1(2)) - abs(fix(coordinateLT1(2))));
L1495x = sign(coordinateLT2(3))*(abs(coordinateLT2(3)) - abs(fix(coordinateLT2(3))));
L1495y = sign(coordinateLT2(1))*(abs(coordinateLT2(1)) - abs(fix(coordinateLT2(1))));
L1495z = sign(coordinateLT2(2))*(abs(coordinateLT2(2)) - abs(fix(coordinateLT2(2))));
L1490x = sign(coordinateLT3(3))*(abs(coordinateLT3(3)) - abs(fix(coordinateLT3(3))));
L1490y = sign(coordinateLT3(1))*(abs(coordinateLT3(1)) - abs(fix(coordinateLT3(1))));
L1490z = sign(coordinateLT3(2))*(abs(coordinateLT3(2)) - abs(fix(coordinateLT3(2))));
%Adjust to tenths of a millimeter
```

```

R1500z = R1500z/10;
R1495z = R1495z/10;
R1490z = R1490z/10;
L1500z = L1500z/10;
L1495z = L1495z/10;
L1490z = L1490z/10;
R1500y = R1500y/10;
R1495y = R1495y/10;
R1490y = R1490y/10;
L1500y = L1500y/10;
L1495y = L1495y/10;
L1490y = L1490y/10;
R1500x = R1500x/10;
R1495x = R1495x/10;
R1490x = R1490x/10;
L1500x = L1500x/10;
L1495x = L1495x/10;
L1490x = L1490x/10;
%source activity given as air kerma rate.
activity = infoRP.SourceSequence.Item_1.ReferenceAirKermaRate;
% Partial dwell-time weights..
% Subtract--> BrachyControlPointSequence.Item_y (even# - odd#)
part1500R = (infoRP.ApplicationSetupSequence.Item_1.ChannelSequence.Item_5.Brachy...
    ControlPointSequence.Item_2.CumulativeTimeWeight)-(infoRP.ApplicationSetup...
    Sequence.Item_1.ChannelSequence.Item_5.BrachyControlPointSequence.Item_1.Cumu...
    lativeTimeWeight);
part1495R = (infoRP.ApplicationSetupSequence.Item_1.ChannelSequence.Item_5.Brachy...
    ControlPointSequence.Item_4.CumulativeTimeWeight)-(infoRP.ApplicationSetup...
    Sequence.Item_1.ChannelSequence.Item_5.BrachyControlPointSequence.Item_3.Cumu...
    lativeTimeWeight);
part1490R = (infoRP.ApplicationSetupSequence.Item_1.ChannelSequence.Item_5.Brachy...
    ControlPointSequence.Item_6.CumulativeTimeWeight)-(infoRP.ApplicationSetup...
    Sequence.Item_1.ChannelSequence.Item_5.BrachyControlPointSequence.Item_5.Cumu...
    lativeTimeWeight);
%total time weight
finalR = infoRP.ApplicationSetupSequence.Item_1.ChannelSequence.Item_5.FinalCumu...
    lativeTimeWeight;
% Total dwell-time
channeltimeR = infoRP.ApplicationSetupSequence.Item_1.ChannelSequence.Item_5.Chan...
    nelTotalTime;
% Calculate dwell-time
dwelltime1500R = double((part1500R)/(finalR)*(channeltimeR));
dwelltime1495R = double((part1495R)/(finalR)*(channeltimeR));
dwelltime1490R = double((part1490R)/(finalR)*(channeltimeR));
% LOvoid,difference x--> infoRP.ApplicationSetupSequence.Item_1.ChannelSequence.Item_x
part1500L = (infoRP.ApplicationSetupSequence.Item_1.ChannelSequence.Item_4.Brachy...
    ControlPointSequence.Item_2.CumulativeTimeWeight)-(infoRP.ApplicationSetup...
    Sequence.Item_1.ChannelSequence.Item_4.BrachyControlPointSequence.Item_1.Cumu...

```

```

    lativeTimeWeight);
part1495L = (infoRP.ApplicationSetupSequence.Item_1.ChannelSequence.Item_4.Brachy...
    ControlPointSequence.Item_4.CumulativeTimeWeight)-(infoRP.ApplicationSetup...
    Sequence.Item_1.ChannelSequence.Item_4.BrachyControlPointSequence.Item_3.Cumu...
    lativeTimeWeight);
part1490L = (infoRP.ApplicationSetupSequence.Item_1.ChannelSequence.Item_4.Brachy...
    ControlPointSequence.Item_6.CumulativeTimeWeight)-(infoRP.ApplicationSetup...
    Sequence.Item_1.ChannelSequence.Item_4.BrachyControlPointSequence.Item_5.Cumu...
    lativeTimeWeight);
%total time weight
finalL = infoRP.ApplicationSetupSequence.Item_1.ChannelSequence.Item_4.FinalCumu...
    lativeTimeWeight;
%Total dwell-time
channeltimeL = infoRP.ApplicationSetupSequence.Item_1.ChannelSequence.Item_4.Chan...
    nelTotalTime;
%Calculate dwell-time
dwelltime1500L = double((part1500L)/(finalL)*(channeltimeL));
dwelltime1495L = double((part1495L)/(finalL)*(channeltimeL));
dwelltime1490L = double((part1490L)/(finalL)*(channeltimeL));
%Calculate the MC conversion factor for each dwell-position
%Rotation parameters searches RD DICOM
%x,y,z unit vectors along primary axis
x = [1;0;0];
y = [0;1;0];
z = [0;0;1];
array = infoRD.GridFrameOffsetVector;
checkarray = array';
dimension = (infoRD.ImagePositionPatient);
DCMframes = infoRD.NumberOfFrames;
DCMrows = infoRD.Rows;
DCMcolumns = infoRD.Columns;
% Subtract coordinates to get a vector originating from first and ending at
% the second. Results in a vector originating from (0, 0, 0) to second
% dwell coordinate (should be approximately 5mm in length)
differenceR1 = R1490 - R1495;
% Vector in the xy plane
xycalc = [differenceR1(1); differenceR1(2); 0];
%Use geometry to solve for angles to orient seeds (This just solves for the
%angle in the dot product of two vectors)
zangleR = ((-acosd((dot(differenceR1,z))/(norm(z)*norm(differenceR1)))));
xangleR = acosd((dot(xycalc,x))/(norm(x)*norm(xycalc)));
yangleR = acosd((dot(xycalc,y))/(norm(y)*norm(xycalc)))-90;
%Get unit vector pointing in the direction of the bottom dwells
differenceL1 = L1490 - L1495;
% Vector in the xy plane
xycalc = [differenceL1(1); differenceL1(2); 0];
%Use geometry to solve for angles to orient seeds
zangleL = ((-acosd((dot(differenceL1,z))/(norm(z)*norm(differenceL1)))));

```

```

xangleL = acosd((dot(xycalc,x))/(norm(x)*norm(xycalc)));
yangleL = acosd((dot(xycalc,y))/(norm(y)*norm(xycalc)))-90;
%Parameters to expand small dose grids to larger so that a rotation can be
%applied.
%50 used because grid dimensions were 101x101x101
MCexpand=201;
shift = (MCexpand - 101)/2;
DICOMxgrid = (dimension(1)+50);
DICOMygrid = (dimension(3)+50);
DICOMzgrid = -(dimension(2)+50);
DICOMsetxgrid = dimension(1);
DICOMsetygrid = dimension(3);
DICOMsetzgrid = dimension(2);
%Dose grid indexes for MC dose grid
xgridMC = (0:0.1:0.1*(MCexpand-1))-((MCexpand-1)/20);
ygridMC = (0:0.1:0.1*(MCexpand-1))-((MCexpand-1)/20);
zgridMC = (0:0.1:0.1*(MCexpand-1))-((MCexpand-1)/20);
%Dose grid indexes compiled from DICOM file.. should match above
xgrid = checkarray + dimension(1);
xgrid = xgrid./10;
ygrid = checkarray + dimension(3);
ygrid = ygrid./10;
zgrid = checkarray + dimension(2);
zgrid = zgrid./10;

```

Appendix 5 Dose Grid 3D Rotation

```
%filename (listed in interpolate function) is dose file to be rotated
%Frames, rows, columns defined in DICOM
m = frames;
n = rows;
q = columns;

%Create a list of coordinates from indexes
%e.g. xgridMC = 0:0.1:0.1*101
[X1 Y1 Z1] = meshgrid(xgridMC, ygridMC, zgridMC);
%Rotation matrix for each axis
xaxis = [ 1      0      0      ;...
          0      cosd(xangleL)  -sind(xangleL)  ;...
          0      sind(xangleL)   cosd(xangleL)  ];
yaxis = [ cosd(yangleL)  0      sind(yangleL)  ;...
          0              1      0              ;...
          -sind(yangleL)  0      cosd(yangleL)  ];
zaxis = [ cosd(zangleL1) -sind(zangleL1)  0      ;...
          sind(zangleL1)  cosd(zangleL1)  0      ;...
          0              0              1      ];

%Use matrix multiplication to rotate all at once
rotation_matrix = yaxis*xaxis*zaxis;

%Apply coordinate rotation
XYZ_rotated = (C1)*[X1(:) Y1(:) Z1(:)].';

%Map rotation from old coordinates to new coordinates
newXYZlist = interp3(X1,Y1,Z1,filename,XL1,YL1,ZL1);

%reshape dose grid from blocklist format to a cube
XYZmatrix = reshape(newXYZlist,[m n q]);
XYZmatrix (isnan(XYZmatrix))=0;
```

Vita

Bobby Chon Mathews was born in Bitburg, Germany, in February, 1984. He completed his Bachelor of Science degree in both general physics and mathematics from the University of Arkansas in Little Rock where he lived from 2003 – 2007. He received his master's degree in medical physics and health physics in the Department of Physics and Astronomy at Louisiana State University in the fall of 2007. He currently plans to begin a career as a clinical medical physicist in Little Rock, Arkansas at Central Arkansas Radiation Therapy Institute (CARTI).